Eur. Phys. J. C (2021) 81:1023
https://doi.org/10.1140/epjc/s10052-021-09761-x

THE EUROPEAN PHYSICAL JOURNAL C



Regular Article - Experimental Physics

# Search for R-parity-violating supersymmetry in a final state containing leptons and many jets with the ATLAS experiment using $\sqrt{s} = 13$ TeV proton–proton collision data

**ATLAS Collaboration**[⋆]

CERN, 1211 Geneva 23, Switzerland

Received: 18 June 2021 / Accepted: 19 October 2021 / Published online: 23 November 2021


**Abstract** A search for R-parity-violating supersymmetry in final states characterized by high jet multiplicity, at least one isolated light lepton and either zero or at least three $b$-tagged jets is presented. The search uses 139 fb$^{-1}$ of $\sqrt{s} =$ 13 TeV proton–proton collision data collected by the ATLAS experiment during Run 2 of the Large Hadron Collider. The results are interpreted in the context of R-parity-violating supersymmetry models that feature gluino production, top-squark production, or electroweakino production. The dominant sources of background are estimated using a data-driven model, based on observables at medium jet multiplicity, to predict the $b$-tagged jet multiplicity distribution at the higher jet multiplicities used in the search. Machine-learning techniques are used to reach sensitivity to electroweakino production, extending the data-driven background estimation to the shape of the machine-learning discriminant. No significant excess over the Standard Model expectation is observed and exclusion limits at the 95% confidence level are extracted, reaching as high as 2.4 TeV in gluino mass, 1.35 TeV in top-squark mass, and 320 (365) GeV in higgsino (wino) mass.

## 1 Introduction

Supersymmetry (SUSY) [1–6] is a theoretical extension of the Standard Model (SM) which fundamentally relates fermions and bosons. It is an alluring theoretical possibility given its potential to solve the hierarchy problem [7–10]. An ad hoc conserved quantity, R-parity [11], is often introduced in SUSY models to avoid rapid proton decay, rendering the lightest supersymmetric particle (LSP) stable and therefore a potential dark-matter candidate [12,13]. There is no fundamental theoretical reason to impose strict R-parity conservation, and R-parity-violating (RPV) SUSY models are well motivated, with fewer experimental constraints than many R-parity-conserving (RPC) models [14,15], and allow for more natural supersymmetric mass spectra.

This article presents a search for pair production of supersymmetric particles with subsequent RPV decays in a final state with at least one isolated lepton (electron or muon), at least eight to fifteen jets (depending on the jet transverse momentum threshold), several of which may contain $b$-flavoured hadrons ($b$-jets), and with no requirement on the missing transverse momentum. Such a final state is commonly predicted in RPV models with either baryon-number-violating [16,17] or lepton-number-violating couplings [18]. Events are assigned to one of two categories according to their lepton content. The first category contains events with two leptons with the same electric charge ($2\ell^{\text{sc}}$), while the second category contains all other events and is dominated by single-lepton events ($1\ell$). Electrons and muons from $\tau$-lepton decays are also considered. A multi-bin fit in each lepton category to the two-dimensional space of jet multiplicity and $b$-jet multiplicity is used to constrain parameters of benchmark RPV simplified signal models [19–21]. A third variable, based on a machine-learning discriminant, is introduced to improve the sensitivity of the search when only testing for the electroweak production of supersymmetric particles. This search has potential sensitivity to a large number of beyond the Standard Model (BSM) physics models, and model-independent limits on the possible contribution of BSM physics to several single-bin signal regions are shown.

The dominant Standard Model background in the $1\ell$ category arises from top-quark pair production and $W/Z$ + jets production, with at least one lepton produced in the vector-boson decay. In the $2\ell^{\text{sc}}$ category, the production of a top-quark pair in association with a $W$ boson ($t\bar{t}W$), or with a misidentified lepton, constitutes the main background. The theoretical modelling of these backgrounds at high jet multiplicity suffers from large uncertainties, so they are estimated from the data by extrapolating the $b$-jet multiplicity distri-

⋆ e-mail: atlas.publications@cern.ch

bution extracted at moderate jet multiplicities to the high jet multiplicities of the search region.

This analysis is an update to a previous ATLAS search [22] for new phenomena in a final state with a lepton and high jet multiplicity, which was performed with 36 fb$^{-1}$ of $\sqrt{s} = 13$ TeV proton–proton collision data. It improves upon the previous result owing to the larger luminosity, the dedicated categorization and analysis of events with two leptons with the same electric charge, and the introduction of multivariate discriminants. This search represents the first LHC result to obtain sensitivity to electroweak production of SUSY particles promptly decaying to quarks, as predicted in baryon-number-violating RPV models. Previous searches targeting similar RPV SUSY models have been carried out by the ATLAS and CMS collaborations [23–33]. The result is also sensitive to SM four-top-quark production, and a validation of the background estimation methods is performed by fitting the normalization of the four-top-quark process relative to the Standard Model value. Previous searches for four-top-quark production were carried out by the ATLAS [34] and CMS [35] collaborations.

## 2 Signal models

Simulated signal events from five SUSY benchmark simplified models (representative production diagrams shown in Fig. 1) are used to guide the analysis selections and to estimate the expected signal yields for different signal-mass hypotheses used to interpret the analysis results. In all models considered, the RPV couplings and the SUSY particle masses are chosen to ensure prompt decays of the SUSY particles. The supersymmetric particle content of the models is the partner of the SM gluon (gluino), the partner of the right-handed top quark (stop), and one or more electroweakinos. The electroweakinos are massive fermions resulting from the mixing between the partners of SM electroweak and Higgs bosons.[1] Three different possibilities for the electroweakino composition are tested: pure bino, pure wino or pure higgsino. In all cases the lightest neutralino ($\tilde{\chi}_1^0$) is the LSP. When considering a wino (higgsino) LSP, the corresponding chargino $\tilde{\chi}_1^\pm$ (and second neutralino $\tilde{\chi}_2^0$) is assumed to be effectively mass degenerate with the LSP, as predicted by theory [36,37], and share the same composition as the LSP. All the electroweakinos that are present under the hypothesis of a given composition are considered in both the production and decay processes. All other electroweakinos are assumed to be decoupled and not considered in the model. The gluino and stop branching ratios, as well as the electroweakino production cross-section, are determined by the nature of the electroweakino. Table 1 summarizes the gluino and stop branching ratios, and shows example cross-sections for direct electroweakino production [38–42], for each electroweakino type. In each case, the electroweakinos decay through a non-zero RPV coupling large enough to ensure prompt decays for the particle masses considered, and small enough to avoid more complex decay patterns involving mixtures of both RPC and RPV decays that are not considered here. Within this scenario the analysis results are independent of the value of the coupling.

Four of the simplified models are inspired by a common natural RPV SUSY model assuming the minimal flavour violation hypothesis [16,17]. The coupling $\lambda''_{323}$ is chosen, as it is predicted to be dominant.[2] With the chosen model parameters, the electroweakinos decay as $\tilde{\chi}_{1/2}^0 \to tbs$ and $\tilde{\chi}_1^\pm \to bbs$, with a branching ratio of 100%. At the lowest order in perturbation theory, signal events in these models contain four, six, or eight $b$-jets in the final state, depending on the production mode. In the first model, gluino production is considered, with decays to heavy-flavour quarks and the electroweakino, which in turn decays via the RPV coupling. The stop, with a mass assumed to be above the gluino mass, is not considered in the model. A signal diagram for this model is shown in Fig. 1a. The second model considers gluino pair production, with each gluino decaying into a top quark and a stop, as shown in Fig. 1b. In this model the RPV coupling is assumed to be large, so that the stop decays via an RPV mode into an $s$-quark and a $b$-quark. The absence of RPC decays of the stop render the electroweakino mass irrelevant in this model. The third scenario considered involves stop pair production with the stop decaying into an electroweakino and a top or bottom quark, while the gluino is set to a very high mass and not considered in the model. An example signal diagram is shown in Fig. 1c. In the fourth model, only electroweakino production is considered, with the stop and gluino assigned a very high mass and not considered in the model. Figure 1d considers the production of $\tilde{\chi}_1^\pm \tilde{\chi}_1^0$. In the case of a higgsino LSP, a similar diagram produces $\tilde{\chi}_1^\pm \tilde{\chi}_2^0$, and a further diagram producing $\tilde{\chi}_1^0 \tilde{\chi}_2^0$ is enabled, as shown in Fig. 1e. Production of $\tilde{\chi}_1^\pm \tilde{\chi}_{1,2}^0$ contributes only to the $1\ell$ category, while the production of $\tilde{\chi}_1^0 \tilde{\chi}_2^0$ contributes to both the $1\ell$ and $2\ell^{\text{sc}}$ categories. Production of $\tilde{\chi}_1^\pm \tilde{\chi}_1^\pm$ is not considered because the decays produce a final state with no leptons. Production of $\tilde{\chi}_1^0 \tilde{\chi}_1^0$ vanishes and is not considered. Therefore electroweak production in the pure bino scenario is not considered.

The fifth and last simplified RPV model considers gluino pair production, where each gluino decays into two first- or second-generation quarks ($q \equiv (u, d, s, c)$) and a $\tilde{\chi}_1^0$,

[1] In SUSY, the Higgs sector is enriched by the presence of an additional complex doublet.

[2] The results apply equally to the coupling $\lambda''_{313}$ since it leads to the same experimental final state.

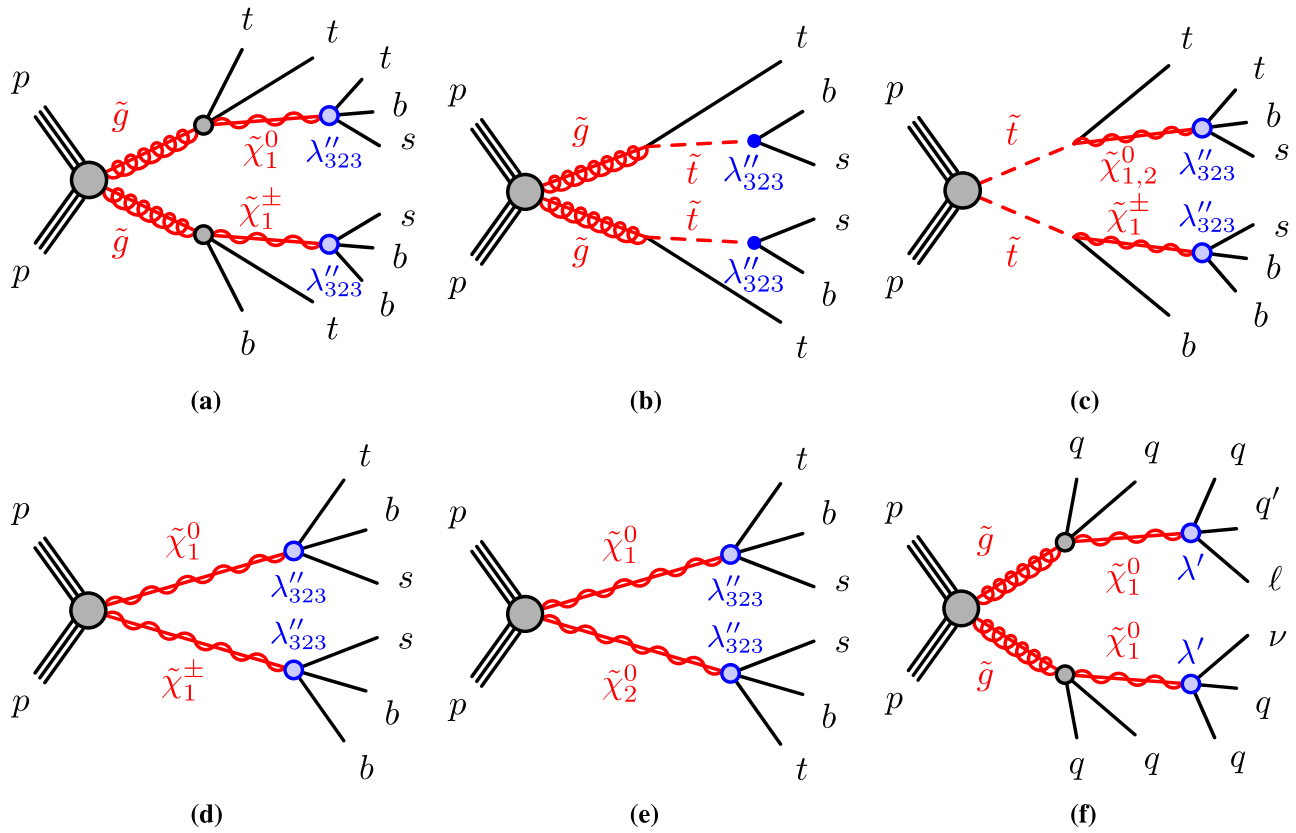


**Fig. 1** Examples of signal diagrams for the simplified RPV models considered in this article. Cases where both of the gluinos (or the stops) decay in the same way are also considered, and $\tilde{\chi}_1^{\pm}\tilde{\chi}_2^0$ pair production is also considered for the higgsino LSP type. For simplicity particles and anti-particles are shown using the same symbols, omitting the anti-particle notation

**Table 1** Stop and gluino branching ratios, as well as cross-sections for direct electroweakino production, as a function of the LSP type. For a pure bino/wino/higgsino LSP, the electroweakino states considered are $\tilde{\chi}_1^0/\tilde{\chi}_1^0\tilde{\chi}_1^{\pm}/\tilde{\chi}_1^0\tilde{\chi}_1^{\pm}\tilde{\chi}_2^0$, respectively. When relevant, decays to $\tilde{\chi}_1^0$ and $\tilde{\chi}_2^0$ are merged as they are assumed to be mass degenerate and both decay in the same way. The production cross-sections are given for an electroweakino mass of $m(\tilde{\chi}_1^0, \tilde{\chi}_1^{\pm}, \tilde{\chi}_2^0) = 300$ GeV

| LSP type | Branching ratios | | | | | Cross-section [fb] for direct production | | |
|---|---|---|---|---|---|---|---|---|
| | Stop | | Gluino | | | $\tilde{\chi}_1^{\pm}\tilde{\chi}_1^0$ | $\tilde{\chi}_1^{\pm}\tilde{\chi}_2^0$ | $\tilde{\chi}_2^0\tilde{\chi}_1^0$ |
| | $t\tilde{\chi}_{1,2}^0$ | $b\tilde{\chi}_1^{\pm}$ | $tt\tilde{\chi}_{1,2}^0$ | $bb\tilde{\chi}_{1,2}^0$ | $tb\tilde{\chi}_1^{\pm}$ | | | |
| Bino | 100% | 0% | 100% | 0% | 0% | 0 | 0 | 0 |
| Wino | 33% | 67% | 17% | 17% | 66% | 387 | 0 | 0 |
| Higgsino | 50% | 50% | 50% | 0% | 50% | 91 | 91 | 52 |

which is the LSP. The $\tilde{\chi}_1^0$ decays into two additional first- or second-generation quarks and a charged lepton or a neutrino ($\tilde{\chi}_1^0 \to q\bar{q}'\ell$ or $\tilde{\chi}_1^0 \to q\bar{q}\nu$, labelled as $\tilde{\chi}_1^0 \to q\bar{q}\ell/\nu$). The decay proceeds via a $\lambda'$ RPV coupling, where each RPV decay can produce any of the four first- or second-generation leptons ($e^{\pm}$, $\mu^{\pm}$, $\nu_e$, $\nu_\mu$) with equal probability. An example signal diagram is shown in Fig. 1f. Signal decays from this model yield a final state with high jet multiplicity and zero $b$-jets.

## 3 ATLAS detector

The ATLAS experiment [43] at the LHC is a multipurpose particle detector with a forward–backward symmetric cylindrical geometry and nearly $4\pi$ coverage in solid angle.[3] It

[3] ATLAS uses a right-handed coordinate system with its origin at the nominal interaction point (IP) in the centre of the detector and the $z$-axis along the beam pipe. The $x$-axis points from the IP to the centre of the LHC ring, and the $y$-axis points upwards. Cylindrical coordinates

consists of an inner tracking detector (ID) surrounded by a thin superconducting solenoid providing a 2 T axial magnetic field, electromagnetic (EM) and hadron calorimeters, and a muon spectrometer (MS). The inner tracking detector covers the pseudorapidity range $|\eta| < 2.5$. It consists of silicon pixel, silicon microstrip and transition radiation tracking detectors; the innermost layer is 33 mm from the beamline [44,45]. Lead/liquid-argon (LAr) sampling calorimeters provide electromagnetic energy measurements with high granularity. A steel/scintillator-tile hadron calorimeter covers the central pseudorapidity range ($|\eta| < 1.7$). The endcap and forward regions are instrumented with LAr calorimeters for both the EM and hadronic energy measurements up to $|\eta| = 4.9$. The muon spectrometer surrounds the calorimeters and is based on three large superconducting air-core toroidal magnets with eight coils each. The field integral of the toroids ranges between 2.0 and 6.0 T·m across most of the detector. The muon spectrometer includes a system of precision tracking chambers and fast detectors for triggering. A two-level trigger system is used to select events [46]. The first-level trigger is implemented in hardware and uses a subset of the detector information to keep the accepted rate below approximately 100 kHz. This is followed by a software-based trigger that reduces the accepted event rate to approximately 1 kHz on average depending on the data-taking conditions. An extensive software suite [47] is used for real and simulated data reconstruction and analysis, for operation and in the trigger and data acquisition systems of the experiment.

## 4 Monte Carlo event simulation

Signal and background events produced in proton–proton collisions were simulated with various Monte Carlo (MC) generators. The simulated events are used in the optimization of event selection criteria, in the neural network training, to estimate systematic uncertainties, to validate the background estimation procedure employed for the dominant background sources, and to predict yields for the subdominant background contributions and for possible signals. The signal and background events were passed through the GEANT4 [48] simulation of the ATLAS detector [49] and reconstructed using the same algorithms as are used for the data.

The generation of the simulated event samples includes the effect of multiple proton–proton interactions per bunch crossing, as well as the impact on the detector response due to interactions from bunch crossings before or after the one containing the hard interaction. The effect of multiple interactions in the same and neighbouring bunch crossings (pile-up) is modelled by overlaying the hard-scattering event with simulated inelastic proton–proton events generated by PYTHIA 8.186 [50] using the `NNPDF2.3lo` set of parton distribution functions (PDF) [51] and the A3 set of tuned parameters [52]. The MC events are weighted to reproduce the distribution of the average number of interactions per bunch crossing ($\langle\mu\rangle$) observed in the data. The EVTGEN [53] program was used to simulate properties of the $b$- and $c$- flavoured hadron decays.

The signal event samples were generated using the MADGRAPH5_aMC@NLO [54] generator interfaced to PYTHIA 8 for the modelling of the parton showering, hadronization, and underlying event. The matrix element (ME) calculation was performed at tree level and includes the emission of up to two additional partons. The signal samples were processed through a fast simulation of the ATLAS detector [49,55]. Gluino and stop signal cross-sections are calculated to approximate next-to-next-to-leading order in the strong coupling constant, adding the resummation of soft gluon emission at next-to-next-to-leading-logarithm accuracy (approximate NNLO+NNLL) [56–66]. The cross-sections for electroweakino production are calculated to next-to-leading order in the strong coupling constant, adding the resummation of soft gluon emission at next-to-leading-logarithm accuracy (NLO+NLL) [38–42].

The production of $t\bar{t}$, $t\bar{t}H$, and single-top events was modelled at NLO using the POWHEGBOX [72–75,93] generator. Additional $t\bar{t}$ samples were generated with MADGRAPH5_aMC@NLO interfaced with PYTHIA 8, and with POWHEGBOX interfaced with HERWIG 7 [83,84], for modelling comparisons and evaluation of systematic uncertainties.

The production of $t\bar{t}V$ ($V = W, Z$) events was modelled using the SHERPA generator. The ME was calculated for up to one additional parton at NLO and up to two partons at LO using the COMIX [94] and OPENLOOPS libraries [95,96], and merged with the SHERPA parton shower using the MEPS@NLO prescription [97–101]. Alternative $t\bar{t}V$ samples produced with the MADGRAPH5_aMC@NLO generator at NLO were used to evaluate systematic uncertainties associated with the modelling of additional QCD radiation.

The production of $t\bar{t}t\bar{t}$, $t\bar{t}t$, $tWZ$, $tZ$, $t\bar{t}WW$, and $t\bar{t}WZ$ events was modelled using the MADGRAPH5_aMC@NLO generator at NLO, and interfaced with PYTHIA 8. An alternative $t\bar{t}t\bar{t}$ sample showered with HERWIG 7, was used to evaluate systematic uncertainties related to the choice of parton-shower model.

The production of an electroweak gauge boson or virtual photon in association with jets ($V$+jets) was simulated with the SHERPA generator using NLO matrix elements for up to two partons, and LO matrix elements for up to four partons. Alternative $V$+jets samples used to validate the analy-

Footnote 3 continued
$(r, \phi)$ are used in the transverse plane, $\phi$ being the azimuthal angle around the $z$-axis. The pseudorapidity is defined in terms of the polar angle $\theta$ as $\eta = -\ln\tan(\theta/2)$. Angular distance is measured in units of $\Delta R \equiv \sqrt{(\Delta y)^2 + (\Delta\phi)^2}$.

**Table 2** Simulated background event samples: the corresponding event generator, parton-shower modelling, cross-section normalization, PDF set and underlying-event parameter tune are shown. The samples marked with (*) are alternative samples used to validate the background estimation method or to assess systematic uncertainties in the modelling. The abbreviation MG5_aMC is used to label the MADGRAPH5_aMC@NLO generator. Samples produced with SHERPA use the default set of tuned parameters of the generator

| Physics process | Event generator | Parton-shower modelling | Cross-section normalization | PDF set | Tune |
|---|---|---|---|---|---|
| $W(\to \ell\nu)$ + jets | SHERPA 2.2.1 [67] | SHERPA 2.2.1 | NNLO [68] | `NNPDF3.0nnlo` [69] | SHERPA |
| $W(\to \ell\nu)$ + jets (*) | MG5_aMC 2.2.2 [54] | PYTHIA 8.186 [70] | NNLO | `NNPDF3.0nlo` [69] | A14 [71] |
| $Z/\gamma^*(\to \ell\ell)$ + jets | SHERPA 2.2.1 | SHERPA 2.2.1 | NNLO [68] | `NNPDF3.0nnlo` | SHERPA |
| $t\bar{t}$ + jets | POWHEGBOX v2 [72–75] | PYTHIA 8.230 [50] | NNLO+NNLL [76–82] | `NNPDF3.0nlo` | A14 |
| $t\bar{t}$ + jets (*) | POWHEGBOX v2 | HERWIG 7.04 [83,84] | NNLO+NNLL | `MMHT2014lo` [85] | H7UE [84] |
| $t\bar{t}$ + jets (*) | MG5_aMC 2.6.0 | PYTHIA 8.230 | NNLO+NNLL | `NNPDF3.0nlo` | A14 |
| Single-top | POWHEGBOX v2 [86–88] | PYTHIA 8.230 | NNLO+NNLL [89–91] | `NNPDF3.0nlo` | A14 |
| $t\bar{t} + W/Z$ | SHERPA 2.2.1 | SHERPA 2.2.1 | NLO [92] | `NNPDF3.0nnlo` | SHERPA |
| $t\bar{t} + t\bar{t}/t/WW/WZ$ | MG5_aMC 2.3.3 [54] | PYTHIA 8.230 | NLO [92] ($t\bar{t}t$ LO) | `NNPDF2.3lo` [51] | A14 |
| $t\bar{t}t\bar{t}$ (*) | MG5_aMC 2.3.3 | HERWIG 7.04 | NLO [54] | `MMHT2014lo` | H7UE |
| $t\bar{t}H$ | POWHEGBOX v2 | PYTHIA 8.230 | NLO | `NNPDF3.0nlo` | A14 |
| $tWZ, tZ$ | MG5_aMC 2.3.3 | PYTHIA 8.212, 8.210 | NLO | `NNPDF3.0nlo` | A14 |
| $VV$ and $VVV$ | SHERPA 2.2.1, 2.2.2, 2.2.4 | SHERPA | NLO | `NNPDF3.0nnlo` | SHERPA |

sis methods were simulated with MADGRAPH5_aMC@NLO using LO-accurate MEs with up to four final-state partons.

Event samples with diboson ($VV$) and triboson ($VVV$) final states were simulated with the SHERPA generator, including off-shell effects and Higgs boson contributions, where appropriate. The $VV$ processes were simulated using matrix elements at NLO accuracy in QCD for up to one additional parton and at LO accuracy for up to three additional parton emissions. The production of triboson ($VVV$) events was simulated with the SHERPA generator using factorized gauge-boson decays.

A summary of the background samples used, together with the event generator configurations, can be found in Table 2.

## 5 Event reconstruction and object identification

Proton–proton collision data recorded by the ATLAS detector between 2015 and 2018 are used to perform the analysis. In this period, the LHC delivered colliding beams with a peak instantaneous luminosity up to $L = 2.1 \times 10^{34}\,\text{cm}^{-2}\text{s}^{-1}$, achieved in 2018, and an average number of $pp$ interactions per bunch crossing of 33.7. After applying beam, detector, and data-quality criteria the total integrated luminosity of the dataset is 139 $\text{fb}^{-1}$ [102]. The uncertainty in the combined 2015–2018 integrated luminosity is 1.7% [103], obtained using the LUCID-2 detector [104] for the primary luminosity measurements.

Proton–proton interaction vertices are reconstructed from charged-particle tracks with $p_T > 500$ MeV [105,106] in the ID. The presence of at least one such vertex with a minimum of two associated tracks is required, and the vertex with the largest sum of $p_{\text{T}}^2$ of associated tracks is chosen as the primary vertex.

Jet candidates are reconstructed up to $|\eta| = 4.9$ using the anti-$k_t$ algorithm [107,108] with radius parameter $R = 0.4$. It uses particle-flow objects as inputs, combining tracking and calorimetric information as detailed in Ref. [109]. The jets are calibrated using the methodology described in Ref. [110]. Any event that contains jets induced by calorimeter noise or non-collision background, according to criteria similar to those described in Ref. [111], is removed. Jets up to $p_T = 60$ GeV containing a large energy contribution from pile-up interactions are suppressed with the jet-vertex tagging (JVT) algorithm that uses tracking and primary vertex information to determine if a given jet originates from the primary vertex [112]. Jets with $p_T > 20$ GeV and $|\eta| < 2.5$ are defined as signal jets, and used further in the analysis.

Signal jets containing $b$-flavoured hadrons are identified with the DL1r $b$-tagging algorithm [113,114] with an average identification efficiency of 70% in simulated $t\bar{t}$ events. The rejection factor is measured to be approximately 300 for jets initiated by light quarks and gluons and approximately 9 for jets initiated by charm quarks [113].

Electron candidates are reconstructed as tracks in the ID matched to energy clusters in the EM calorimeter, within $|\eta| < 2.47$ [115]. The analysis considers only candidate electrons with $p_{\text{T}} > 10$ GeV and not in the transition region between the barrel and endcap calorimeters ($1.37 < |\eta| < 1.52$). The electron identification is based on a multivariate likelihood-based discriminant that uses the shower shapes in the EM calorimeter and the associated track properties measured in the ID. The electron candidates must satisfy the 'Medium' identification criteria described in Ref. [115],

while the signal electrons must satisfy the 'Tight' identification for better rejection of non-prompt or misidentified electrons. The electron identification efficiency varies with increasing $p_{\mathrm{T}}$ in $Z \to ee$ events, from 65% at $p_T = 10$ GeV to 88% at 100 GeV for the Tight operating point, and from 75% at 20 GeV to 94% at 100 GeV for the Medium operating point.

For candidate and signal electrons, the longitudinal impact parameter of the electron track, $z_0$, is required to satisfy $|z_0 \sin\theta| < 0.5$ mm, where $\theta$ is the polar angle of the track. For signal electrons, the transverse impact parameter divided by its uncertainty, $|d_0|/\sigma(d_0)$, is required to be at most five.

For all signal electrons there must be no association with a vertex from a reconstructed photon conversion [115] in the detector material. To further reduce the photon conversion background, additional requirements are applied to the signal electrons [34]: (i) the candidate must not have a reconstructed displaced vertex with a conversion radius $r > 20$ mm whose reconstruction uses the track associated with the electron, (ii) the invariant mass of the system formed by the track associated with the electron and the closest track (in $\Delta R$) at the primary vertex or a conversion vertex is required to be larger than 100 MeV. This photon conversion veto has an average efficiency of 99% for prompt electrons while providing a rejection factor of 4 for electrons from photon conversion.

In the $2\ell^{\mathrm{sc}}$ category, signal electrons with wrongly reconstructed charge (charge-flip) are suppressed using a boosted decision tree (BDT) discriminant exploiting additional tracks in the vicinity of the electron and track-to-cluster matching variables [115]. A rejection factor of around 9 for electrons with a wrong charge assignment is achieved, while selecting properly measured electrons with an efficiency of 98%, in simulated $Z \to ee$ events selected with the Tight identification and isolation operating points [115].

Muon candidates are reconstructed in the region $|\eta| < 2.5$ from MS tracks matching ID tracks. Only muons with $p_T > 10$ GeV satisfying the 'Medium' quality requirements defined in Ref. [116] are considered. The muon reconstruction efficiency is approximately 98% in simulated $Z \to \mu\mu$ events. The same longitudinal impact parameter selection as for candidate and signal electrons is applied, while $|d_0|/\sigma(d_0)$ is required to be at most three.

For signal electrons and muons the identification criteria are complemented by an isolation requirement, which is based on the energy in a cone around the lepton candidate calculated using either reconstructed tracks or energy clusters. Non-prompt electrons and muons from the decays of $b$- and $c$-flavoured hadrons are further rejected using a BDT discriminant based on isolation and secondary vertex information, referred to as the non-prompt-lepton veto [117]. The efficiency of the combined isolation and non-prompt-lepton veto is on average above 80% for prompt leptons with $p_T > 30$ GeV in simulated diboson events. Finally, all signal leptons are required to have $p_T > 15$ GeV.

A sequential overlap removal procedure to resolve ambiguities between candidate jets and candidate leptons is carried out before the signal selection as follows. First, candidate electrons sharing their track with a muon candidate are removed. Furthermore, any non-$b$-jet candidate lying within an angular distance $\Delta R = 0.2$ of a candidate electron is discarded; non-$b$-jets within $\Delta R = 0.4$ of candidate muons are removed if the number of tracks associated with the jet is less than three. Finally, any lepton candidate remaining within a distance $\Delta R = \min\{0.4, 0.04 + 10\,\mathrm{GeV}/p_T(\ell)\}$ of any surviving jet candidate is discarded since they likely arise from decays of $b$- or $c$-flavoured hadrons.

Similar to the electron candidates, the photon candidates are reconstructed from calorimeter energy clusters and identified using the 'Tight' criteria [115]. They are required to be in the region $|\eta| < 2.37$ and have $p_T > 145$ GeV. Signal photons must satisfy the 'Tight' calorimeter-based isolation requirements [115], and are used to validate the background estimation technique detailed in Sect. 7.1.

The missing transverse momentum, with magnitude $E_{\mathrm{T}}^{\mathrm{miss}}$, is defined as the negative vector sum of the transverse momenta of all identified objects (muon, electron and jet candidates) and an additional soft term [118,119]. The soft term is added to recover the contributions from other low-$p_{\mathrm{T}}$ objects, and is constructed from all tracks that are matched to the primary vertex but are not associated with any other object. A dedicated overlap removal procedure, based on removing duplicated energy contributions, is applied. The $E_{\mathrm{T}}^{\mathrm{miss}}$ variable is used to define control regions enriched in certain types of background, as discussed in Sect. 7.4, and as input for the multivariate discriminant.

## 6 Event selection and analysis strategy

Two complementary analysis strategies are defined, namely the 'jet counting analysis' and the electroweak analysis, labelled 'EWK analysis'. While the first approach is designed to be very generic and offers a large variety of signal interpretations for strong production models, the second approach is specifically tailored to reach sensitivity for electroweakino production. In both analyses, events are assigned to one of two categories according to their lepton content, and further categorized into regions based on jet multiplicity and $b$-jet multiplicity. This categorization provides a set of regions that are sensitive to decays from all the possible signal models considered in this search, amplifying the ability of the search to discriminate signal from background. The EWK analysis is an extension of the jet counting analysis, where a third variable, a neural network (NN) discriminant, is introduced in some of the jet and $b$-jet multiplicity regions in order to

improve the separation of signal from background. Additional kinematic selections are also applied at the preselection level, tailored to the electroweakino signals.

Events were selected for read-out using single-lepton triggers that require the electron or muon to satisfy identification criteria similar to those used in the offline reconstruction and isolation requirements [120,121]. For the analysis selection, at least four jets and at least one signal electron or muon, matched to the trigger lepton, are required in the event. The highest-$p_{\mathrm{T}}$ lepton in the event has to pass the signal requirements and satisfy $p_{\mathrm{T}} > 27\,\mathrm{GeV}$, in order to be above the trigger threshold. Two disjoint event categories are defined according to the lepton content: a same-charge dilepton selection ($2\ell^{\mathrm{sc}}$), and all other events with at least one lepton ($1\ell$). Events are placed in the $2\ell^{\mathrm{sc}}$ category if they contain exactly two signal leptons with same electric charge, and no additional candidate leptons. In order to reduce backgrounds containing a $Z$ boson decaying into electrons, where one electron has its charge misidentified, events with two electrons have to satisfy a $|m_{ee} - m_Z| > 10\,\mathrm{GeV}$ requirement. Events with at least three signal leptons, with one same-flavour pair satisfying $|m_{\ell\ell} - m_Z| < 10\,\mathrm{GeV}$ and exactly zero $b$-jets, are included as a separate subregion of the $2\ell^{\mathrm{sc}}$ category, in order to be used for background estimation. All events passing further selections, but which do not enter the $2\ell^{\mathrm{sc}}$ category, are assigned to the $1\ell$ category, including events containing more than one candidate lepton. The regions with seven or fewer jets and zero $b$-jets in the $1\ell$ category are further divided into three subregions. The first subregion is defined by selecting events with two same-flavour candidate leptons fulfilling an invariant-mass requirement, $|m_{\ell\ell} - m_Z| < 10\,\mathrm{GeV}$. The remaining events are divided into two subregions according to the electric charge of the highest-$p_{\mathrm{T}}$ lepton. This division in subregions provides additional information that allows more accurate constraints to be placed on the $W$+jets and $Z$+jets backgrounds.

The jet counting analysis is carried out with five jet-$p_{\mathrm{T}}$ thresholds to provide sensitivity to a broad range of possible signals. These thresholds are applied to all jets in the event and are at $p_{\mathrm{T}} = 20$, 40, 60, 80, and 100 GeV. The optimal jet $p_{\mathrm{T}}$ threshold depends on the model and particle masses being tested. The jet multiplicity is binned from a minimum of four jets to a maximum number ($N_{\mathrm{last}}$) that depends on the $p_{\mathrm{T}}$ threshold and the lepton category. In the $1\ell$ category the last bin corresponds to 15 or more jets for the 20 GeV threshold, and 12, 11, 10, and 8 or more jets for the other thresholds in increasing order. In the $2\ell^{\mathrm{sc}}$ category it corresponds to 10, 8, 7, 7, and 6 or more jets respectively. The highest jet-multiplicity bin for each $p_{\mathrm{T}}$ threshold is inclusive of larger jet multiplicities. For each jet multiplicity bin, there are five exclusive bins in the $b$-jet multiplicity (four exclusive bins from zero to three $b$-jets, with an additional inclusive four-or-more bin). The regions defined in the jet counting analysis are summarised in Table 3. For a given jet $p_{\mathrm{T}}$ threshold all regions are orthogonal and are analysed simultaneously. However, regions defined for different jet $p_{\mathrm{T}}$ thresholds can overlap. The number of bins used in the search ranges from 110 when considering the 20 GeV jet threshold, including the different subregions with zero $b$-jets, to 51 bins when considering the 100 GeV jet threshold. In this article, the notation $N_{j,b}^{\mathrm{process}}$ is used to denote the number of events predicted by the background fit model, with $j$ jets and $b$ $b$-jets for a given process, e.g. $N_{j,b}^{t\bar{t}\text{+jets}}$ for $t\bar{t}$+jets events. The quantity $N_{j}^{\mathrm{process}}$, referred to as a jet slice, is the number of events with $j$ jets for the considered physics process, and it is inclusive in the number of $b$-jets.

**Table 3** Summary of regions considered in the jet counting analysis. The notation N$b$ is used to indicate a requirement on the $b$-jet multiplicity. The highest jet multiplicity considered ($N_{\mathrm{last}}$) depends on the jet $p_{\mathrm{T}}$ threshold and the lepton category. In the $1\ell$ category it corresponds to 15, 12, 11, 10, and 8 jets for the different jet $p_{\mathrm{T}}$ thresholds in increasing order. In the $2\ell^{\mathrm{sc}}$ category it corresponds to 10, 8, 7, 7, and 6 jets respectively

| Lepton category | Jet multiplicity | Analysis regions |
|---|---|---|
| $1\ell$ category | 4…7 jets | $0b\ \ell^-$, $0b\ \ell^+$, $0b\ m_{\ell\ell}$, $1b$, $2b$, $3b$, $\geq 4b$ |
| | 8…$\geq N_{\mathrm{last}}^{1\ell}$ jets | $0b$, $1b$, $2b$, $3b$, $\geq 4b$ |
| $2\ell^{\mathrm{sc}}$ category | 4…$\geq N_{\mathrm{last}}^{2\ell^{\mathrm{sc}}}$ jets | $0b\ 3\ell$, $0b$, $1b$, $2b$, $3b$, $\geq 4b$ |

In order to improve the sensitivity of the search to the model with electroweakino production, the EWK analysis is introduced, which extends the jet counting analysis at the 20 GeV jet-$p_{\mathrm{T}}$ threshold. In the $1\ell$ category only, a separate NN discriminant is trained in each jet slice with eight or fewer jets, to discriminate the higgsino signal from the $t\bar{t}$ background. The full distribution of the NN output, binned in four even-width bins with approximately equal signal fraction, is fitted in each of the regions with at least one $b$-jet. The NN training is performed with the constraint that the NN output distribution of the $t\bar{t}$ background be invariant with respect to the $b$-jet multiplicity. This property is later exploited in order to estimate the background from data, as described in Sect. 7. The invariance of the NN output with respect to the $b$-jet multiplicity is achieved with distance-correlation training [122,123]. The NNs are trained on a mixture of higgsino samples as the signal, and $t\bar{t}$ as the only background.

The NN discriminant is constructed from a combination of low-level and high-level inputs. The low-level variables considered are the jet and leading-lepton momenta, the individual pseudo-continuous $b$-jet score [113] of all jets, and the $E_{\mathrm{T}}^{\mathrm{miss}}$ magnitude and direction. The high-level inputs correspond to the jet and $b$-jet multiplicity of the event, minimum distance between the leading lepton and any jet, scalar $p_{\mathrm{T}}$ sum of all jets ($H_{\mathrm{T}}$), scalar $p_{\mathrm{T}}$ sum of all $b$-jets, $m^{\mathrm{jets}}$ (defined below),

invariant mass of the three-jet system with highest system $p_{\mathrm{T}}$, and invariant mass of the 3j + $\ell$ + $\mathbf{p}^{\mathrm{miss}}$ system with highest system $p_{\mathrm{T}}$ (assuming that the $z$-component of the missing momentum $\mathbf{p}^{\mathrm{miss}}$ is zero). The two invariant mass variables attempt to reconstruct $\tilde{\chi}_1^{\pm} \to bbs$ and $\tilde{\chi}_{1,2}^0 \to tbs$ decays respectively. The $m^{\mathrm{jets}}$ variable is defined as follows. All the jets in the event are split into two groups, where both groups have to contain at least one jet. All possible combinations are tested, including those where the number of jets in each group is very different. For each grouping, the higher of the masses of the two groups is selected, and then the minimum across all possible groupings is taken. The $m^{\mathrm{jets}}$ distribution has an endpoint for signal events at $m(\tilde{\chi}_1^0)$ that is reached in events where all partons were reconstructed. For most events, the value is lower, since the lepton and $E_{\mathrm{T}}^{\mathrm{miss}}$ components are ignored. Backgrounds, however, do not show such an endpoint. In addition, the shape of this variable has only a weak dependence on the number of $b$-jets, which helps the NN to achieve separation while not introducing sensitivity to the $b$-jet multiplicity.

The inputs are connected to a single output node via two fully connected hidden layers of 100 neurons. The NNs are trained using PyTorch [124] and the Adam optimizer [125]. Events in the training dataset are sampled according to the inverse of the $b$-jet fraction (defined as the fraction of events in a given $b$-jet bin with respect to the total number of events in the jet slice) in order to flatten the $b$-jet spectrum. In order to achieve invariance of the NN output with respect to the $b$-jet multiplicity, the loss function of the training contains a term that penalizes a high distance correlation between the output and the $b$-jet multiplicity [123]. A hyperparameter $\lambda$ controls the weight of this penalty term, with a value $\lambda = 15$ which was optimized to achieve the highest sensitivity to the signal, accounting for both the separation and the systematic uncertainties derived from non-invariance of the NN, as described in Sect. 8. The invariance and separation achieved is shown in Fig. 2. After training, the variables ranked highest in importance (using the integrated gradients method described in Ref. [126]) are $H_{\mathrm{T}}$, the individual pseudo-continuous $b$-jet score of all jets, number of $b$-jets, invariant mass of the 3j + $\ell$ + $\mathbf{p}^{\mathrm{miss}}$ system with highest system $p_{\mathrm{T}}$, and $m^{\mathrm{jets}}$. The $b$-jet multiplicity is highly ranked despite the NN output being independent of it since it can be used to offset the effect from variables that are correlated with the number of $b$-jets such as $H_{\mathrm{T}}$.

In the $2\ell^{\mathrm{sc}}$ category, signal events are produced via the leptonic decays of two top quarks. However, the dominant backgrounds contain only one leptonic top decay, while the second lepton is a misidentified or non-prompt lepton, or originates from a $W$ boson that is not produced in a top decay ($t\bar{t}W$). This property is exploited by introducing an additional requirement of $m^{\ell j} < 155\,\mathrm{GeV}$, where the observable $m^{\ell j}$

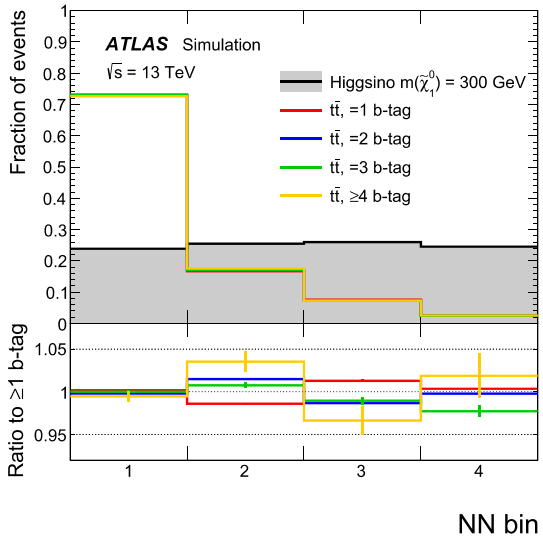


**Fig. 2** Output distribution of the NN discriminant in the six-jet slice, evaluated over a signal sample and $t\bar{t}$ background split into the different $b$-jet regions. The bottom panel shows the ratio of the NN output distribution for $t\bar{t}$ background in each $b$-jet region to the distribution in an inclusive region with at least one $b$-jet. The NN output distribution is invariant with respect to the number of $b$-jets in the selection, with differences per bin below 4%

is defined as $m^{\ell j} = \min_{a,b}\left\{\max\left(m(\ell_0, \mathrm{jet}_a), m(\ell_1, \mathrm{jet}_b)\right)\right\}$, with $\mathrm{jet}_a \neq \mathrm{jet}_b$, for all possible permutations of $\mathrm{jet}_a$ and $\mathrm{jet}_b$ taken from the four leading jets. No $b$-tag information is used in the selection of the jets, to avoid differences in the variable across the different $b$-tag regions. The signal has an endpoint in this variable at $m^{\ell j} = \sqrt{m_{\mathrm{top}}^2 - m_W^2} \approx 152\,\mathrm{GeV}$, while background events tend to have larger values.

In order to probe a specific BSM model, all the regions in both lepton categories are simultaneously fit to data to constrain the model, in what is called a model-dependent fit. Separate fits are performed for each analysis and jet $p_{\mathrm{T}}$ threshold, and the configuration providing the best expected sensitivity is used to probe the model. In the search for a generic BSM signal, dedicated discovery signal regions (SRs) are defined which could be populated by a signal, and where the SM contribution is expected to be small. The background in these SRs is estimated from a fit excluding the SR being tested, in what is called a model-independent fit. The discovery SR definitions used in the jet counting analysis are shown in Table 4.

Two additional discovery SRs are defined targeting a possible electroweakino signal making use of the EWK analysis. The first SR is defined in the $1\ell$ category, with exactly six jets with $p_{\mathrm{T}} > 20\,\mathrm{GeV}$, at least four $b$-jets, and a selection on the NN discriminant. The NN selection corresponds to a signal efficiency of 25% on the higgsino model with a mass of 300 GeV and a background rejection of 40 for the $t\bar{t}$ background, which corresponds to bin four in Fig. 2. The

**Table 4** The discovery signal regions used in jet counting and NN analyses, in the search for a generic BSM signal. For every jet $p_{\mathrm{T}}$ threshold, four signal regions are defined in the jet counting analysis, leading to a total of 20 discovery signal regions in the jet counting analysis. Two additional discovery signal regions are defined in the EWK analysis

| Jet counting analysis discovery SRs | | | |
|---|---|---|---|
| Jet $p_{\mathrm{T}}$ threshold | Number of jets $1\ell$ category | Number of jets $2\ell^{\mathrm{sc}}$ category | Number of $b$-jets |
| 20 GeV | $\geq 15$ | $\geq 10$ | $= 0, \geq 3$ |
| 40 GeV | $\geq 12$ | $\geq 8$ | $= 0, \geq 3$ |
| 60 GeV | $\geq 11$ | $\geq 7$ | $= 0, \geq 3$ |
| 80 GeV | $\geq 10$ | $\geq 7$ | $= 0, \geq 3$ |
| 100 GeV | $\geq 8$ | $\geq 6$ | $= 0, \geq 3$ |
| EWK analysis discovery SRs | | | |
| Jet $p_{\mathrm{T}}$ threshold | Lepton category and selection | Number of jets | Number of $b$-jets |
| 20 GeV | $1\ell$, NN bin 4 | $= 6$ | $\geq 4$ |
| 20 GeV | $2\ell^{\mathrm{sc}}$, $m^{\ell j} < 155$ GeV | $= 6$ | $\geq 3$ |

second SR is defined in the $2\ell^{\mathrm{sc}}$ category, with exactly six jets with $p_{\mathrm{T}} > 20$ GeV, and at least three $b$-jets. The discovery SR definitions used in the EWK analysis are also shown in Table 4.

The dominant background processes are $t\bar{t}$+jets and $W/Z$+jets in the $1\ell$ category, and $t\bar{t}W$, $t\bar{t}$ with a misidentified lepton, and diboson production in the $2\ell^{\mathrm{sc}}$ category. The estimation of the dominant backgrounds is carried out using a combined fit to the jet and $b$-jet multiplicity bins described above. For these backgrounds, the normalization per jet slice is derived using parameterized extrapolations from lower jet multiplicities. The $b$-jet multiplicity shape per jet slice is taken from MC simulation for the $W/Z$+jets and diboson backgrounds, whereas for background processes involving top quarks it is predicted from the data using a parameterized extrapolation based on observables at medium jet multiplicities. A separate likelihood fit is carried out for each jet $p_{\mathrm{T}}$ threshold, with the fit parameters of the background model determined separately in each fit. The assumptions used in the parameterization are validated using data and MC simulation.

## 7 Background estimation

The dominant background in the $1\ell$ category arises from $W/Z$+jets production in the zero $b$-jet regions, and top-quark pair production in the regions with at least one $b$-jet. In the $2\ell^{\mathrm{sc}}$ category the dominant background in the zero $b$-jet regions originates from diboson production with fully leptonic decays, in particular $WZ$ where one lepton from the $Z$ boson decay is lost. In the regions with at least one $b$-jet the main backgrounds are the associated production of a top-quark pair and a $W$ boson, dileptonic $t\bar{t}$ where an electron has its charge misidentified, and semileptonic $t\bar{t}$ with a jet misidentified as a lepton, or with a non-prompt lepton. These three background components are merged and labelled as $t\bar{t}X^{\mathrm{sc}}$, and estimated simultaneously.

The theoretical modelling of all these backgrounds at high jet multiplicity suffers from large uncertainties, so they are estimated from the data by extrapolating the jet and $b$-jet multiplicity distributions extracted at moderate jet multiplicities to the high jet multiplicities of the search regions.

### 7.1 Jet multiplicity prediction

A data-driven approach is used to estimate the contribution of the main backgrounds in each jet multiplicity slice. The estimate of the normalization relies on assuming a functional form to describe the evolution of the number of background events for process $X$ as a function of the jet multiplicity, $r^X(j) \equiv N^X_{j+1}/N^X_j$.

Above a certain number of jets, $r(j)$ is assumed to be constant, implying a fixed probability of additional jet radiation, referred to as 'staircase scaling' [127–130]. This behaviour has been observed in $W/Z$+jets by the ATLAS [131,132] and CMS [133] collaborations. For lower jet multiplicities, a different scaling is expected with $r(j) = k/(j+1)$ where $k$ is a constant, referred to as 'Poisson scaling' [130]. The transition point between these scaling behaviours depends on the jet kinematic selections.

For the kinematic phase space relevant for this search, a combination of the two scalings is found to describe the data in dedicated validation regions (described later in this section), as well as in simulated MC samples with an integrated luminosity much larger than that of the data. This combined scaling is parameterized as

$$r^X(j) = c_0^X + c_1^X/(j + c_2^X),$$

where $c_0^X$, $c_1^X$ and $c_2^X$ are process-dependent constants that are extracted from the data. The $c_2^X$ parameter is introduced to take into account the ambiguity in the counting of jets originating from the decay products of the process $X$ and the additional jets. The parameter is fixed to $c_2^X = 1$ in the estimation of $W$+jets, $Z$+jets, and fully leptonic diboson events, as there is no ambiguity in the counting of jets for these processes. However, $c_2^X$ is a free parameter in the estimation of backgrounds containing top quarks, where the jet counting ambiguity remains.

Studies using simulated event samples, both at generator level and after event reconstruction, demonstrate that the flexibility of this parameterization is also able to absorb reconstruction effects related to the decrease in event reconstruction efficiency with increasing jet multiplicity, which are mainly due to the lepton–jet overlap and lepton isolation requirements.

The number of background events from process $X$ in the $j$ jets slice is then parameterized as follows:

$$N_j^X = N_4^X \cdot \prod_{j'=4}^{j'=j-1} r^X(j'),$$

where $N_4^X$ is a free parameter for the absolute normalization in four-jet events. Since the last jet-multiplicity bin used in the analysis is inclusive in the number of jets, the model is used to predict this by iterating to higher jet multiplicities and summing the contribution for each jet multiplicity above the maximum used in the analysis. The four parameters per process, i.e. $N_4^X$, $c_0^X$, $c_1^X$, and $c_2^X$ (if not fixed to one), are allowed to float in the fit, and are therefore extracted from the data along with the other background contributions. Studies in data and MC simulation indicate that the $c_0^X$ and $c_1^X$ parameters for $W$+jets and $Z$+jets are statistically compatible, and are therefore combined into common parameters $c_0^{W/Z\text{+jets}}$ and $c_1^{W/Z\text{+jets}}$. The normalization parameters $N_4^{W\text{+jets}}$ and $N_4^{Z\text{+jets}}$ are kept independent. The $c_i^X$ parameters are independent among the rest of the backgrounds, including $t\bar{t}$ in the $1\ell$ category and $t\bar{t}X^{\text{sc}}$ in the $2\ell^{\text{sc}}$ category.

The jet-scaling assumption is validated in data, using $\gamma$+jets and dileptonic $t\bar{t}$ events. The $\gamma$+jets events are selected using a high-$p_{\text{T}}$ photon trigger, and a high-$p_{\text{T}}$ signal photon is required in the event selection. The dileptonic $t\bar{t}$ data sample is selected by requiring an electron candidate and a muon candidate in the event, with at least two jets of which at least one is a $b$-jet, and the small background predicted by MC simulation is subtracted. The possible signal contamination in this sample is negligible as the selection is inclusive over the number of $b$-jets. In this sample, the scaling behaviour can be tested for up to 13 jets, which corresponds to 15 jets for a semileptonic $t\bar{t}$+jets sample. Simulated $W$+jets, $Z$+jets, semileptonic $t\bar{t}$ (both the nominal sample and the alternative samples described in Sect. 4), and $t\bar{t}X^{\text{sc}}$ samples are also found to be consistent with the jets-scaling assumption.

Figure 3 shows the $r(j)$ ratio for various processes used to validate the jet-scaling parameterization. Each panel shows the $r(j)$ ratio for data or MC simulation with the fitted parameterization overlaid as a line.

### 7.2 Prediction of $b$-jet multiplicity

The number of background events from process $X$ in a given jet and $b$-jet multiplicity region can be expressed as follows:

$$N_{j,b}^X = f_{j,b}^X \cdot N_j^X$$

where $f_{j,b}^X$ is the fraction of events from process $X$ with $b$ number of $b$-jets in the $j$ jet slice, and satisfies $\sum_{b=0}^{4} f_{j,b}^X = 1$. A data-driven model is used to estimate the $b$-jet fraction in background processes containing top quarks. The basic concept of this model is based on the extraction of an initial template of the $b$-jet fraction distribution in events with four jets and the parameterization of the evolution of this template to higher jet multiplicities. Each jet slice is constrained in the fit as discussed later in this section. The $b$-jet fractions for $W$+jets, $Z$+jets and diboson backgrounds are taken from MC simulation.

The extrapolation of the $b$-jet multiplicity distribution to higher jet multiplicities starts from the assumption that the difference between the $b$-jet multiplicity distribution in events with $j$ and $j+1$ jets arises mainly from the production of additional jets, and can be described by a fixed probability that the additional jet is a $b$-jet. Given the small mis-tag rate, this probability is dominated by the probability that the additional jet is a heavy-flavour jet which is $b$-tagged. In order to account for acceptance effects due to the different kinematics in events with high jet multiplicity, the probability of further $b$-tagged jets entering the acceptance is also taken into account. The extrapolation to one additional jet can be parameterized as:

$$f_{(j+1),b} = f_{j,b} \cdot x_0 + f_{j,(b-1)} \cdot x_1 + f_{j,(b-2)} \cdot x_2, \qquad (1)$$

where the parameters $x_i$ describe the probability of one additional jet to be either not $b$-tagged ($x_0$), $b$-tagged ($x_1$), or $b$-tagged and causing a second jet to be $b$-tagged ($x_2$). The latter is dominated by cases where the extra jet influences the event kinematics such that a second $b$-jet, previously not $b$-tagged, becomes $b$-tagged. This parameter aims to model the increase in $b$-tagging efficiency with jet $p_{\text{T}}$. Given that the $x_i$ parameters describe probabilities, the sum $\sum_i x_i$ is normalized to unity. Terms with a negative number of $b$-tagged jets ($f_{j,b<0}$) are set to zero. Subsequent application of this parameterization produces a $b$-jet template for arbitrarily high jet multiplicities.

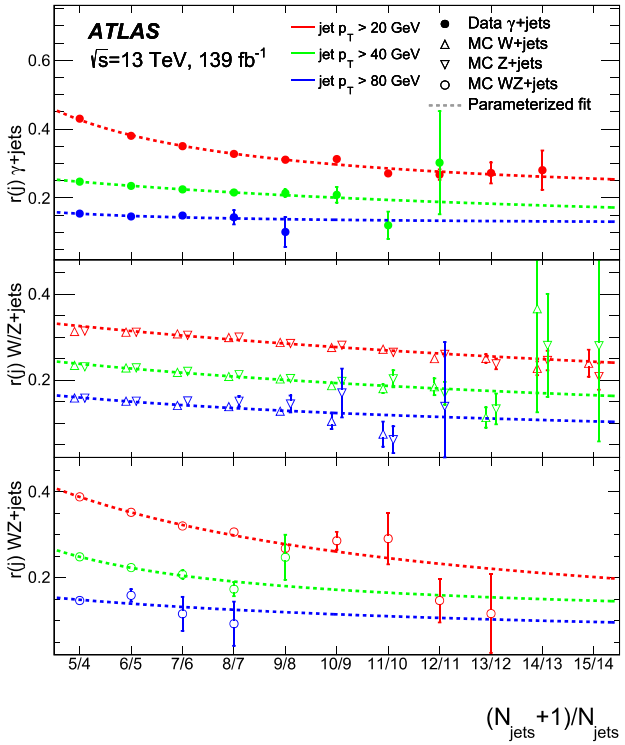


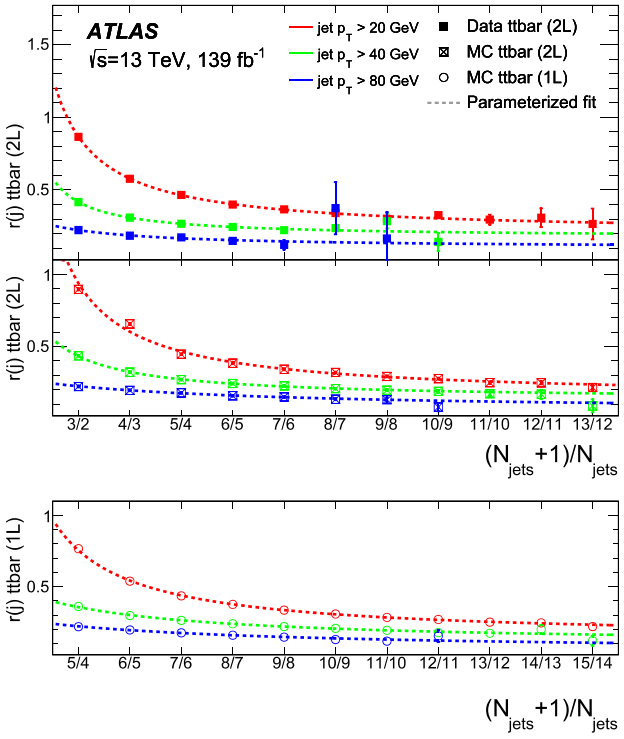


**Fig. 3** The ratio of the number of events with $(j+1)$ jets to the number with $j$ jets in various event samples (details in the legend), used to validate the jet-scaling parameterization. In the MC samples of $W/Z/WZ$+jets the vector bosons are forced to decay to leptons. Each panel shows the ratio for data or MC simulation with the fitted parameterization overlaid as a dashed line. The uncertainties shown are statistical

Studies based on MC simulated events with sample sizes corresponding to equivalent luminosities much larger than the collected dataset, as well as studies using fully efficient generator-level $b$-tagging, indicate the necessity to add a fit parameter that allows for correlated production of two $b$-jets as may be expected with $b$-jet production from gluon splitting. This is implemented by changing the evolution described in Eq. (1) such that any term with $x_1 \cdot x_1$ is replaced by $x_1 \cdot x_1 \cdot \rho_{11}$, where $\rho_{11}$ describes the correlated production of two $b$-jets. The value of $\rho_{11}$ is a free parameter and is determined in the fit.

The initial $b$-jet multiplicity template is extracted from data events with four jets after subtracting all non-$t\bar{t}$ background processes, and is denoted by $f_{4,b}$ and scaled by the absolute normalization $N_4^{t\bar{t}+\text{jets}}$ in order to obtain the model in the four-jet bin:

$$N_{4,b}^{t\bar{t}+\text{jets}} = N_4^{t\bar{t}+\text{jets}} \cdot f_{4,b},$$

where the sum of $f_{4,b}$ over the four $b$-jet bins is normalized to unity. The zero $b$-jet component of the initial $t\bar{t}$ template, exhibits an anti-correlation with the absolute $W$+jets normalization, which is extracted in the same region. The division into subregions separated in leading-lepton charge, detailed in Sect. 6, provides a handle to extract the absolute $W$+jets normalization, due to the charge asymmetry in $W^{\pm}$ production. The remaining anti-correlation does not affect the total background estimate. For these regions, the $t\bar{t}$+jets process is assumed to be charge symmetric and the model is simply split into two halves for these bins.

The model described above is based on the assumption that any change in the $b$-jet multiplicity distribution is due to additional jet radiation with a certain probability to lead to $b$-jets. There is, however, also a small increase in the acceptance for $b$-jets produced in the decay of the $t\bar{t}$ system, when increasing the jet multiplicity, due to the higher jet momentum on average. The effect amounts to up to 5% in the one- and two-$b$-jet bins for high jet multiplicities, and is taken into account using a correction to the initial template extracted from simulated $t\bar{t}$ events.

The parameters that model the production of additional $b$-jets $(x_i, \rho_{11})$ are correlated in the $1\ell$ and $2\ell^{\text{sc}}$ categories. The initial $b$-jet multiplicity parameters $(f_{4,b})$, and the acceptance correction to the initial template are independent in each lepton category.

### 7.3 Neural network template prediction

The NN is only introduced in regions with at least one $b$-jet, where the dominant background is $t\bar{t}$ production. The NN output distribution is obtained from MC simulation for

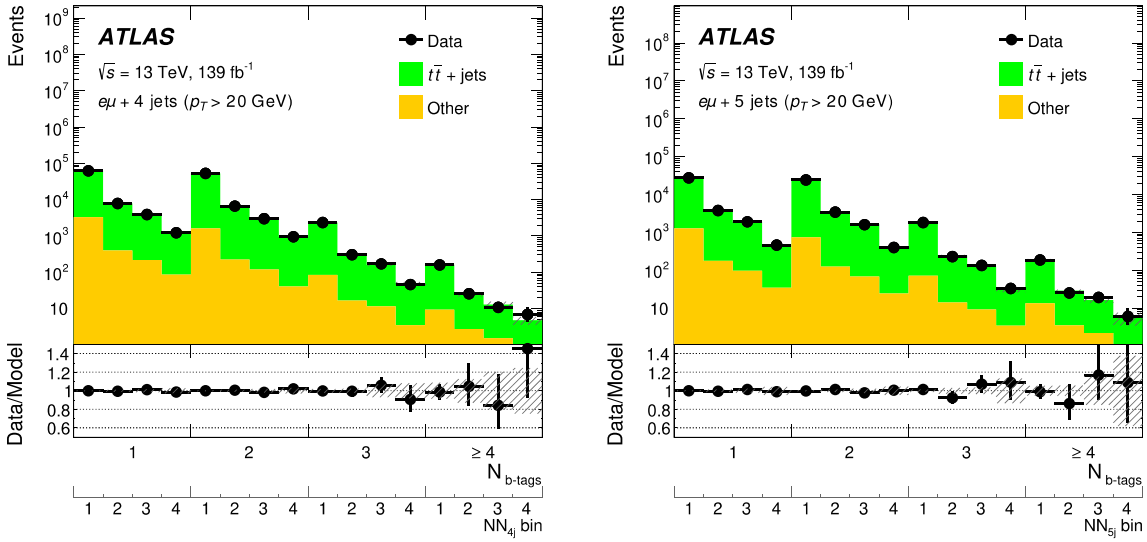


**Fig. 4** Observed data and the corresponding background estimation in regions with one electron, one muon, and four jets (left) or five jets (right). All uncertainties, which may be correlated across the bins, are included in the error bands (shaded regions). The shape of the NN template for the $t\bar{t}$ background is required to be identical in all $b$-jet regions. Good agreement between the data and estimated background confirms the invariance of the NN output with respect to the $b$-jet region

all the subdominant backgrounds. A data-driven method is developed in order to predict the NN output distribution for $t\bar{t}$ background events, making use of the invariance of the NN output with respect to the number of $b$-jets in the event. The $t\bar{t}$ background in a given bin of the NN output is parameterized as:

$$N_{j,b,i}^{t\bar{t}+\text{jets}} = n_{j,i} \cdot N_{j,b}$$

where $n_{j,i}$ is the fraction of $t\bar{t}$ events in bin $i$ of the NN output in the $j$ jet slice, and is independent of the $b$-jet region. The fractions in each jet slice are free parameters and are fitted simultaneously to all $b$-jet regions, constrained by the sum $\sum_i n_j^i$ being normalized to unity. Given the large statistical power of the one- and two-$b$-jet regions, the fitted NN templates are determined in these regions and not biased by a possible signal entering the high $b$-jet regions.

This method relies on the invariance of the NN output with respect to the number of $b$-jets. This property is validated in large samples of MC simulated $t\bar{t}$ events, including the alternative samples described in Sect. 4. The invariance is also confirmed in data by using a pure sample of dileptonic $t\bar{t}$ events, with a selection requiring one electron, one muon, and at least one $b$-jet. The signal contamination in this dataset is at most 2% in the last NN bin of the 4 b-tag region. The only process that is not negligible given this selection is $\tilde{\chi}_1^0\tilde{\chi}_2^0$ production, which has a lower cross-section than the $\tilde{\chi}_1^\pm\tilde{\chi}_{1,2}^0$ process, that contributes most to the 1-lepton selection. Figure 4 shows that good agreement between data and estimated background is observed in this region, confirming in data the invariance of the NN output with respect to the $b$-jet region.

### 7.4 Fake and non-prompt lepton background

The contribution from events with a fake or non-prompt (FNP) lepton (such as hadrons misidentified as leptons, leptons originating from the decay of heavy-flavour hadrons, and electrons from photon conversions), constitutes a minor but non-negligible background.

The multi-jet background in the $1\ell$ category is estimated from the data with a matrix method similar to that described in Ref. [134]. In this method, two types of lepton identification criteria are defined: *'tight'*, corresponding to the default signal lepton criteria described in Sect. 5, and *'loose'*, corresponding to candidate leptons after overlap removal. The matrix method relates the numbers of observed events in which a *loose* lepton candidate does or does not satisfy the *tight* selection criteria. The probability for *loose* prompt leptons to satisfy the *tight* selection criteria is obtained using a $Z \to \ell\ell$ data sample and is modelled as a function of the lepton $p_{\text{T}}$. The probability for *loose* FNP leptons to satisfy the *tight* selection criteria is determined from a data control region enriched in non-prompt leptons that requires a *loose* lepton, multiple jets, low $E_{\text{T}}^{\text{miss}}$ [135,136], and low transverse mass.[4] This data sample is recorded with prescaled lepton triggers without an isolation requirement. The efficiencies

[4] The transverse mass of the lepton–$E_{\text{T}}^{\text{miss}}$ system is defined as: $m_{\text{T}} = \sqrt{2p_{\text{T}}^{\ell}E_{\text{T}}^{\text{miss}}(1-\cos(\Delta\phi(\ell, E_{\text{T}}^{\text{miss}})))}$.

are measured as a function of lepton candidate $p_{\mathrm{T}}$ after subtracting the contribution from prompt-lepton processes, and are assumed to be independent of the jet multiplicity.[5]

In the $2\ell^{\mathrm{sc}}$ category, the background from FNP leptons in association with a top-quark pair is estimated as part of the $t\bar{t}X^{\mathrm{sc}}$ background as described above. Other contributions from FNP leptons constitute less than 10% of the total background in the zero-$b$-jet bin, with a negligible contribution in the $b$-jet regions, and are taken from MC simulation. The estimation is validated in a dedicated validation region requiring zero $b$-jets, two same-flavour leptons satisfying $|m_{\ell\ell} - m_Z| < 10\,\mathrm{GeV}$, and an additional candidate lepton failing the signal requirement. This region is dominated by $Z$ boson events containing a FNP lepton, and is used to verify the modelling of FNP leptons in the MC simulation.

### 7.5 Minor backgrounds

The minor background contributions from single-top production, $t\bar{t}H$, and SM four-top-quark production are estimated using MC simulation. In the $1\ell$ category the diboson and $t\bar{t}V$ backgrounds are also estimated from MC simulation, while the estimates are both data-driven ($t\bar{t}V$ as part of the $t\bar{t}X^{\mathrm{sc}}$ background) in the $2\ell^{\mathrm{sc}}$ category. In all but the highest jet slices considered, the sum of these backgrounds contributes no more than 10% of the SM expectation in any of the $b$-jet bins; for the highest jet slices this can rise to 35%.

### 7.6 Fit configuration and validation

Two different fit configurations are used in the search. When testing a specific BSM model the model-dependent fit set-up is used, where for each jet $p_{\mathrm{T}}$ threshold all the regions in both lepton categories are simultaneously fit to data to constrain the model. The expected signal contribution in all bins is taken into account, including bins with low jet or $b$-jet multiplicity. The jet counting analysis is used to constrain the models with strong production and the EWK analysis for the models with electroweakino production. Separate fits are performed for each jet $p_{\mathrm{T}}$ threshold, and the threshold with best expected sensitivity for the given signal mass point is used to set limits. In the search for a generic BSM signal in a particular SR the model-independent fit set-up is used, where for each jet $p_{\mathrm{T}}$ threshold the simultaneous fit includes all regions except the SR being tested. Possible signal leakage to the control regions can produce a bias in the background estimation, leading to conservative limits. Such limits have hence been obtained assuming negligible signal contributions in regions outside of the SR. Signal processes with final states that the search is targeting generally have negligible leakage into these regions, as is the case for the benchmark models considered.

The number of freely floating parameters in the background model is 26 in the jet counting analysis, and 41 in the EWK analysis. The different parameters for each background are summarized in Table 5. The number of fitted bins varies between 51 and 110 in the jet counting analysis, depending on the jet $p_{\mathrm{T}}$ threshold used, and is 170 in the EWK analysis, leading to an over-constrained system in all cases.

The fit set-up was extensively tested using MC simulated events, and was demonstrated to give excellent agreement on a background-only dataset, and a negligible bias in the fitted signal yields. This level of agreement is seen both in the cases where the background-only distributions are fit, and when a signal is injected into the fitted data.

## 8 Systematic uncertainties

The dominant backgrounds are estimated from the data without the use of MC simulation, and therefore the main systematic uncertainties related to the estimation of these backgrounds arise from the assumptions made in the construction of the parameterized model. Uncertainties related to the theoretical modelling of the specific processes and due to the modelling of the detector response in simulated events are only relevant for the minor backgrounds, which are taken from MC simulation, and for the estimates of the signal yields after selections.

For the $W/Z$+jets background estimation, the uncertainty related to the assumed jet scaling is taken from studies of this behaviour in $W$+jets and $Z$+jets MC simulation, as well as in $\gamma$+jets data control regions chosen to be kinematically similar to the search selection. Deviations from the assumed scaling behaviour are assigned as a systematic uncertainty, uncorrelated in each jet slice. In the case of no deviation the statistical precision of the validation is assigned. The uncertainty in the lower jet multiplicities is at the percent level for all jet $p_{\mathrm{T}}$ thresholds, and up to 50% in the highest jet multiplicities, driven by the statistical precision of the method. The uncertainty related to the parameterization of the jet multiplicity of the $t\bar{t}$ background is determined with the same strategy, and is derived from MC simulation closure tests (including alternative MC generators), as well as dileptonic $t\bar{t}$ control regions in data. No evidence of a deviation from the assumed scaling behaviour is seen, and the statistical precision of the closure in data is used as an uncertainty.

The expected uncertainty of the charge asymmetry in $W$+jets production is 3%–5% from PDF variations [137], but in the seven-jet region the uncertainty is dominated by the

[5] To minimize the dependence on the number of jets, the event selection considers only the highest-$p_{\mathrm{T}}$ candidate lepton when checking the more stringent identification and isolation criteria of the signal lepton definitions.

**Table 5** Summary of all the free floating parameters in the background model. There are a total of 26 such parameters in the jet counting analysis and 41 in the EWK analysis

| Parameters | $t\bar{t}$ +jets | $t\bar{t}X^{\mathrm{sc}}$ | $W$+jets | $Z$+jets | $VV$+jets | Constraints |
|---|---|---|---|---|---|---|
| Normalization | $N_4^{t\bar{t}}$ | $N_4^{t\bar{t}X^{\mathrm{sc}}}$ | $N_4^W$ | $N_4^Z$ | $N_4^{VV}$ | – |
| Jet scaling, $i \in \{0, 1, 2\}$ | $c_i^{t\bar{t}}$ | $c_i^{t\bar{t}X^{\mathrm{sc}}}$ | $c_i^{W/Z}$ | | $c_i^{VV}$ | $c_2^{W/Z} = c_2^{VV} = 1$ |
| Initial $b$-jet fractions, $i \in \{0 \ldots 4\}$ | $f_{4,i}^{t\bar{t}}$ | $f_{4,i}^{t\bar{t}X^{\mathrm{sc}}}$ | – | – | – | $\sum_i f_{4,i} = 1$ |
| Extra heavy-flavour jets, $i \in \{0, 1, 2\}$ | $x_i$, $\rho_{11}$ | | – | – | – | $\sum_i x_i = 1$ |
| NN shape, $i \in \{1 \ldots 4\}$, $j \in \{4 \ldots 8\}$ | $n_{j,i}$ | – | – | – | – | $\sum_i n_{j,i} = 1$ |

limited number of MC events (up to 10% for the 80 GeV jet-$p_{\mathrm{T}}$ threshold). The uncertainty in the shape of the $b$-jet multiplicity distribution in $W$+jets, $Z$+jets, and diboson events is derived by comparing different MC generator configurations (e.g. varying the renormalization and factorization scale and the parton-shower model parameters). It is seen to grow as a function of jet multiplicity and is about 50% for events with five jets, after which the MC statistical uncertainty becomes very large. A conservative uncertainty of 50% per additional heavy-flavour quark that is generated is assigned to the fractional contribution from $V(V)$+$b$ and $V(V)$+$c$ events, uncorrelated among the three backgrounds. This uncertainty has a negligible impact on the final result as the background from $W/Z$ boson or diboson production with additional heavy-flavour jets is small compared to that from top-quark pair production. In addition, the uncertainties related to the $b$-tagging efficiency and mis-tag rate are taken into account in the uncertainty in the $W/Z$+jets $b$-jet template.

The $b$-jet fraction estimation method exhibits good closure in studies based on MC simulated events with sample sizes corresponding to integrated luminosities much larger than that of the collected dataset, as well as studies using fully efficient generator-level $b$-tagging, so no systematic uncertainty related to these studies is assigned. A small uncertainty related to the acceptance correction for the initial $b$-jet multiplicity template is derived by varying the MC generator configuration for the $t\bar{t}$ sample used to estimate the correction. This leads to a 3% uncertainty in the correction, and has no significant effect on the final uncertainty.

The prediction of the NN template in $t\bar{t}$ events relies on the invariance of the NN output with respect to the number of $b$-jets in the event. This assumption is tested in MC simulation (both the nominal sample and the alternative samples described in Sect. 4), and seen to hold within 5% in the five-jet and six-jet slices, where the best signal-to-background ratio is expected, and within 10% in the rest. The largest deviation from the $b$-jet-inclusive template that is seen per bin across $b$-jet regions is assigned as an uncorrelated uncertainty in each bin and ranges from 1% to 10%.

The dominant uncertainty in the multi-jet background estimate arises from the number of data events in the control regions. An uncertainty in the subtraction of electroweak backgrounds from these control regions is estimated at 20% of the expected yield of these background processes. Additional uncertainties are assessed to cover the possible dependencies of the prompt and FNP lepton efficiencies [134] on variables other than lepton $p_{\mathrm{T}}$ (for example the dependence on the number of jets in the event). The total uncertainty in the multi-jet background yields is about 50%.

The uncertainty in the expected yields of the minor backgrounds includes theoretical uncertainties in the cross-sections and in the modelling of the kinematics by the MC generator, as well as experimental uncertainties related to the modelling of the detector response in the simulation. The uncertainties assigned to cover the theoretical estimate of these backgrounds in the relevant regions are 50% for diboson in the $1\ell$ category and single top-quark production, and 30% for $t\bar{t}V/H$ production. An additional uncertainty of 50% is assigned to the contribution from $t\bar{t}V + b$ and $t\bar{t}V + c$ events. These uncertainties are conservative estimates based on the impact seen from renormalization and factorization scale variations, PDF variations, and comparisons with samples with an alternative parton-shower model.

Uncertainties in the modelling of $t\bar{t}t\bar{t}$ are assigned from renormalization and factorization scale variations, as well as from a comparison with simulated samples with an alternative parton-shower model. An uncertainty of 100% is assigned to the cross-section to cover the difference between the predicted and measured cross-sections [34]. Using instead the central value and uncertainty from the ATLAS measurement leads to a 1% decrease in expected sensitivity.

The final uncertainty in the background estimate in the SRs is dominated by the uncertainty in the fitted model parameter values, which stems from the statistical uncertainty of the data events in the different jet slices. Systematic uncertainties do not contribute significantly in the jet counting analysis, and cause only a 1% loss in sensitivity. The leading systematic uncertainty in the EWK analysis is related to the NN

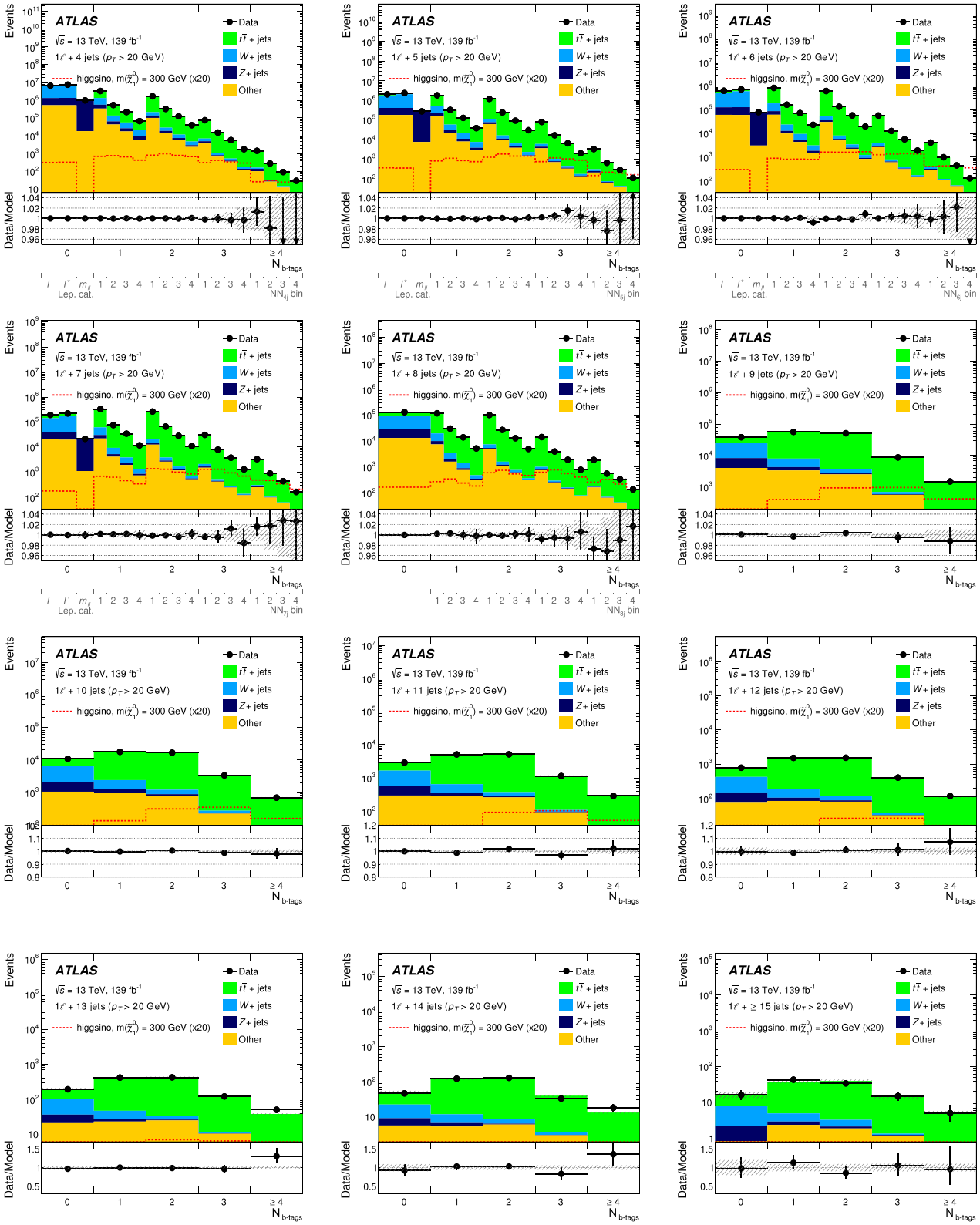


**Fig. 5** The observed data event yields and the corresponding estimates for the backgrounds in the different $b$-jet multiplicity bins for the 20 GeV jet-$p_{\mathrm{T}}$ threshold regions defined for the EWK analysis in the $1\ell$ category. The background shown is estimated by including all bins in the fit. All uncertainties, which may be correlated across the bins, are included in the error bands (shaded regions). The expected signal distribution for the higgsino LSP $m(\tilde{\chi}_1^0) = 300$ GeV hypothesis normalized to 20 times its expected cross-section is also overlaid

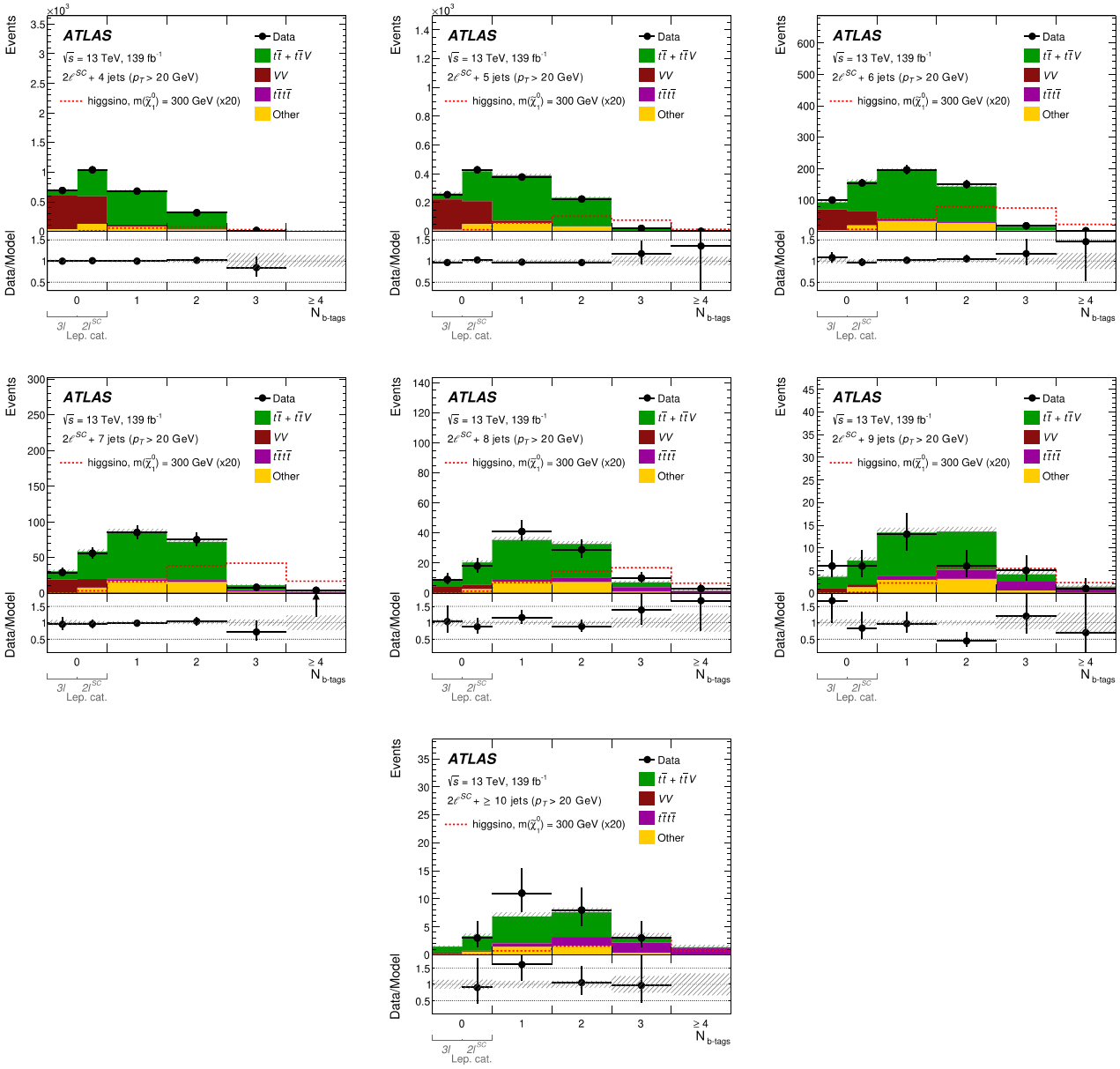


**Fig. 6** The observed data event yields and the corresponding estimates for the backgrounds in the different $b$-jet multiplicity bins for the 20 GeV jet-$p_{\mathrm{T}}$ threshold regions defined for the EWK analysis in the $2\ell^{\mathrm{sc}}$ category. The background shown is estimated by including all bins in the fit. All uncertainties, which may be correlated across the bins, are included in the error bands (shaded regions). The expected signal distribution for the higgsino LSP $m(\tilde{\chi}_1^0) = 300$ GeV hypothesis normalized to 20 times its expected cross-section is also overlaid

invariance assumption and causes a 30% loss in sensitivity, while other systematic uncertainties are subdominant.

The uncertainties assigned to the expected signal yields for the SUSY benchmark processes considered include the experimental uncertainties related to the detector modelling, which are dominated by the modelling of the jet energy scale, and the $b$-tagging efficiencies and mis-tagging rates. For example, for a signal model with four $b$-quarks, the $b$-tagging uncertainties are $\approx 10\%$, and the jet-related uncertainties are typically $\approx 5\%$. The uncertainty in the signal cross-sections used is discussed in Sect. 4. The uncertainty in the signal yields related to the modelling of additional jet radiation is studied by varying the factorization, renormalization, and jet-matching scales as well as the parton-shower tune in the simulation. The corresponding uncertainty is small for most of the signal parameter space, but is as large as 30% for very light or very heavy LSPs, where the contribution from additional jet radiation is relevant. The difference between fast

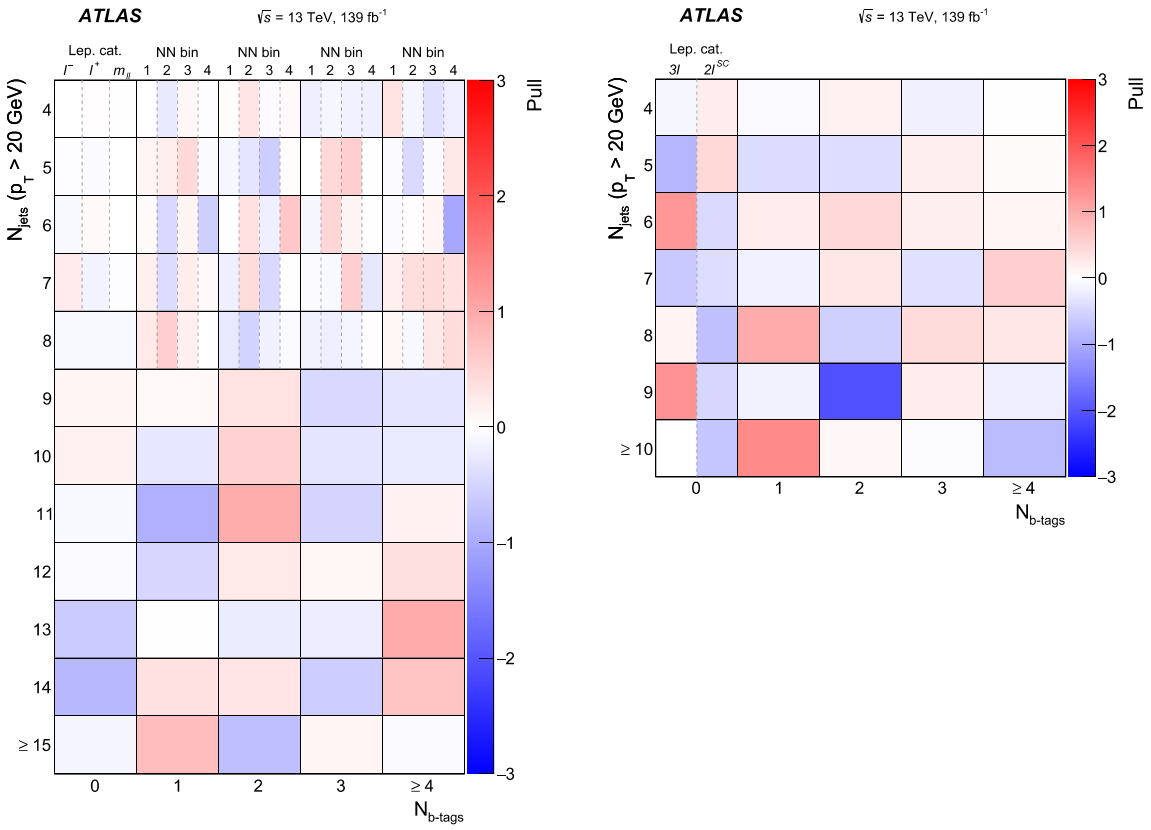


**Fig. 7** The observed pulls in all the regions considered in the EWK analysis, in the $1\ell$ category (left) and the $2\ell^{\text{SC}}$ category (right). The pull is defined as the difference between the observed number of events and the total expected number of events determined by the fit divided by the total uncertainty. The total uncertainty is the sum in quadrature of the statistical error of the observed data and the uncertainty in the predicted background

and full simulation is evaluated for selected signal points. The jet multiplicity, $b$-jet multiplicity, and NN output distributions are found to be statistically compatible, so no additional uncertainty is considered due to the usage of fast simulation.

## 9 Results

Results are provided both as model-independent limits on the contribution from BSM physics to the dedicated SRs, and in the context of the five SUSY benchmark models discussed in Sect. 2. As described in Sect. 7.6, two different fit configurations are used for the two sets of results. In both cases, the profile likelihood-ratio test [138] is used to establish 95% confidence intervals using the $\text{CL}_\text{s}$ prescription [139]. The parameter of interest is the signal strength, defined as the cross-section of the hypothetical contribution from physics beyond the SM in units of the cross-section of the benchmark model.

The $b$-jet multiplicity distributions are shown in Figs. 5 and 6 for the EWK analysis defined with a 20 GeV jet-$p_\text{T}$ threshold, for the $1\ell$ and $2\ell^{\text{SC}}$ categories respectively. Figure 7 summarizes the observed pulls in all analysis regions, defined as the difference between the observed number of events and the total expected number of events determined by the fit divided by the total uncertainty. The total uncertainty is the sum in quadrature of the statistical error of the observed data and the uncertainty in the predicted background. The pulls follow a gaussian distribution centered at zero. Figure 8 shows the $b$-jet multiplicity distribution for the last jet-multiplicity bin defined for each of the jet $p_\text{T}$ thresholds, in both the $1\ell$ and $2\ell^{\text{SC}}$ categories, which contains the discovery SRs at zero $b$-jet and high $b$-jet multiplicity. The likelihood fit is configured using the model-dependent configuration where all bins are input to the fit, and fixing the signal-strength parameter to zero.

### 9.1 Model-independent results

The observed data event yields and the corresponding estimates for the backgrounds in the discovery SRs defined for the $1\ell$ and $2\ell^{\text{SC}}$ categories are shown in Tables 6 and 7. For each SR a fit is performed to predict the background using the model-independent set-up, which excludes the SR

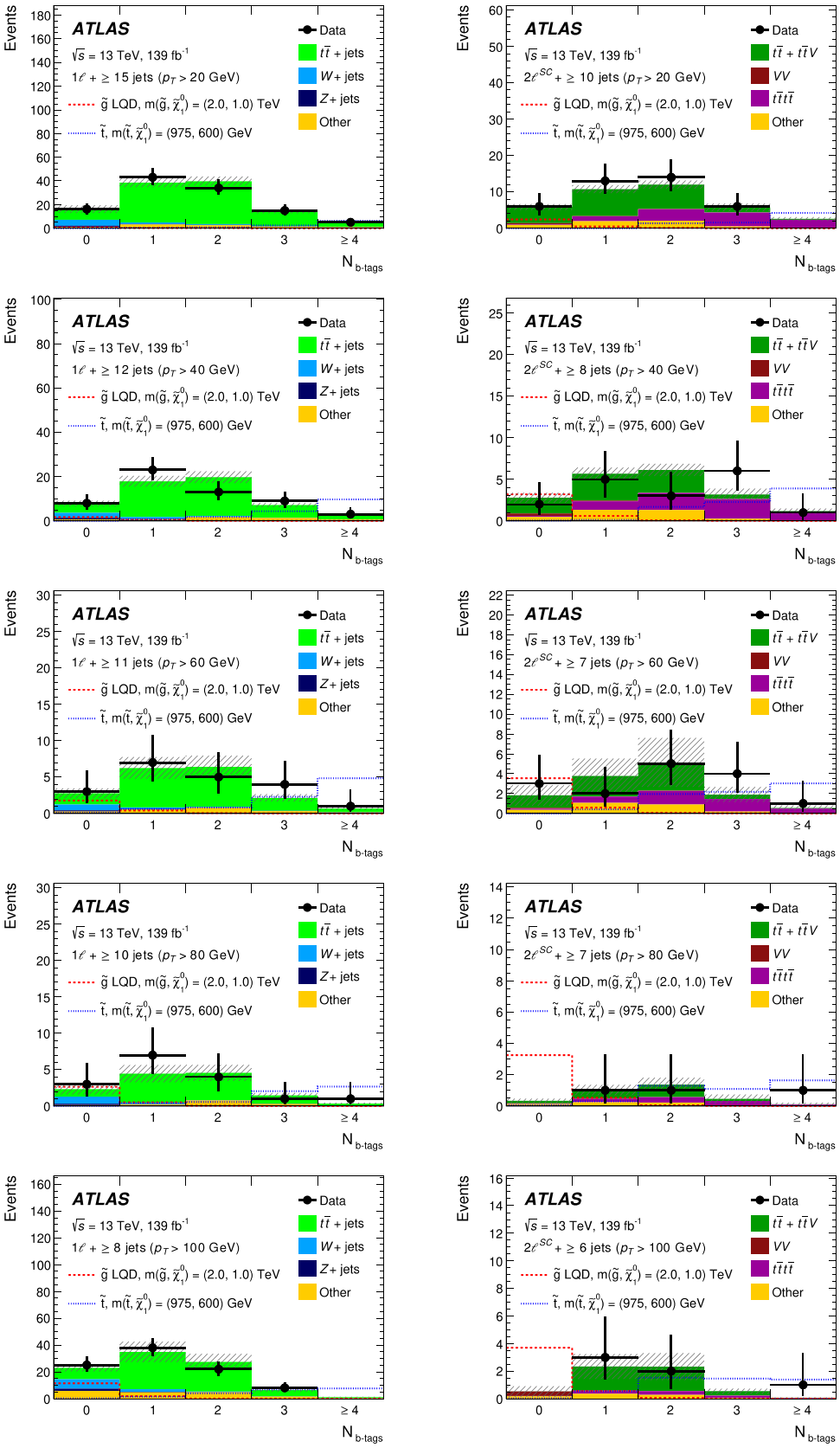


**Fig. 8** The observed data event yields and the corresponding estimates for the backgrounds in the different last jet-multiplicity bins defined for the $1\ell$ (left) and $2\ell^{\mathrm{sc}}$ (right) categories. The background shown is estimated by including all bins in the fit. All uncertainties, which may be correlated across the bins, are included in the error bands (shaded regions). Hypothetical contributions from representative RPV SUSY scenarios are displayed as dashed and dotted lines

**Table 6** Data event yields compared with the expected contributions from relevant background sources, in the discovery signal regions defined for the $1\ell$ category. The $p_0$-value, and corresponding significance (Z), as well as the observed and expected 95% CL model-independent upper limits on the product of cross-section, acceptance and efficiency (in ab) are also shown ($\sigma^{\text{excl}}$). In SRs with a deficit of data compared to the background prediction the $p_0$-value is capped at 0.5. The parameters of the background model are determined in a fit to a reduced set of bins, corresponding to the model-independent fit discussed in the text

| Jet $p_{\text{T}}$ threshold | Selection †=NN bin 4 | Total background | Data | $p_0$ | Z | $\sigma^{\text{excl}}$ obs. [ab] | $\sigma^{\text{excl}}$ exp. [ab] |
|---|---|---|---|---|---|---|---|
| 20 GeV | $= 6j, \geq 4b$,† | $145 \pm 6$ | 126 | 0.5 | 0 | 130 | $200^{+80}_{-60}$ |
| | $\geq 15j, = 0b$ | $16.3 \pm 5.2$ | 16 | 0.5 | 0 | 100 | $100^{+40}_{-30}$ |
| | $\geq 15j, \geq 3b$ | $17.0 \pm 1.9$ | 20 | 0.26 | 0.7 | 92 | $74^{+29}_{-21}$ |
| 40 GeV | $\geq 12j, = 0b$ | $7.8 \pm 1.5$ | 8 | 0.47 | 0.1 | 55 | $53^{+21}_{-15}$ |
| | $\geq 12j, \geq 3b$ | $8.6 \pm 1.1$ | 12 | 0.17 | 0.9 | 76 | $55^{+21}_{-15}$ |
| 60 GeV | $\geq 11j, = 0b$ | $2.7 \pm 0.8$ | 3 | 0.44 | 0.2 | 38 | $35^{+14}_{-10}$ |
| | $\geq 11j, \geq 3b$ | $2.3 \pm 0.6$ | 5 | 0.1 | 1.3 | 56 | $33^{+13}_{-9}$ |
| 80 GeV | $\geq 10j, = 0b$ | $2.1 \pm 1.1$ | 3 | 0.38 | 0.3 | 42 | $34^{+13}_{-9}$ |
| | $\geq 10j, \geq 3b$ | $1.7 \pm 1.5$ | 2 | 0.47 | 0.1 | 35 | $33^{+13}_{-9}$ |
| 100 GeV | $\geq 8j, = 0b$ | $22.7 \pm 1.9$ | 25 | 0.38 | 0.3 | 96 | $85^{+33}_{-24}$ |
| | $\geq 8j, \geq 3b$ | $7.5 \pm 1.0$ | 8 | 0.41 | 0.2 | 55 | $51^{+20}_{-14}$ |

**Table 7** Data event yields compared with the expected contributions from relevant background sources, in the discovery signal regions defined for the $2\ell^{\text{sc}}$ category. The $p_0$-value, and corresponding significance (Z), as well as the observed and expected 95% CL model-independent upper limits on the product of cross-section, acceptance and efficiency (in ab) are also shown. In SRs with a deficit of data compared to the background prediction the $p_0$-value is capped at 0.5. The parameters of the background model are determined in a fit to a reduced set of bins, corresponding to the model-independent fit discussed in the text

| Jet $p_{\text{T}}$ threshold | Selection †=$m^{\ell j} < 155$ GeV | Total background | Data | $p_0$ | Z | $\sigma^{\text{excl}}$ obs. [ab] | $\sigma^{\text{excl}}$ exp. [ab] |
|---|---|---|---|---|---|---|---|
| 20 GeV | $= 6j, \geq 3b$,† | $16.1 \pm 1.2$ | 20 | 0.21 | 0.8 | 92 | $69^{+27}_{-19}$ |
| | $\geq 10j, = 0b$ | $5.8 \pm 0.8$ | 6 | 0.46 | 0.1 | 48 | $45^{+18}_{-13}$ |
| | $\geq 10j, \geq 3b$ | $8.2 \pm 1.5$ | 6 | 0.5 | 0 | 41 | $54^{+21}_{-15}$ |
| 40 GeV | $\geq 8j, = 0b$ | $2.8 \pm 0.7$ | 2 | 0.5 | 0 | 31 | $35^{+14}_{-10}$ |
| | $\geq 8j, \geq 3b$ | $3.6 \pm 1.2$ | 7 | 0.13 | 1.1 | 67 | $39^{+15}_{-11}$ |
| 60 GeV | $\geq 7j, = 0b$ | $1.71 \pm 0.35$ | 3 | 0.2 | 0.8 | 41 | $29^{+12}_{-8}$ |
| | $\geq 7j, \geq 3b$ | $2.0 \pm 0.7$ | 5 | 0.09 | 1.3 | 58 | $32^{+13}_{-9}$ |
| 80 GeV | $\geq 7j, = 0b$ | $0.34 \pm 0.13$ | 0 | 0.5 | 0 | 22 | $22^{+9}_{-0}$ |
| | $\geq 7j, \geq 3b$ | $0.54 \pm 0.20$ | 1 | 0.34 | 0.4 | 27 | $22^{+9}_{-0}$ |
| 100 GeV | $\geq 6j, = 0b$ | $0.5 \pm 0.4$ | 0 | 0.5 | 0 | 22 | $22^{+9}_{-0}$ |
| | $\geq 6j, \geq 3b$ | $0.52 \pm 0.22$ | 1 | 0.28 | 0.6 | 28 | $22^{+9}_{-0}$ |

under consideration. In addition, the discovery $p_0$-values and corresponding gaussian significance (Z) are shown, which measure the compatibility of the observed data with the background-only (zero signal strength) hypothesis relative to fluctuations of the background. Larger values indicate greater relative compatibility. No significant excess of data over the expected event yields is observed in any of the SRs. The two largest excesses are observed in the 60 GeV, $\geq$ 11 jets, $\geq$ 3 $b$-jets SR defined for the $1\ell$ category and in the 60 GeV, $\geq$ 7 jets, $\geq$ 3 $b$-jets SR defined for the $2\ell^{\text{sc}}$ category, and both correspond to a significance of 1.3 standard deviations. Upper limits on the product of cross-section, acceptance, and efficiency are set at 95% CL, ranging from 22 to 200 ab, depending on the SR.

### 9.2 Model-dependent results

For each signal model probed, the fit is configured using the model-dependent configuration. No significant excess is observed in any of the model-dependent fits. Figure 9 shows the observed and expected exclusion limits for the strong production signal models featuring gluino and stop pair production, as a function of the gluino mass or stop mass. Gluino masses up to 2.4 TeV are excluded for high LSP masses, and

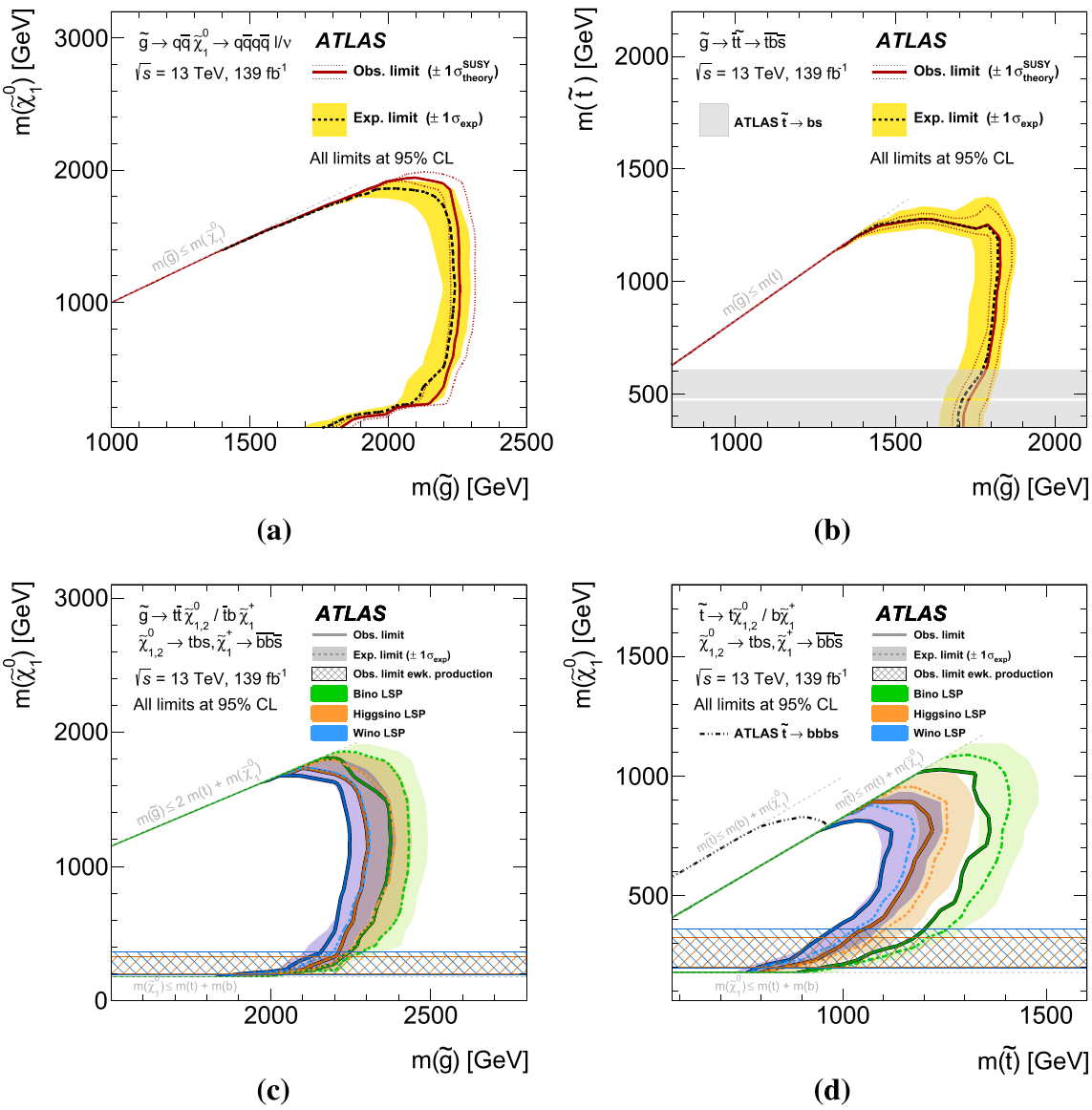


**Fig. 9** Observed and expected exclusion contours for the RPV models with strong production. The results are shown for **a** $\tilde{g} \to q\bar{q}\tilde{\chi}_1^0 \to q\bar{q}q\bar{q}\ell/\nu$, **b** $\tilde{g} \to t\bar{t}\tilde{t} \to t\bar{t}b\bar{s}$, **c** $\tilde{g} \to t\bar{t}\tilde{\chi}_{1,2}^0 \to t\bar{t}tbs$ and **d** stop pair production. The contours of the band around the expected limit are the $\pm 1\sigma$ variations, including all uncertainties. The dotted lines around the observed limit illustrate the change in the observed limit as the nominal signal cross-section is scaled up and down by the theoretical uncertainty. All limits are computed at 95% CL. The diagonal line indicates the kinematic limit for the decays in each specified scenario. The limits on direct electroweakino production obtained with the EWK analysis are displayed as horizontal hatched bands in **c** and **d**. When relevant, the limit on the stop mass from Refs. [23,27] is also shown. A small range in stop mass between 460 and 470 GeV is not excluded by the search for $\tilde{t} \to bs$ [27]

up to 2 TeV for low LSP masses. Stop masses are excluded up to 1–1.3 TeV, depending on the LSP mass. The sensitivity decreases for low LSP masses due to the high boost of the LSP, resulting in close-by decay products that lead to reconstruction and isolation inefficiencies. The best sensitivity is achieved for a bino LSP, while the wino LSP exhibits the worst sensitivity due to the lower number of top quarks in the final state. The exclusion limits for the models with gluino or stop production are stronger than in the previous version of the analysis documented in Ref. [22], thanks to the larger dataset and the inclusion of the same-sign lepton category.

Figure 10 shows exclusion limits in the electroweakino pair-production model, versus the LSP mass. The limits for pure higgsino and wino LSPs are shown separately, taking into account the processes discussed in Sect. 2. The wino signal can only contribute to the $1\ell$ category, via $\tilde{\chi}_1^\pm \tilde{\chi}_1^0$ production, while the higgsino signal is also present in the $2\ell^{\text{sc}}$ category through $\tilde{\chi}_2^0 \tilde{\chi}_1^0$ production. This leads to differences in

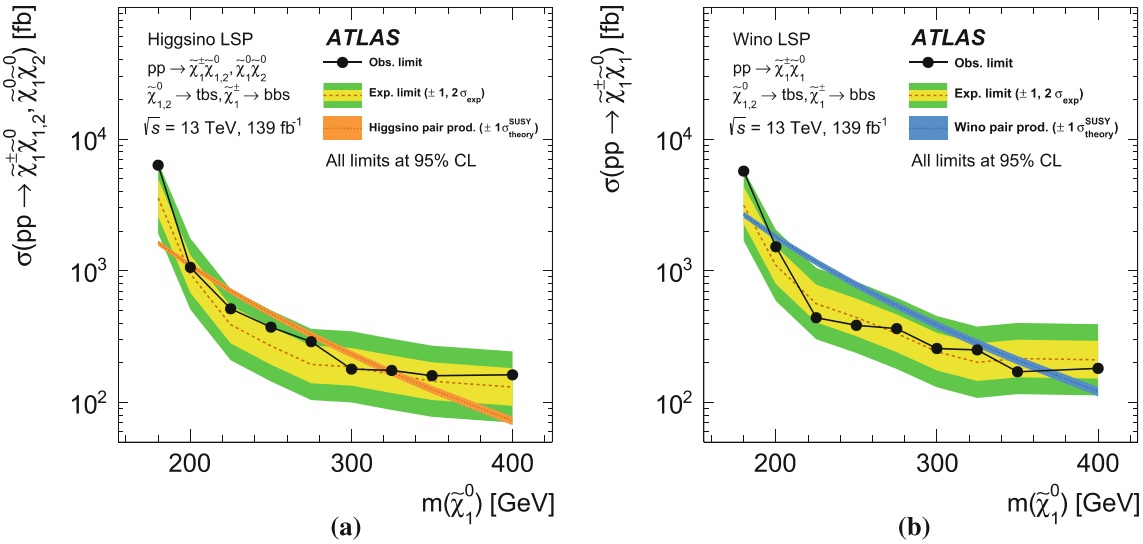


**Fig. 10** Observed and expected exclusion contours for the RPV models with electroweakino production models with **a** higgsino and **b** wino LSP hypotheses. The yellow and green contours of the band around the expected limit are the $\pm 1\sigma$ and $\pm 2\sigma$ variations including all uncertainties, respectively. The theoretical prediction is also shown, with the uncertainties in the prediction shown as a coloured band. The production of $\tilde{\chi}_1^{\pm}\tilde{\chi}_1^{\pm}$ is not considered as it decays to a final state with no leptons

the observed limits between the two models. Depending on the LSP hypothesis, LSP masses between 200 (197) GeV and 320 (365) GeV are excluded for a higgsino (wino) LSP.

The analysis is also sensitive to SM $t\bar{t}t\bar{t}$ production, which produces a final state similar to the targeted signals. An additional model-dependent fit is performed where the $t\bar{t}t\bar{t}$ normalization is a free parameter. The fitted normalization of the four-top process relative to the Standard Model value is $\mu_{t\bar{t}t\bar{t}} = 2.0^{+0.9}_{-0.7}$. Modelling uncertainties due to scale variations and parton-shower variation are taken into account, as is a 20% cross-section uncertainty for the reference SM prediction of $\sigma_{t\bar{t}t\bar{t}}$ [92]. This is in agreement with the measured value in Ref. [34] of $\mu_{t\bar{t}t\bar{t}} = 2.0^{+0.8}_{-0.6}$. Both analyses are based on the same dataset and have overlapping selections, but have completely different background estimation methods. The best sensitivity is obtained with the 40 GeV jet-$p_{\mathrm{T}}$ threshold. Compatible results, albeit with larger uncertainties, are obtained with the 20 GeV and 60 GeV jet-$p_{\mathrm{T}}$ thresholds. A fit with two independent signal strengths in each lepton category yields consistent values in both categories.

## 10 Conclusion

A search for RPV supersymmetry events with at least one isolated lepton (electron or muon) and high jet multiplicity is presented. In order to improve the sensitivity of the search, events with two leptons with the same electric charge, and events with at least one lepton are analysed separately. The selection also relies on the number of $b$-jets in the event. In order to ensure the highest sensitivity to the electroweak production models, a neural-network-based analysis was introduced. Data-based techniques are used to estimate the dominant backgrounds from $t\bar{t}$+jets, $W/Z$+jets, diboson, and $t\bar{t}W$ production. The analysis is performed with proton–proton collision data at $\sqrt{s} = 13$ TeV collected from 2015 to 2018 with the ATLAS detector at the LHC, corresponding to an integrated luminosity of 139 fb$^{-1}$.

With no significant excess over the Standard Model expectation observed, results are interpreted in the framework of simplified models featuring gluino, stop, or electroweakino pair production in RPV supersymmetry scenarios. In a benchmark model with $\tilde{g} \to t\bar{t}\tilde{\chi}_1^0 \to t\bar{t}tbs$, gluino masses up to 2.38 TeV are excluded at 95% confidence level. Top squarks with masses up to 1.36 TeV are excluded in a model with direct stop production and RPV decays of the LSP. In both models, three hypotheses for the LSP are tested: pure bino, pure wino, and pure higgsino. In a model with $\tilde{g} \to t\bar{t}\tilde{}$ and $\tilde{t} \to b\bar{s}$, gluino masses up to 1.83 TeV are excluded, whereas in a model with $\tilde{g} \to q\bar{q}\tilde{\chi}_1^0 \to q\bar{q}q\bar{q}\ell/\nu$, gluino masses up to 2.25 TeV are excluded. Direct electroweak production of electroweakinos is also tested, and higgsino (wino) masses between 200 (197) GeV and 320 (365) GeV are excluded.

These results improve upon the previously existing LHC limits for the gluino and stop production models considered, owing to the larger luminosity, the dedicated categorization and analysis of events with two leptons with the same electric charge, and the introduction of multivariate discriminants. The results for the electroweak production model also improve upon the limits on hadronic RPV decays of elec-

troweakinos from LEP [140–142]. Model-independent limits are also set on the contribution of new phenomena to the signal-region yields.

**Acknowledgements** We thank CERN for the very successful operation of the LHC, as well as the support staff from our institutions without whom ATLAS could not be operated efficiently. We acknowledge the support of ANPCyT, Argentina; YerPhI, Armenia; ARC, Australia; BMWFW and FWF, Austria; ANAS, Azerbaijan; SSTC, Belarus; CNPq and FAPESP, Brazil; NSERC, NRC and CFI, Canada; CERN; ANID, Chile; CAS, MOST and NSFC, China; Minciencias, Colombia; MSMT CR, MPO CR and VSC CR, Czech Republic; DNRF and DNSRC, Denmark; IN2P3-CNRS and CEA-DRF/IRFU, France; SRNSFG, Georgia; BMBF, HGF and MPG, Germany; GSRT, Greece; RGC and Hong Kong SAR, China; ISF and Benoziyo Center, Israel; INFN, Italy; MEXT and JSPS, Japan; CNRST, Morocco; NWO, Netherlands; RCN, Norway; MNiSW and NCN, Poland; FCT, Portugal; MNE/IFA, Romania; JINR; MES of Russia and NRC KI, Russian Federation; MESTD, Serbia; MSSR, Slovakia; ARRS and MIZŠ, Slovenia; DST/NRF, South Africa; MICINN, Spain; SRC and Wallenberg Foundation, Sweden; SERI, SNSF and Cantons of Bern and Geneva, Switzerland; MOST, Taiwan; TAEK, Turkey; STFC, United Kingdom; DOE and NSF, United States of America. In addition, individual groups and members have received support from BCKDF, CANARIE, Compute Canada, CRC and IVADO, Canada; Beijing Municipal Science & Technology Commission, China; COST, ERC, ERDF, Horizon 2020 and Marie Sk1ℓodowska-Curie Actions, European Union; Investissements d'Avenir Labex, Investissements d'Avenir Idex and ANR, France; DFG and AvH Foundation, Germany; Herakleitos, Thales and Aristeia programmes co-financed by EU-ESF and the Greek NSRF, Greece; BSF-NSF and GIF, Israel; La Caixa Banking Foundation, CERCA Programme Generalitat de Catalunya and PROMETEO and GenT Programmes Generalitat Valenciana, Spain; Göran Gustafssons Stiftelse, Sweden; The Royal Society and Leverhulme Trust, United Kingdom. The crucial computing support from all WLCG partners is acknowledged gratefully, in particular from CERN, the ATLAS Tier-1 facilities at TRIUMF (Canada), NDGF (Denmark, Norway, Sweden), CC-IN2P3 (France), KIT/GridKA (Germany), INFN-CNAF (Italy), NL-T1 (Netherlands), PIC (Spain), ASGC (Taiwan), RAL (UK) and BNL (USA), the Tier-2 facilities worldwide and large non-WLCG resource providers. Major contributors of computing resources are listed in Ref. [143].

**Data Availability Statement** This manuscript has no associated data or the data will not be deposited. [Authors' comment: All ATLAS scientific output is published in journals, and preliminary results are made available in Conference Notes. All are openly available, without restriction on use by external parties beyond copyright law and the standard conditions agreed by CERN. Data associated with journal publications are also made available: tables and data from plots (e.g. cross section values, likelihood profiles, selection efficiencies, cross section limits, ...) are stored in appropriate repositories such as HEPDATA (http://hepdata.cedar.ac.uk/). ATLAS also strives to make additional material related to the paper available that allows a reinterpretation of the data in the context of new theoretical models. For example, an extended encapsulation of the analysis is often provided for measurements in the framework of RIVET (http://rivet.hepforge.org/).]



Funded by SCOAP[3].

## References

1. Y. Golfand, E. Likhtman, Extension of the algebra of Poincare group generators and violation of P invariance. JETP Lett. **13**, 323 (1971) [Pisma Zh. Eksp. Teor. Fiz. **13** (1971) 452]
2. D. Volkov, V. Akulov, Is the neutrino a goldstone particle? Phys. Lett. B **46**, 109 (1973)
3. J. Wess, B. Zumino, Supergauge transformations in four dimensions. Nucl. Phys. B **70**, 39 (1974)
4. J. Wess, B. Zumino, Supergauge invariant extension of quantum electrodynamics. Nucl. Phys. B **78**, 1 (1974)
5. S. Ferrara, B. Zumino, Supergauge invariant Yang-Mills theories. Nucl. Phys. B **79**, 413 (1974)
6. A. Salam, J. Strathdee, Super-symmetry and non-Abelian gauges. Phys. Lett. B **51**, 353 (1974)
7. N. Sakai, Naturalness in supersymmetric GUTS. Z. Phys. C **11**, 153 (1981)
8. S. Dimopoulos, S. Raby, F. Wilczek, Supersymmetry and the scale of unification. Phys. Rev. D **24**, 1681 (1981)
9. L.E. Ibáñez, G.G. Ross, Low-energy predictions in supersymmetric grand unified theories. Phys. Lett. B **105**, 439 (1981)
10. S. Dimopoulos, H. Georgi, Softly broken supersymmetry and SU(5). Nucl. Phys. B **193**, 150 (1981)
11. G.R. Farrar, P. Fayet, Phenomenology of the production, decay, and detection of new hadronic states associated with supersymmetry. Phys. Lett. B **76**, 575 (1978)
12. H. Goldberg, Constraint on the photino mass from cosmology. Phys. Rev. Lett. **50**, 1419 (1983) [Erratum: Phys. Rev. Lett. **103**, 1419 (2009)]
13. J. Ellis, J. Hagelin, D.V. Nanopoulos, K.A. Olive, M. Srednicki, Supersymmetric relics from the big bang. Nucl. Phys. B **238**, 453 (1984)
14. J.A. Evans, Y. Kats, D. Shih, M.J. Strassler, Toward full LHC coverage of natural supersymmetry. JHEP **07**, 101 (2014). arXiv:1310.5758 [hep-ph]
15. B. Batell, T. Lin, L.-T. Wang, Flavored dark matter and R-parity violation. JHEP **01**, 075 (2014). arXiv:1309.4462 [hep-ph]
16. G. D'Ambrosio, G.F. Giudice, G. Isidori, A. Strumia, Minimal Flavour Violation: an effective field theory approach. Nucl. Phys. B **645**, 155 (2002). arXiv:hep-ph/0207036
17. C. Csáki, Y. Grossman, B. Heidenreich, MFV SUSY: a natural theory for R-parity violation. Phys. Rev. D **85**, 095009 (2012). arXiv:1111.1239 [hep-ph]
18. D.E. Lopez-Fogliani, C. Munoz, Proposal for a supersymmetric standard model. Phys. Rev. Lett. **97**, 041801 (2006). arXiv:hep-ph/0508297
19. J. Alwall, M.-P. Le, M. Lisanti, J.G. Wacker, Searching for directly decaying gluinos at the Tevatron. Phys. Lett. B **666**, 34 (2008). arXiv:0803.0019 [hep-ph]
20. J. Alwall, P. Schuster, N. Toro, Simplified models for a first characterization of new physics at the LHC. Phys. Rev. D **79**, 075020 (2009). arXiv:0810.3921 [hep-ph]
21. D. Alves et al., Simplified models for LHC new physics searches. J. Phys. G **39**, 105005 (2012). arXiv:1105.2838 [hep-ph]
22. ATLAS Collaboration, Search for new phenomena in a lepton plus high jet multiplicity final state with the ATLAS experiment using

$\sqrt{s}$ = 13 TeV proton-proton collision data. JHEP **09**, 088 (2017). arXiv:1704.08493 [hep-ex]
23. ATLAS Collaboration, Search for phenomena beyond the Standard Model in events with large b-jet multiplicity using the ATLAS detector at the LHC. Eur. Phys. J. C **81**, 11 (2021). arXiv:2010.01015 [hep-ex]
24. ATLAS Collaboration, Search for squarks and gluinos in final states with same-sign leptons and jets using 139 fb$^{-1}$ of data collected with the ATLAS detector. JHEP **06**, 046 (2020). arXiv:1909.08457 [hep-ex]
25. ATLAS Collaboration, Search for supersymmetry in events with four or more leptons in $\sqrt{s}$ = 13 TeV pp collisions with ATLAS. Phys. Rev. D **98**, 032009 (2018). arXiv:1804.03602 [hep-ex]
26. ATLAS Collaboration, Search for R-parity-violating supersymmetric particles in multi-jet final states produced in p-p collisions at $\sqrt{s}$ = 13 TeV using the ATLAS detector at the LHC. Phys. Lett. B **785**, 136 (2018). arXiv:1804.03568 [hep-ex]
27. ATLAS Collaboration, A search for pair-produced resonances in four-jet final states at $\sqrt{s}$ = 13 TeV with the ATLAS detector. Eur. Phys. J. C **78**, 250 (2018). arXiv:1710.07171 [hep-ex]
28. ATLAS Collaboration, Search for B-L R-parity-violating top squarks in $\sqrt{s}$ =13 TeV pp collisions with the ATLAS experiment. Phys. Rev. D **97**, 032003 (2018). arXiv:1710.05544 [hep-ex]
29. ATLAS Collaboration, Search for supersymmetry in final states with two same-sign or three leptons and jets using 36 fb$^{-1}$ of $\sqrt{s}$ = 13 TeV pp collision data with the ATLAS detector. JHEP **09**, 084 (2017). arXiv:1706.03731 [hep-ex] [Erratum: JHEP **08**, 121 (2019)]
30. C.M.S. Collaboration, Search for R-parity violating supersymmetry in pp collisions at $\sqrt{s}$ = 13 TeV using $b$ jets in a final state with a single lepton, many jets, and high sum of large-radius jet masses. Phys. Lett. B **783**, 114 (2018). arXiv:1712.08920 [hep-ex]
31. C.M.S. Collaboration, Searches for R-parity-violating supersymmetry in pp collisions at $\sqrt{(s)}$ = 8 TeV in final states with 0–4 leptons. Phys. Rev. D **94**, 112009 (2016). arXiv:1606.08076 [hep-ex]
32. C.M.S. Collaboration, Search for top squarks in R-parity-violating supersymmetry using three or more leptons and B-tagged jets. Phys. Rev. Lett. **111**, 221801 (2013). arXiv:1306.6643 [hep-ex]
33. C.M.S. Collaboration, Search for top squarks in final states with two top quarks and several light flavor jets in proton-proton collisions at $\sqrt{s}$ = 13 TeV. Phys. Rev. D **104**, 032006 (2021). arXiv:2102.06976 [hep-ex]
34. ATLAS Collaboration, Evidence for $t\bar{t}t\bar{t}$ production in the multilepton final state in proton-proton collisions at $\sqrt{s}$ = 13 TeV with the ATLAS detector. Eur. Phys. J. C **80**, 1085 (2020). arXiv:2007.14858 [hep-ex]
35. CMS Collaboration, Search for standard model production of four top quarks in proton-proton collisions at $\sqrt{s}$ = 13 TeV (2017). arXiv:1702.06164 [hep-ex]
36. M. Ibe, S. Matsumoto, R. Sato, Mass splitting between charged and neutral winos at two-loop level. Phys. Lett. B **721**, 252 (2013). arXiv:1212.5989 [hep-ph]
37. N. Nagata, S. Shirai, Higgsino dark matter in high-scale supersymmetry. JHEP **01**, 029 (2015). arXiv:1410.4549 [hep-ph]
38. W. Beenakker et al., Production of charginos/neutralinos and sleptons at hadron colliders. Phys. Rev. Lett. **83**, 3780 (1999). arXiv:hep-ph/9906298 [Erratum: Phys. Rev. Lett. **100**, 029901 (2008)]
39. G. Bozzi, B. Fuks, M. Klasen, Threshold resummation for slepton-pair production at hadron colliders. Nucl. Phys. B **777**, 157 (2007). arXiv:hep-ph/0701202
40. B. Fuks, M. Klasen, D.R. Lamprea, M. Rothering, Precision predictions for electroweak superpartner production at hadron colliders with RESUMMINO. Eur. Phys. J. C **73**, 2480 (2013). arXiv:1304.0790 [hep-ph]
41. B. Fuks, M. Klasen, D.R. Lamprea, M. Rothering, Revisiting slepton pair production at the large hadron collider. JHEP **01**, 168 (2014). arXiv:1310.2621 [hep-ph]
42. J. Fiaschi, M. Klasen, Slepton pair production at the LHC in NLO+NLL with resummation improved parton densities. JHEP **03**, 094 (2018). arXiv:1801.10357 [hep-ph]
43. ATLAS Collaboration, The ATLAS experiment at the CERN large hadron collider. JINST **3**, S08003 (2008)
44. ATLAS Collaboration, ATLAS Insertable B-Layer Technical Design Report, ATLAS-TDR-19 (2010). https://cds.cern.ch/record/1291633 (ATLAS Insertable B-Layer Technical Design Report Addendum, ATLAS-TDR-19-ADD-1 (2012). https://cds.cern.ch/record/1451888)
45. B. Abbott et al., Production and integration of the ATLAS Insertable B-Layer. JINST **13**, T05008 (2018). arXiv:1803.00844 [physics.ins-det]
46. ATLAS Collaboration, The performance of the jet trigger for the ATLAS detector during data taking. Eur. Phys. J. C **76**, 526 (2016). arXiv:1606.07759 [hep-ex]
47. ATLAS Collaboration, The ATLAS Collaboration Software and Firmware, ATL-SOFT-PUB-2021-001 (2021). https://cds.cern.ch/record/2767187
48. S. Agostinelli et al., GEANT4 A simulation toolkit. Nucl. Instrum. Meth. **A506**, 250 (2003)
49. ATLAS Collaboration, The ATLAS simulation infrastructure. Eur. Phys. J. C **70**, 823 (2010). arXiv:1005.4568 [physics.ins-det]
50. T. Sjöstrand et al., An introduction to PYTHIA 8.2. Comput. Phys. Commun. **191**, 159 (2015). arXiv:1410.3012 [hep-ph]
51. R.D. Ball et al., Parton distributions with LHC data. Nucl. Phys. B **867**, 244 (2013). arXiv:1207.1303 [hep-ph]
52. ATLAS Collaboration, The Pythia 8 A3 tune description of ATLAS minimum bias and inelastic measurements incorporating the Donnachie–Landshoff diffractive model. ATL-PHYS-PUB-2016-017 (2016). https://cds.cern.ch/record/2206965
53. D.J. Lange, The EvtGen particle decay simulation package. Nucl. Instrum. Meth. A **462**, 152 (2001)
54. J. Alwall et al., The automated computation of tree-level and next-to-leading order differential cross sections, and their matching to parton shower simulations. JHEP **07**, 079 (2014). arXiv:1405.0301 [hep-ph]
55. ATLAS Collaboration, The simulation principle and performance of the ATLAS fast calorimeter simulation FastCaloSim. ATL-PHYS-PUB-2010-013 (2010). https://cds.cern.ch/record/1300517
56. W. Beenakker, C. Borschensky, M. Krämer, A. Kulesza, E. Laenen, NNLL-fast: predictions for coloured supersymmetric particle production at the LHC with threshold and Coulomb resummation. JHEP **12**, 133 (2016). arXiv:1607.07741 [hep-ph]
57. W. Beenakker et al., NNLL resummation for squark and gluino production at the LHC. JHEP **12**, 023 (2014). arXiv:1404.3134 [hep-ph]
58. W. Beenakker et al., Towards NNLL resummation: hard matching coefficients for squark and gluino hadroproduction. JHEP **10**, 120 (2013). arXiv:1304.6354 [hep-ph]
59. W. Beenakker et al., NNLL resummation for squark-antisquark pair production at the LHC. JHEP **01**, 076 (2012). arXiv:1110.2446 [hep-ph]
60. W. Beenakker et al., Soft-gluon resummation for squark and gluino hadroproduction. JHEP **12**, 041 (2009). arXiv:0909.4418 [hep-ph]
61. A. Kulesza, L. Motyka, Soft gluon resummation for the production of gluino-gluino and squark antisquark pairs at the LHC. Phys. Rev. D **80**, 095004 (2009). arXiv:0905.4749 [hep-ph]
62. A. Kulesza, L. Motyka, Threshold resummation for squark-antisquark and gluino-pair production at the LHC. Phys. Rev. Lett. **102**, 111802 (2009). arXiv:0807.2405 [hep-ph]

63. W. Beenakker, R. Höpker, M. Spira, P. Zerwas, Squark and gluino production at hadron colliders. Nucl. Phys. B **492**, 51 (1997). arXiv:hep-ph/9610490
64. W. Beenakker, M. Krämer, T. Plehn, M. Spira, P. Zerwas, Stop production at hadron colliders. Nucl. Phys. B **515**, 3 (1998). arXiv:hep-ph/9710451
65. W. Beenakker et al., Supersymmetric top and bottom squark production at hadron colliders. JHEP **08**, 098 (2010). arXiv:1006.4771 [hep-ph]
66. W. Beenakker et al., NNLL resummation for stop pair-production at the LHC. JHEP **05**, 153 (2016). arXiv:1601.02954 [hep-ph]
67. E. Bothmann et al., Event generation with Sherpa 2.2. SciPost Phys. **7**, 034 (2019). arXiv:1905.09127 [hep-ph]
68. C. Anastasiou, L.J. Dixon, K. Melnikov, F. Petriello, High precision QCD at hadron colliders: electroweak gauge boson rapidity distributions at next-to-next-to leading order. Phys. Rev. D **69**, 094008 (2004). arXiv:hep-ph/0312266
69. R.D. Ball et al., Parton distributions for the LHC run II. JHEP **04**, 040 (2015). arXiv:1410.8849 [hep-ph]
70. T. Sjöstrand, S. Mrenna, P. Skands, A brief introduction to PYTHIA 8.1. Comput. Phys. Commun. **178**, 852 (2008). arXiv:0710.3820 [hep-ph]
71. ATLAS Collaboration, ATLAS Pythia 8 tunes to 7 TeV data, ATL-PHYS-PUB-2014-021 (2014). https://cds.cern.ch/record/1966419
72. S. Frixione, P. Nason, G. Ridolfi, A positive-weight next-to-leading-order Monte Carlo for heavy flavour hadroproduction. JHEP **09**, 126 (2007). arXiv:0707.3088 [hep-ph]
73. P. Nason, A new method for combining NLO QCD with shower Monte Carlo algorithms. JHEP **11**, 040 (2004). arXiv:hep-ph/0409146
74. S. Frixione, P. Nason, C. Oleari, Matching NLO QCD computations with parton shower simulations: the POWHEG method. JHEP **11**, 070 (2007). arXiv:0709.2092 [hep-ph]
75. S. Alioli, P. Nason, C. Oleari, E. Re, A general framework for implementing NLO calculations in shower Monte Carlo programs: the POWHEG BOX. JHEP **06**, 043 (2010). arXiv:1002.2581 [hep-ph]
76. M. Beneke, P. Falgari, S. Klein, C. Schwinn, Hadronic top-quark pair production with NNLL threshold resummation. Nucl. Phys. B **855**, 695 (2012). arXiv:1109.1536 [hep-ph]
77. M. Cacciari, M. Czakon, M. Mangano, A. Mitov, P. Nason, Top-pair production at hadron colliders with next-to-next-to-leading logarithmic soft-gluon resummation. Phys. Lett. B **710**, 612 (2012). arXiv:1111.5869 [hep-ph]
78. P. Bärnreuther, M. Czakon, A. Mitov, Percent-level-precision physics at the Tevatron: next-to-next-to-leading order QCD corrections to $q\bar{q} \longrightarrow t\bar{t} + X$. Phys. Rev. Lett. **109**, 132001 (2012). arXiv:1204.5201 [hep-ph]
79. M. Czakon, A. Mitov, NNLO corrections to top-pair production at hadron colliders: the all-fermionic scattering channels. JHEP **12**, 054 (2012). arXiv:1207.0236 [hep-ph]
80. M. Czakon, A. Mitov, NNLO corrections to top pair production at hadron colliders: the quark-gluon reaction. JHEP **01**, 080 (2013). arXiv:1210.6832 [hep-ph]
81. M. Czakon, P. Fiedler, A. Mitov, Total top-quark pair-production cross section at hadron colliders through $O(\alpha_S^4)$. Phys. Rev. Lett. **110**, 252004 (2013). arXiv:1303.6254 [hep-ph]
82. M. Czakon, A. Mitov, Top++: a program for the calculation of the top-pair cross-section at hadron colliders. Comput. Phys. Commun. **185**, 2930 (2014). arXiv:1112.5675 [hep-ph]
83. M. Bähr et al., Herwig++ physics and manual. Eur. Phys. J. C **58**, 639 (2008). arXiv:0803.0883 [hep-ph]
84. J. Bellm et al., Herwig 7.0/Herwig++ 3.0 release note. Eur. Phys. J. C **76**, 196 (2016). arXiv:1512.01178 [hep-ph]
85. L. Harland-Lang, A. Martin, P. Motylinski, R. Thorne, Parton distributions in the LHC era: MMHT 2014 PDFs. Eur. Phys. J. C **75**, 204 (2015). arXiv:1412.3989 [hep-ph]
86. S. Alioli, P. Nason, C. Oleari, E. Re, NLO single-top production matched with shower in POWHEG: s- and t-channel contributions. JHEP **09**, 111 (2009). arXiv:0907.4076 [hep-ph] [Erratum: JHEP **02**, 011 (2010)]
87. E. Re, Single-top Wt-channel production matched with parton showers using the POWHEG method. Eur. Phys. J. C **71**, 1547 (2011). arXiv:1009.2450 [hep-ph]
88. R. Frederix, E. Re, P. Torrielli, Single-top t-channel hadroproduction in the four-flavour scheme with POWHEG and aMC@NLO. JHEP **09**, 130 (2012). arXiv:1207.5391 [hep-ph]
89. N. Kidonakis, Next-to-next-to-leading-order collinear and soft gluon corrections for t-channel single top quark production. Phys. Rev. D **83**, 091503 (2011). arXiv:1103.2792 [hep-ph]
90. N. Kidonakis, Two-loop soft anomalous dimensions for single top quark associated production with a $W^-$ or $H^-$. Phys. Rev. D **82**, 054018 (2010). arXiv:1005.4451 [hep-ph]
91. N. Kidonakis, Top Quark Production, Proceedings, Helmholtz International Summer School on Physics of Heavy Quarks and Hadrons (HQ 2013) 139 (2013). arXiv:1311.0283 [hep-ph]
92. R. Frederix, D. Pagani, M. Zaro, Large NLO corrections in $t\bar{t}W^{\pm}$ and $t\bar{t}t\bar{t}$ hadroproduction from supposedly subleading EW contributions. JHEP **02**, 031 (2018). arXiv:1711.02116 [hep-ph]
93. H.B. Hartanto, B. Jäger, L. Reina, D. Wackeroth, Higgs boson production in association with top quarks in the POWHEG BOX. Phys. Rev. D **91**, 094003 (2015). arXiv:1501.04498 [hep-ph]
94. T. Gleisberg, S. Höche, Comix, a new matrix element generator. JHEP **12**, 039 (2008). arXiv:0808.3674 [hep-ph]
95. F. Cascioli, P. Maierhöfer, S. Pozzorini, Scattering amplitudes with open loops. Phys. Rev. Lett. **108**, 111601 (2012). arXiv:1111.5206 [hep-ph]
96. A. Denner, S. Dittmaier, L. Hofer, Collier: a fortran-based complex one-loop library in extended regularizations. Comput. Phys. Commun. **212**, 220 (2017). arXiv:1604.06792 [hep-ph]
97. S. Schumann, F. Krauss, A parton shower algorithm based on Catani-Seymour dipole factorisation. JHEP **03**, 038 (2008). arXiv:0709.1027 [hep-ph]
98. S. Höche, F. Krauss, M. Schönherr, F. Siegert, A critical appraisal of NLO+PS matching methods. JHEP **09**, 049 (2012). arXiv:1111.1220 [hep-ph]
99. S. Höche, F. Krauss, M. Schönherr, F. Siegert, QCD matrix elements + parton showers. The NLO case. JHEP **04**, 027 (2013). arXiv:1207.5030 [hep-ph]
100. S. Catani, F. Krauss, R. Kuhn, B.R. Webber, QCD matrix elements + parton showers. JHEP **11**, 063 (2001). arXiv:hep-ph/0109231
101. S. Höche, F. Krauss, S. Schumann, F. Siegert, QCD matrix elements and truncated showers. JHEP **05**, 053 (2009). arXiv:0903.1219 [hep-ph]
102. ATLAS Collaboration, ATLAS data quality operations and performance for 2015–2018 data-taking. JINST **15**, P04003 (2020). arXiv:1911.04632 [physics.ins-det]
103. ATLAS Collaboration, Luminosity determination in pp collisions at $\sqrt{s}$ = 13 TeV using the ATLAS detector at the LHC. ATLAS-CONF-2019-021 (2019). https://cds.cern.ch/record/2677054
104. G. Avoni et al., The new LUCID-2 detector for luminosity measurement and monitoring in ATLAS. JINST **13**, P07017 (2018)
105. ATLAS Collaboration, Vertex reconstruction performance of the ATLAS detector at $\sqrt{s}$ = 13 TeV, ATL-PHYS-PUB-2015-026 (2015). https://cds.cern.ch/record/2037717
106. ATLAS Collaboration, Reconstruction of primary vertices at the ATLAS experiment in Run 1 proton–proton collisions at the LHC. Eur. Phys. J. C **77**, 332 (2017). arXiv:1611.10235 [hep-ex]
107. M. Cacciari, G.P. Salam, G. Soyez, The anti-$k_t$ jet clustering algorithm. JHEP **04**, 063 (2008). arXiv:0802.1189 [hep-ph]

108. M. Cacciari, G.P. Salam, G. Soyez, FastJet user manual. Eur. Phys. J. C **72**, 1896 (2012). arXiv:1111.6097 [hep-ph]
109. ATLAS Collaboration, Jet reconstruction and performance using particle flow with the ATLAS detector. Eur. Phys. J. C **77**, 466 (2017). arXiv:1703.10485 [hep-ex]
110. ATLAS Collaboration, Jet energy scale and resolution measured in proton–proton collisions at $\sqrt{s}$ = 13 TeV with the ATLAS detector (2020). arXiv:2007.02645 [hep-ex]
111. ATLAS Collaboration, Selection of jets produced in 13 TeV proton–proton collisions with the ATLAS detector. ATLAS-CONF-2015-029 (2015). https://cds.cern.ch/record/2037702
112. ATLAS Collaboration, Performance of pile-up mitigation techniques for jets in pp collisions at $\sqrt{s}$ = 8 TeV using the ATLAS detector. Eur. Phys. J. C **76**, 581 (2016). arXiv:1510.03823 [hep-ex]
113. ATLAS Collaboration, ATLAS b-jet identification performance and efficiency measurement with $t\bar{t}$ events in pp collisions at $\sqrt{s}$ = 13 TeV. Eur. Phys. J. C **79**, 970 (2019). arXiv:1907.05120 [hep-ex]
114. ATLAS Collaboration, Optimisation and performance studies of the ATLAS b-tagging algorithms for the 2017–18 LHC run. ATL-PHYS-PUB-2017-013 (2017). https://cds.cern.ch/record/2273281
115. ATLAS Collaboration, Electron and photon performance measurements with the ATLAS detector using the 2015–2017 LHC proton–proton collision data. JINST **14**, P12006 (2019). arXiv:1908.00005 [hep-ex]
116. ATLAS Collaboration, Muon reconstruction and identification efficiency in ATLAS using the full Run 2 pp collision data set at $\sqrt{s}$ = 13 TeV (2020). arXiv:2012.00578 [hep-ex]
117. ATLAS Collaboration, Evidence for the associated production of the Higgs boson and a top quark pair with the ATLAS detector. Phys. Rev. D **97**, 072003 (2018). arXiv:1712.08891 [hep-ex]
118. ATLAS Collaboration, Performance of missing transverse momentum reconstruction with the ATLAS detector using proton–proton collisions at $\sqrt{s}$ = 13 TeV. Eur. Phys. J. C **78**, 903 (2018). arXiv:1802.08168 [hep-ex]
119. ATLAS Collaboration, $E_T^{miss}$ performance in the ATLAS detector using 2015–2016 LHC pp collisions. ATLAS-CONF-2018-023 (2018). https://cds.cern.ch/record/2625233
120. ATLAS Collaboration, Performance of the ATLAS muon triggers in Run 2. JINST **15**, P09015 (2020). arXiv:2004.13447 [hep-ex]
121. ATLAS Collaboration, Performance of electron and photon triggers in ATLAS during LHC Run 2. Eur. Phys. J. C **80**, 47 (2020). arXiv:1909.00761 [hep-ex]
122. G.J. Székely, M.L. Rizzo, N.K. Bakirov, Measuring and testing dependence by correlation of distances. Ann. Stat. **35**, 2769 (2007). https://doi.org/10.1214/009053607000000505
123. G. Kasieczka, D. Shih, Robust jet classifiers through distance correlation. Phys. Rev. Lett. **125**, 122001 (2020). arXiv:2001.05310 [hep-ph]
124. A. Paszke et al., *PyTorch: an imperative style, high-performance deep learning library, Advances in Neural Information Processing Systems*, vol. 32 (Inc, Curran Associates, 2019), p. 8024
125. D.P. Kingma, J. Ba, Adam: a method for stochastic, optimization (2017). arXiv:1412.6980 [cs.LG]
126. M. Sundararajan, A. Taly, Q. Yan, Axiomatic attribution for deep networks (2017). arXiv:1703.01365 [cs.LG]
127. S.D. Ellis, R. Kleiss, W.J. Stirling, W's, Z's and Jets. Phys. Lett. B **154**, 435 (1985)
128. F.A. Berends, W.T. Giele, H. Kuijf, R.H. Kleiss, W.J. Stirling, Multijet production in W, Z events at $p\bar{p}$ colliders. Phys. Lett. B **224**, 237 (1989)
129. W. Giele, W. Stirling, Top search at fermilab: multijet signals and backgrounds. Nucl. Phys. B **343**, 14 (1990)
130. E. Gerwick, T. Plehn, S. Schumann, P. Schichtel, Scaling patterns for QCD jets. JHEP **10**, 162 (2012). arXiv:1208.3676 [hep-ph]
131. ATLAS Collaboration, Measurement of the production cross section of jets in association with a Z boson in pp collisions at $\sqrt{s}$ = 7 TeV with the ATLAS detector. JHEP **07**, 032 (2013). arXiv:1304.7098 [hep-ex]
132. ATLAS Collaboration, Measurements of the production cross section of a Z boson in association with jets in pp collisions at $\sqrt{s}$ = 13 TeV with the ATLAS detector. Eur. Phys. J. C **77**, 361 (2017). arXiv:1702.05725 [hep-ex]
133. C.M.S. Collaboration, Jet production rates in association with W and Z bosons in pp collisions at $\sqrt{s}$ = 7 TeV. JHEP **01**, 010 (2012). arXiv:1110.3226 [hep-ex]
134. ATLAS Collaboration, Search for supersymmetry at $\sqrt{s}$ = 13 TeV in final states with jets and two same-sign leptons or three leptons with the ATLAS detector. Eur. Phys. J. C 7**6**, 259 (2016). arXiv:1602.09058 [hep-ex]
135. ATLAS Collaboration, Performance of missing transverse momentum reconstruction with the ATLAS detector in the first proton–proton collisions at $\sqrt{s}$ = 13 TeV, ATL-PHYS-PUB-2015-027 (2015). https://cds.cern.ch/record/2037904
136. ATLAS Collaboration, Expected performance of missing transverse momentum reconstruction for the ATLAS detector at $\sqrt{s}$ = 13 TeV, ATL-PHYS-PUB-2015-023 (2015). https://cds.cern.ch/record/2037700
137. M. Botje et al., The PDF4LHC Working Group Interim Recommendations (2011). arXiv:1101.0538 [hep-ph]
138. G. Cowan, K. Cranmer, E. Gross, O. Vitells, Asymptotic formulae for likelihood-based tests of new physics. Eur. Phys. J. C **71**, 1554 (2011). arXiv:1007.1727 [physics.data-an] [Erratum: Eur. Phys. J. C **73**, 2501 (2013)]
139. A.L. Read, Presentation of search results: the CLs technique. J. Phys. G **28**, 2693 (2002)
140. DELPHI Collaboration, Search for supersymmetric particles assuming R-parity non-conservation in $e^+e^-$ collisions at $\sqrt{s}$ = 192 GeV to 208 GeV. Eur. Phys. J. C **36**, 1 (2004). arXiv:hep-ex/0406009 [Erratum: Eur. Phys. J. C **37**, 129 (2004)]
141. ALEPH Collaboration, Search for supersymmetric particles with R parity violating decays in $e^+e^-$ collisions at $\sqrt{s}$ up to 209 GeV. Eur. Phys. J. C **31**, 1 (2003). arXiv:hep-ex/0210014
142. L3 Collaboration, Search for R-parity violating decays of supersymmetric particles in $e^+e^-$ collisions at LEP. Phys. Lett. B **524**, 65 (2002). arXiv:hep-ex/0110057
143. ATLAS Collaboration, ATLAS, Computing Acknowledgements (ATL-SOFT-PUB-2020-001). https://cds.cern.ch/record/2717821

## ATLAS Collaboration

G. Aad[99], B. Abbott[125], D. C. Abbott[100], A. Abed Abud[34], K. Abeling[51], D. K. Abhayasinghe[91], S. H. Abidi[27], H. Abramowicz[158], H. Abreu[157], Y. Abulaiti[5], A. C. Abusleme Hoffman[143a], B. S. Acharya[64a,64b,p], B. Achkar[51], L. Adam[97], C. Adam Bourdarios[4], L. Adamczyk[81a], L. Adamek[163], J. Adelman[117], A. Adiguzel[11c,ae], S. Adorni[52], T. Adye[140], A. A. Affolder[142], Y. Afik[157], C. Agapopoulou[62], M. N. Agaras[12], J. Agarwala[68a,68b], A. Aggarwal[115], C. Agheorghiesei[25c], J. A. Aguilar-Saavedra[136a,136f,ad], A. Ahmad[34], F. Ahmadov[77], W. S. Ahmed[101], X. Ai[44], G. Aielli[71a,71b], S. Akatsuka[83], M. Akbiyik[97], T. P. A. Åkesson[94], A. V. Akimov[108], K. Al Khoury[37], G. L. Alberghi[21b], J. Albert[172], M. J. Alconada Verzini[86], S. Alderweireldt[48], M. Aleksa[34], I. N. Aleksandrov[77], C. Alexa[25b], T. Alexopoulos[9], A. Alfonsi[116], F. Alfonsi[21a,21b], M. Alhroob[125], B. Ali[138], S. Ali[155], M. Aliev[162], G. Alimonti[66a], C. Allaire[34], B. M. M. Allbrooke[153], P. P. Allport[19], A. Aloisio[67a,67b], F. Alonso[86], C. Alpigiani[145], E. Alunno Camelia[71a,71b], M. Alvarez Estevez[96], M. G. Alviggi[67a,67b], Y. Amaral Coutinho[78b], A. Ambler[101], L. Ambroz[131], C. Amelung[34], D. Amidei[103], S. P. Amor Dos Santos[136a], S. Amoroso[44], C. S. Amrouche[52], C. Anastopoulos[146], N. Andari[141], T. Andeen[10], J. K. Anders[18], S. Y. Andrean[43a,43b], A. Andreazza[66a,66b], V. Andrei[59a], S. Angelidakis[8], A. Angerami[37], A. V. Anisenkov[118a,118b], A. Annovi[69a], C. Antel[52], M. T. Anthony[146], E. Antipov[126], M. Antonelli[49], D. J. A. Antrim[16], F. Anulli[70a], M. Aoki[79], J. A. Aparisi Pozo[170], M. A. Aparo[153], L. Aperio Bella[44], N. Aranzabal[34], V. Araujo Ferraz[78a], C. Arcangeletti[49], A. T. H. Arce[47], E. Arena[88], J-F. Arguin[107], S. Argyropoulos[50], J.-H. Arling[44], A. J. Armbruster[34], A. Armstrong[167], O. Arnaez[163], H. Arnold[34], Z. P. Arrubarrena Tame[111], G. Artoni[131], H. Asada[113], K. Asai[123], S. Asai[160], N. A. Asbah[57], E. M. Asimakopoulou[168], L. Asquith[153], J. Assahsah[33d], K. Assamagan[27], R. Astalos[26a], R. J. Atkin[31a], M. Atkinson[169], N. B. Atlay[17], H. Atmani[58b], P. A. Atmasiddha[103], K. Augsten[138], S. Auricchio[67a,67b], V. A. Austrup[178], G. Avolio[34], M. K. Ayoub[13c], G. Azuelos[107,ak], D. Babal[26a], H. Bachacou[141], K. Bachas[159], F. Backman[43a,43b], A. Badea[57], P. Bagnaia[70a,70b], H. Bahrasemani[149], A. J. Bailey[170], V. R. Bailey[169], J. T. Baines[140], C. Bakalis[9], O. K. Baker[179], P. J. Bakker[116], E. Bakos[14], D. Bakshi Gupta[7], S. Balaji[154], R. Balasubramanian[116], E. M. Baldin[118a,118b], P. Balek[139], E. Ballabene[66a,66b], F. Balli[141], W. K. Balunas[131], J. Balz[97], E. Banas[82], M. Bandieramonte[135], A. Bandyopadhyay[17], L. Barak[158], E. L. Barberio[102], D. Barberis[53a,53b], M. Barbero[99], G. Barbour[92], K. N. Barends[31a], T. Barillari[112], M-S. Barisits[34], J. Barkeloo[128], T. Barklow[150], B. M. Barnett[140], R. M. Barnett[16], A. Baroncelli[58a], G. Barone[27], A. J. Barr[131], L. Barranco Navarro[43a,43b], F. Barreiro[96], J. Barreiro Guimarães da Costa[13a], U. Barron[158], S. Barsov[134], F. Bartels[59a], R. Bartoldus[150], G. Bartolini[99], A. E. Barton[87], P. Bartos[26a], A. Basalaev[44], A. Basan[97], I. Bashta[72a,72b], A. Bassalat[62], M. J. Basso[163], C. R. Basson[98], R. L. Bates[55], S. Batlamous[33e], J. R. Batley[30], B. Batool[148], M. Battaglia[142], M. Bauce[70a,70b], F. Bauer[141,*], P. Bauer[22], H. S. Bawa[29], A. Bayirli[11c], J. B. Beacham[47], T. Beau[132], P. H. Beauchemin[166], F. Becherer[50], P. Bechtle[22], H. P. Beck[18,r], K. Becker[174], C. Becot[44], A. J. Beddall[11a], V. A. Bednyakov[77], C. P. Bee[152], T. A. Beermann[178], M. Begalli[78b], M. Begel[27], A. Behera[152], J. K. Behr[44], C. Beirao Da Cruz E Silva[34], J. F. Beirer[34,51], F. Beisiegel[22], M. Belfkir[4], G. Bella[158], L. Bellagamba[21b], A. Bellerive[32], P. Bellos[19], K. Beloborodov[118a,118b], K. Belotskiy[109], N. L. Belyaev[109], D. Benchekroun[33a], Y. Benhammou[158], D. P. Benjamin[5], M. Benoit[27], J. R. Bensinger[24], S. Bentvelsen[116], L. Beresford[34], M. Beretta[49], D. Berge[17], E. Bergeaas Kuutmann[168], N. Berger[4], B. Bergmann[138], L. J. Bergsten[24], J. Beringer[16], S. Berlendis[6], G. Bernardi[132], C. Bernius[150], F. U. Bernlochner[22], T. Berry[91], P. Berta[44], A. Berthold[46], I. A. Bertram[87], O. Bessidskaia Bylund[178], S. Bethke[112], A. Betti[40], A. J. Bevan[90], S. Bhatta[152], D. S. Bhattacharya[173], P. Bhattarai[24], V. S. Bhopatkar[5], R. Bi[135], R. M. Bianchi[135], O. Biebel[111], R. Bielski[34], N. V. Biesuz[69a,69b], M. Biglietti[72a], T. R. V. Billoud[138], M. Bindi[51], A. Bingul[11d], C. Bini[70a,70b], S. Biondi[21a,21b], C. J. Birch-sykes[98], G. A. Bird[19,140], M. Birman[176], T. Bisanz[34], J. P. Biswal[2], D. Biswas[177,k], A. Bitadze[98], C. Bittrich[46], K. Bjørke[130], I. Bloch[44], C. Blocker[24], A. Blue[55], U. Blumenschein[90], J. Blumenthal[97], G. J. Bobbink[116], V. S. Bobrovnikov[118a,118b], D. Bogavac[12], A. G. Bogdanchikov[118a,118b], C. Bohm[43a], V. Boisvert[91], P. Bokan[44], T. Bold[81a], M. Bomben[132], M. Bona[90], M. Boonekamp[141], C. D. Booth[91], A. G. Borbély[55], H. M. Borecka-Bielska[107], L. S. Borgna[92], G. Borissov[87], D. Bortoletto[131], D. Boscherini[21b], M. Bosman[12], J. D. Bossio Sola[101], K. Bouaouda[33a], J. Boudreau[135], E. V. Bouhova-Thacker[87], D. Boumediene[36], R. Bouquet[132], A. Boveia[124], J. Boyd[34], D. Boye[27], I. R. Boyko[77], A. J. Bozson[91], J. Bracinik[19], N. Brahimi[58c,58d], G. Brandt[178], O. Brandt[30], F. Braren[44], B. Brau[100], J. E. Brau[128], W. D. Breaden Madden[55],

K. Brendlinger[44], R. Brener[176], L. Brenner[34], R. Brenner[168], S. Bressler[176], B. Brickwedde[97], D. L. Briglin[19], D. Britton[55], D. Britzger[112], I. Brock[22], R. Brock[104], G. Brooijmans[37], W. K. Brooks[143e], E. Brost[27], P. A. Bruckman de Renstrom[82], B. Brüers[44], D. Bruncko[26b], A. Bruni[21b], G. Bruni[21b], M. Bruschi[21b], N. Bruscino[70a,70b], L. Bryngemark[150], T. Buanes[15], Q. Buat[152], P. Buchholz[148], A. G. Buckley[55], I. A. Budagov[77], M. K. Bugge[130], O. Bulekov[109], B. A. Bullard[57], T. J. Burch[117], S. Burdin[88], C. D. Burgard[44], A. M. Burger[126], B. Burghgrave[7], J. T. P. Burr[44], C. D. Burton[10], J. C. Burzynski[100], V. Büscher[97], P. J. Bussey[55], J. M. Butler[23], C. M. Buttar[55], J. M. Butterworth[92], W. Buttinger[140], C. J. Buxo Vazquez[104], A. R. Buzykaev[118a,118b], G. Cabras[21b], S. Cabrera Urbán[170], D. Caforio[54], H. Cai[135], V. M. M. Cairo[150], O. Cakir[3a], N. Calace[34], P. Calafiura[16], G. Calderini[132], P. Calfayan[63], G. Callea[55], L. P. Caloba[78b], A. Caltabiano[71a,71b], S. Calvente Lopez[96], D. Calvet[36], S. Calvet[36], T. P. Calvet[99], M. Calvetti[69a,69b], R. Camacho Toro[132], S. Camarda[34], D. Camarero Munoz[96], P. Camarri[71a,71b], M. T. Camerlingo[72a,72b], D. Cameron[130], C. Camincher[172], M. Campanelli[92], A. Camplani[38], V. Canale[67a,67b], A. Canesse[101], M. Cano Bret[75], J. Cantero[126], Y. Cao[169], M. Capua[39a,39b], A. Carbone[66a,66b], R. Cardarelli[71a], F. Cardillo[170], G. Carducci[39a,39b], T. Carli[34], G. Carlino[67a], B. T. Carlson[135], E. M. Carlson[164a,172], L. Carminati[66a,66b], M. Carnesale[70a,70b], R. M. D. Carney[150], S. Caron[115], E. Carquin[143e], S. Carrá[44], G. Carratta[21a,21b], J. W. S. Carter[163], T. M. Carter[48], D. Casadei[31c], M. P. Casado[12,h], A. F. Casha[163], E. G. Castiglia[179], F. L. Castillo[59a], L. Castillo Garcia[12], V. Castillo Gimenez[170], N. F. Castro[136a,136e], A. Catinaccio[34], J. R. Catmore[130], A. Cattai[34], V. Cavaliere[27], N. Cavalli[21a,21b], V. Cavasinni[69a,69b], E. Celebi[11b], F. Celli[131], K. Cerny[127], A. S. Cerqueira[78a], A. Cerri[153], L. Cerrito[71a,71b], F. Cerutti[16], A. Cervelli[21b], S. A. Cetin[11b], Z. Chadi[33a], D. Chakraborty[117], M. Chala[136f], J. Chan[177], W. S. Chan[116], W. Y. Chan[88], J. D. Chapman[30], B. Chargeishvili[156b], D. G. Charlton[19], T. P. Charman[90], M. Chatterjee[18], C. C. Chau[32], S. Chekanov[5], S. V. Chekulaev[164a], G. A. Chelkov[77,ag], A. Chen[103], B. Chen[158], C. Chen[58a], C. H. Chen[76], H. Chen[13c], H. Chen[27], J. Chen[58a], J. Chen[37], J. Chen[24], S. Chen[133], S. J. Chen[13c], X. Chen[13b], Y. Chen[58a], Y-H. Chen[44], C. L. Cheng[177], H. C. Cheng[60a], H. J. Cheng[13a], A. Cheplakov[77], E. Cheremushkina[44], R. Cherkaoui El Moursli[33e], E. Cheu[6], K. Cheung[61], L. Chevalier[141], V. Chiarella[49], G. Chiarelli[69a], G. Chiodini[65a], A. S. Chisholm[19], A. Chitan[25b], I. Chiu[160], Y. H. Chiu[172], M. V. Chizhov[77,t], K. Choi[10], A. R. Chomont[70a,70b], Y. Chou[100], Y. S. Chow[116], L. D. Christopher[31f], M. C. Chu[60a], X. Chu[13a,13d], J. Chudoba[137], J. J. Chwastowski[82], D. Cieri[112], K. M. Ciesla[82], V. Cindro[89], I. A. Cioară[25b], A. Ciocio[16], F. Cirotto[67a,67b], Z. H. Citron[176,l], M. Citterio[66a], D. A. Ciubotaru[25b], B. M. Ciungu[163], A. Clark[52], P. J. Clark[48], S. E. Clawson[98], C. Clement[43a,43b], L. Clissa[21a,21b], Y. Coadou[99], M. Cobal[64a,64c], A. Coccaro[53b], J. Cochran[76], R. F. Coelho Barrue[136a], R. Coelho Lopes De Sa[100], S. Coelli[66a], H. Cohen[158], A. E. C. Coimbra[34], B. Cole[37], J. Collot[56], P. Conde Muiño[136a,136h], S. H. Connell[31c], I. A. Connelly[55], E. I. Conroy[131], F. Conventi[67a,al], H. G. Cooke[19], A. M. Cooper-Sarkar[131], F. Cormier[171], L. D. Corpe[34], M. Corradi[70a,70b], E. E. Corrigan[94], F. Corriveau[101,aa], M. J. Costa[170], F. Costanza[4], D. Costanzo[146], B. M. Cote[124], G. Cowan[91], J. W. Cowley[30], J. Crane[98], K. Cranmer[122], R. A. Creager[133], S. Crépé-Renaudin[56], F. Crescioli[132], M. Cristinziani[148], M. Cristoforetti[73a,73b,b], V. Croft[166], G. Crosetti[39a,39b], A. Cueto[4], T. Cuhadar Donszelmann[167], H. Cui[13a,13d], A. R. Cukierman[150], W. R. Cunningham[55], S. Czekierda[82], P. Czodrowski[34], M. M. Czurylo[59b], M. J. Da Cunha Sargedas De Sousa[58a], J. V. Da Fonseca Pinto[78b], C. Da Via[98], W. Dabrowski[81a], T. Dado[45], S. Dahbi[31f], T. Dai[103], C. Dallapiccola[100], M. Dam[38], G. D'amen[27], V. D'Amico[72a,72b], J. Damp[97], J. R. Dandoy[133], M. F. Daneri[28], M. Danninger[149], V. Dao[34], G. Darbo[53b], S. Darmora[5], A. Dattagupta[128], S. D'Auria[66a,66b], C. David[164b], T. Davidek[139], D. R. Davis[47], B. Davis-Purcell[32], I. Dawson[90], K. De[7], R. De Asmundis[67a], M. De Beurs[116], S. De Castro[21a,21b], N. De Groot[115], P. de Jong[116], H. De la Torre[104], A. De Maria[13c], D. De Pedis[70a], A. De Salvo[70a], U. De Sanctis[71a,71b], M. De Santis[71a,71b], A. De Santo[153], J. B. De Vivie De Regie[56], D. V. Dedovich[77], J. Degens[116], A. M. Deiana[40], J. Del Peso[96], Y. Delabat Diaz[44], F. Deliot[141], C. M. Delitzsch[6], M. Della Pietra[67a,67b], D. Della Volpe[52], A. Dell'Acqua[34], L. Dell'Asta[66a,66b], M. Delmastro[4], P. A. Delsart[56], S. Demers[179], M. Demichev[77], S. P. Denisov[119], L. D'Eramo[117], D. Derendarz[82], J. E. Derkaoui[33d], F. Derue[132], P. Dervan[88], K. Desch[22], K. Dette[163], C. Deutsch[22], P. O. Deviveiros[34], F. A. Di Bello[70a,70b], A. Di Ciaccio[71a,71b], L. Di Ciaccio[4], C. Di Donato[67a,67b], A. Di Girolamo[34], G. Di Gregorio[69a,69b], A. Di Luca[73a,73b], B. Di Micco[72a,72b], R. Di Nardo[72a,72b], C. Diaconu[99], F. A. Dias[116], T. Dias Do Vale[136a], M. A. Diaz[143a], F. G. Diaz Capriles[22], J. Dickinson[16], M. Didenko[170], E. B. Diehl[103], J. Dietrich[17], S. Díez Cornell[44], C. Diez Pardos[148], A. Dimitrievska[16], W. Ding[13b], J. Dingfelder[22], I-M. Dinu[25b],

S. J. Dittmeier[59b], F. Dittus[34], F. Djama[99], T. Djobava[156b], J. I. Djuvsland[15], M. A. B. Do Vale[144], D. Dodsworth[24], C. Doglioni[94], J. Dolejsi[139], Z. Dolezal[139], M. Donadelli[78c], B. Dong[58c], J. Donini[36], A. D'onofrio[13c], M. D'Onofrio[88], J. Dopke[140], A. Doria[67a], M. T. Dova[86], A. T. Doyle[55], E. Drechsler[149], E. Dreyer[149], T. Dreyer[51], A. S. Drobac[166], D. Du[58b], T. A. du Pree[116], F. Dubinin[108], M. Dubovsky[26a], A. Dubreuil[52], E. Duchovni[176], G. Duckeck[111], O. A. Ducu[25b,34], D. Duda[112], A. Dudarev[34], M. D'uffizi[98], L. Duflot[62], M. Dührssen[34], C. Dülsen[178], A. E. Dumitriu[25b], M. Dunford[59a], S. Dungs[45], A. Duperrin[99], H. Duran Yildiz[3a], M. Düren[54], A. Durglishvili[156b], B. Dutta[44], D. Duvnjak[1], G. I. Dyckes[133], M. Dyndal[81a], S. Dysch[98], B. S. Dziedzic[82], B. Eckerova[26a], M. G. Eggleston[47], E. Egidio Purcino De Souza[78b], L. F. Ehrke[52], T. Eifert[7], G. Eigen[15], K. Einsweiler[16], T. Ekelof[168], Y. El Ghazali[33b], H. El Jarrari[33e], A. El Moussaouy[33a], V. Ellajosyula[168], M. Ellert[168], F. Ellinghaus[178], A. A. Elliot[90], N. Ellis[34], J. Elmsheuser[27], M. Elsing[34], D. Emeliyanov[140], A. Emerman[37], Y. Enari[160], J. Erdmann[45], A. Ereditato[18], P. A. Erland[82], M. Errenst[178], M. Escalier[62], C. Escobar[170], O. Estrada Pastor[170], E. Etzion[158], G. Evans[136a], H. Evans[63], M. O. Evans[153], A. Ezhilov[134], F. Fabbri[55], L. Fabbri[21a,21b], V. Fabiani[115], G. Facini[174], V. Fadeyev[142], R. M. Fakhrutdinov[119], S. Falciano[70a], P. J. Falke[22], S. Falke[34], J. Faltova[139], Y. Fan[13a], Y. Fang[13a], Y. Fang[13a], G. Fanourakis[42], M. Fanti[66a,66b], M. Faraj[58c], A. Farbin[7], A. Farilla[72a], E. M. Farina[68a,68b], T. Farooque[104], S. M. Farrington[48], P. Farthouat[34], F. Fassi[33e], D. Fassouliotis[8], M. Faucci Giannelli[71a,71b], W. J. Fawcett[30], L. Fayard[62], O. L. Fedin[134,q], M. Feickert[169], L. Feligioni[99], A. Fell[146], C. Feng[58b], M. Feng[13b], M. J. Fenton[167], A. B. Fenyuk[119], S. W. Ferguson[41], J. Ferrando[44], A. Ferrari[168], P. Ferrari[116], R. Ferrari[68a], D. Ferrere[52], C. Ferretti[103], F. Fiedler[97], A. Filipčič[89], F. Filthaut[115], M. C. N. Fiolhais[136a,136c,a], L. Fiorini[170], F. Fischer[148], W. C. Fisher[104], T. Fitschen[19], I. Fleck[148], P. Fleischmann[103], T. Flick[178], B. M. Flierl[111], L. Flores[133], L. R. Flores Castillo[60a], F. M. Follega[73a,73b], N. Fomin[15], J. H. Foo[163], G. T. Forcolin[73a,73b], B. C. Forland[63], A. Formica[141], F. A. Förster[12], A. C. Forti[98], E. Fortin[99], M. G. Foti[131], D. Fournier[62], H. Fox[87], P. Francavilla[69a,69b], S. Francescato[70a,70b], M. Franchini[21a,21b], S. Franchino[59a], D. Francis[34], L. Franco[4], L. Franconi[18], M. Franklin[57], G. Frattari[70a,70b], A. C. Freegard[90], P. M. Freeman[19], B. Freund[107], W. S. Freund[78b], E. M. Freundlich[45], D. Froidevaux[34], J. A. Frost[131], Y. Fu[58a], M. Fujimoto[123], E. Fullana Torregrosa[170], J. Fuster[170], A. Gabrielli[21a,21b], A. Gabrielli[34], P. Gadow[44], G. Gagliardi[53a,53b], L. G. Gagnon[16], G. E. Gallardo[131], E. J. Gallas[131], B. J. Gallop[140], R. Gamboa Goni[90], K. K. Gan[124], S. Ganguly[176], J. Gao[58a], Y. Gao[48], Y. S. Gao[29,n], F. M. Garay Walls[143a], C. García[170], J. E. García Navarro[170], J. A. García Pascual[13a], M. Garcia-Sciveres[16], R. W. Gardner[35], D. Garg[75], S. Gargiulo[50], C. A. Garner[163], V. Garonne[130], S. J. Gasiorowski[145], P. Gaspar[78b], G. Gaudio[68a], P. Gauzzi[70a,70b], I. L. Gavrilenko[108], A. Gavrilyuk[120], C. Gay[171], G. Gaycken[44], E. N. Gazis[9], A. A. Geanta[25b], C. M. Gee[142], C. N. P. Gee[140], J. Geisen[94], M. Geisen[97], C. Gemme[53b], M. H. Genest[56], S. Gentile[70a,70b], S. George[91], T. Geralis[42], L. O. Gerlach[51], P. Gessinger-Befurt[97], M. Ghasemi Bostanabad[172], M. Ghneimat[148], A. Ghosh[167], A. Ghosh[75], B. Giacobbe[21b], S. Giagu[70a,70b], N. Giangiacomi[163], P. Giannetti[69a], A. Giannini[67a,67b], S. M. Gibson[91], M. Gignac[142], D. T. Gil[81b], B. J. Gilbert[37], D. Gillberg[32], G. Gilles[178], N. E. K. Gillwald[44], D. M. Gingrich[2,ak], M. P. Giordani[64a,64c], P. F. Giraud[141], G. Giugliarelli[64a,64c], D. Giugni[66a], F. Giuli[71a,71b], I. Gkialas[8,i], E. L. Gkougkousis[12], P. Gkountoumis[9], L. K. Gladilin[110], C. Glasman[96], G. R. Gledhill[128], M. Glisic[128], I. Gnesi[39b,d], M. Goblirsch-Kolb[24], D. Godin[107], S. Goldfarb[102], T. Golling[52], D. Golubkov[119], J. P. Gombas[104], A. Gomes[136a,136b], R. Goncalves Gama[51], R. Gonçalo[136a,136c], G. Gonella[128], L. Gonella[19], A. Gongadze[77], F. Gonnella[19], J. L. Gonski[37], S. González de la Hoz[170], S. Gonzalez Fernandez[12], R. Gonzalez Lopez[88], C. Gonzalez Renteria[16], R. Gonzalez Suarez[168], S. Gonzalez-Sevilla[52], G. R. Gonzalvo Rodriguez[170], R. Y. González Andana[143a], L. Goossens[34], N. A. Gorasia[19], P. A. Gorbounov[120], H. A. Gordon[27], B. Gorini[34], E. Gorini[65a,65b], A. Gorišek[89], A. T. Goshaw[47], M. I. Gostkin[77], C. A. Gottardo[115], M. Gouighri[33b], V. Goumarre[44], A. G. Goussiou[145], N. Govender[31c], C. Goy[4], I. Grabowska-Bold[81a], K. Graham[32], E. Gramstad[130], S. Grancagnolo[17], M. Grandi[153], V. Gratchev[134], P. M. Gravila[25f], F. G. Gravili[65a,65b], H. M. Gray[16], C. Grefe[22], I. M. Gregor[44], P. Grenier[150], K. Grevtsov[44], C. Grieco[12], N. A. Grieser[125], A. A. Grillo[142], K. Grimm[29,m], S. Grinstein[12,x], J.-F. Grivaz[62], S. Groh[97], E. Gross[176], J. Grosse-Knetter[51], Z. J. Grout[92], C. Grud[103], A. Grummer[114], J. C. Grundy[131], L. Guan[103], W. Guan[177], C. Gubbels[171], J. Guenther[34], J. G. R. Guerrero Rojas[170], F. Guescini[112], D. Guest[17], R. Gugel[97], A. Guida[44], T. Guillemin[4], S. Guindon[34], J. Guo[58c], L. Guo[62], Y. Guo[103], R. Gupta[44], S. Gurbuz[22], G. Gustavino[125], M. Guth[50], P. Gutierrez[125], L. F. Gutierrez Zagazeta[133], C. Gutschow[92], C. Guyot[141], C. Gwenlan[131], C. B. Gwilliam[88], E. S. Haaland[130], A. Haas[122], M. Habedank[17],

C. Haber[16], H. K. Hadavand[7], A. Hadef[97], M. Haleem[173], J. Haley[126], J. J. Hall[146], G. Halladjian[104], G. D. Hallewell[99], L. Halser[18], K. Hamano[172], H. Hamdaoui[33e], M. Hamer[22], G. N. Hamity[48], K. Han[58a], L. Han[13c], L. Han[58a], S. Han[16], Y. F. Han[163], K. Hanagaki[79,v], M. Hance[142], M. D. Hank[35], R. Hankache[98], E. Hansen[94], J. B. Hansen[38], J. D. Hansen[38], M. C. Hansen[22], P. H. Hansen[38], K. Hara[165], T. Harenberg[178], S. Harkusha[105], Y. T. Harris[131], P. F. Harrison[174], N. M. Hartman[150], N. M. Hartmann[111], Y. Hasegawa[147], A. Hasib[48], S. Hassani[141], S. Haug[18], R. Hauser[104], M. Havranek[138], C. M. Hawkes[19], R. J. Hawkings[34], S. Hayashida[113], D. Hayden[104], C. Hayes[103], R. L. Hayes[171], C. P. Hays[131], J. M. Hays[90], H. S. Hayward[88], S. J. Haywood[140], F. He[58a], Y. He[161], Y. He[132], M. P. Heath[48], V. Hedberg[94], A. L. Heggelund[130], N. D. Hehir[90], C. Heidegger[50], K. K. Heidegger[50], W. D. Heidorn[76], J. Heilman[32], S. Heim[44], T. Heim[16], B. Heinemann[44,ai], J. G. Heinlein[133], J. J. Heinrich[128], L. Heinrich[34], J. Hejbal[137], L. Helary[44], A. Held[122], S. Hellesund[130], C. M. Helling[142], S. Hellman[43a,43b], C. Helsens[34], R. C. W. Henderson[87], L. Henkelmann[30], A. M. Henriques Correia[34], H. Herde[150], Y. Hernández Jiménez[152], H. Herr[97], M. G. Herrmann[111], T. Herrmann[46], G. Herten[50], R. Hertenberger[111], L. Hervas[34], N. P. Hessey[164a], H. Hibi[80], S. Higashino[79], E. Higón-Rodriguez[170], K. K. Hill[27], K. H. Hiller[44], S. J. Hillier[19], M. Hils[46], I. Hinchliffe[16], F. Hinterkeuser[22], M. Hirose[129], S. Hirose[165], D. Hirschbuehl[178], B. Hiti[89], O. Hladik[137], J. Hobbs[152], R. Hobincu[25e], N. Hod[176], M. C. Hodgkinson[146], B. H. Hodkinson[30], A. Hoecker[34], J. Hofer[44], D. Hohn[50], T. Holm[22], T. R. Holmes[35], M. Holzbock[112], L. B. A. H. Hommels[30], B. P. Honan[98], T. M. Hong[135], J. C. Honig[50], A. Hönle[112], B. H. Hooberman[169], W. H. Hopkins[5], Y. Horii[113], P. Horn[46], L. A. Horyn[35], S. Hou[155], J. Howarth[55], J. Hoya[86], M. Hrabovsky[127], A. Hrynevich[106], T. Hryn'ova[4], P. J. Hsu[61], S.-C. Hsu[145], Q. Hu[37], S. Hu[58c], Y. F. Hu[13a,13d,am], D. P. Huang[92], X. Huang[13c], Y. Huang[58a], Y. Huang[13a], Z. Hubacek[138], F. Hubaut[99], M. Huebner[22], F. Huegging[22], T. B. Huffman[131], M. Huhtinen[34], R. Hulsken[56], N. Huseynov[77,ab], J. Huston[104], J. Huth[57], R. Hyneman[150], S. Hyrych[26a], G. Iacobucci[52], G. Iakovidis[27], I. Ibragimov[148], L. Iconomidou-Fayard[62], P. Iengo[34], R. Ignazzi[38], R. Iguchi[160], T. Iizawa[52], Y. Ikegami[79], A. Ilg[18], N. Ilic[163], H. Imam[33a], T. Ingebretsen Carlson[43a,43b], G. Introzzi[68a,68b], M. Iodice[72a], V. Ippolito[70a,70b], M. Ishino[160], W. Islam[126], C. Issever[17,44], S. Istin[11c,an], J. M. Iturbe Ponce[60a], R. Iuppa[73a,73b], A. Ivina[176], J. M. Izen[41], V. Izzo[67a], P. Jacka[137], P. Jackson[1], R. M. Jacobs[44], B. P. Jaeger[149], C. S. Jagfeld[111], G. Jäkel[178], K. B. Jakobi[97], K. Jakobs[50], T. Jakoubek[176], J. Jamieson[55], K. W. Janas[81a], G. Jarlskog[94], A. E. Jaspan[88], N. Javadov[77,ab], T. Javůrek[34], M. Javurkova[100], F. Jeanneau[141], L. Jeanty[128], J. Jejelava[156a,ac], P. Jenni[50,e], S. Jézéquel[4], J. Jia[152], Z. Jia[13c], Y. Jiang[58a], S. Jiggins[50], J. Jimenez Pena[112], S. Jin[13c], A. Jinaru[25b], O. Jinnouchi[161], H. Jivan[31f], P. Johansson[146], K. A. Johns[6], C. A. Johnson[63], E. Jones[174], R. W. L. Jones[87], T. J. Jones[88], J. Jovicevic[51], X. Ju[16], J. J. Junggeburth[34], A. Juste Rozas[12,x], A. Kaczmarska[82], M. Kado[70a,70b], H. Kagan[124], M. Kagan[150], A. Kahn[37], C. Kahra[97], T. Kaji[175], E. Kajomovitz[157], C. W. Kalderon[27], A. Kaluza[97], A. Kamenshchikov[119], M. Kaneda[160], N. J. Kang[142], S. Kang[76], Y. Kano[113], J. Kanzaki[79], D. Kar[31f], K. Karava[131], M. J. Kareem[164b], I. Karkanias[159], S. N. Karpov[77], Z. M. Karpova[77], V. Kartvelishvili[87], A. N. Karyukhin[119], E. Kasimi[159], C. Kato[58d], J. Katzy[44], K. Kawade[147], K. Kawagoe[85], T. Kawaguchi[113], T. Kawamoto[141], G. Kawamura[51], E. F. Kay[172], F. I. Kaya[166], S. Kazakos[12], V. F. Kazanin[118a,118b], Y. Ke[152], J. M. Keaveney[31a], R. Keeler[172], J. S. Keller[32], D. Kelsey[153], J. J. Kempster[19], J. Kendrick[19], K. E. Kennedy[37], O. Kepka[137], S. Kersten[178], B. P. Kerševan[89], S. Ketabchi Haghighat[163], M. Khandoga[132], A. Khanov[126], A. G. Kharlamov[118a,118b], T. Kharlamova[118a,118b], E. E. Khoda[171], T. J. Khoo[17], G. Khoriauli[173], E. Khramov[77], J. Khubua[156b], S. Kido[80], M. Kiehn[34], A. Kilgallon[128], E. Kim[161], Y. K. Kim[35], N. Kimura[92], A. Kirchhoff[51], D. Kirchmeier[46], J. Kirk[140], A. E. Kiryunin[112], T. Kishimoto[160], D. P. Kisliuk[163], V. Kitali[44], C. Kitsaki[9], O. Kivernyk[22], T. Klapdor-Kleingrothaus[50], M. Klassen[59a], C. Klein[32], L. Klein[173], M. H. Klein[103], M. Klein[88], U. Klein[88], P. Klimek[34], A. Klimentov[27], F. Klimpel[34], T. Klingl[22], T. Klioutchnikova[34], F. F. Klitzner[111], P. Kluit[116], S. Kluth[112], E. Kneringer[74], T. M. Knight[163], A. Knue[50], D. Kobayashi[85], M. Kobel[46], M. Kocian[150], T. Kodama[160], P. Kodys[139], D. M. Koeck[153], P. T. Koenig[22], T. Koffas[32], N. M. Köhler[34], M. Kolb[141], I. Koletsou[4], T. Komarek[127], K. Köneke[50], A. X. Y. Kong[1], T. Kono[123], V. Konstantinides[92], N. Konstantinidis[92], B. Konya[94], R. Kopeliansky[63], S. Koperny[81a], K. Korcyl[82], K. Kordas[159], G. Koren[158], A. Korn[92], S. Korn[51], I. Korolkov[12], E. V. Korolkova[146], N. Korotkova[110], B. Kortman[116], O. Kortner[112], S. Kortner[112], V. V. Kostyukhin[146,162], A. Kotsokechagia[62], A. Kotwal[47], A. Koulouris[34], A. Kourkoumeli-Charalampidi[68a,68b], C. Kourkoumelis[8], E. Kourlitis[5], R. Kowalewski[172], W. Kozanecki[141], A. S. Kozhin[119], V. A. Kramarenko[110], G. Kramberger[89], D. Krasnopevtsev[58a], M. W. Krasny[132], A. Krasznahorkay[34], J. A. Kremer[97], J. Kretzschmar[88], K. Kreul[17], P. Krieger[163],

F. Krieter[111], S. Krishnamurthy[100], A. Krishnan[59b], M. Krivos[139], K. Krizka[16], K. Kroeninger[45], H. Kroha[112], J. Kroll[137], J. Kroll[133], K. S. Krowpman[104], U. Kruchonak[77], H. Krüger[22], N. Krumnack[76], M. C. Kruse[47], J. A. Krzysiak[82], A. Kubota[161], O. Kuchinskaia[162], S. Kuday[3b], D. Kuechler[44], J. T. Kuechler[44], S. Kuehn[34], T. Kuhl[44], V. Kukhtin[77], Y. Kulchitsky[105,af], S. Kuleshov[143c], M. Kumar[31f], N. Kumari[99], M. Kuna[56], A. Kupco[137], T. Kupfer[45], O. Kuprash[50], H. Kurashige[80], L. L. Kurchaninov[164a], Y. A. Kurochkin[105], A. Kurova[109], M. G. Kurth[13a,13d], E. S. Kuwertz[34], M. Kuze[161], A. K. Kvam[145], J. Kvita[127], T. Kwan[101], C. Lacasta[170], F. Lacava[70a,70b], H. Lacker[17], D. Lacour[132], N. N. Lad[92], E. Ladygin[77], R. Lafaye[4], B. Laforge[132], T. Lagouri[143d], S. Lai[51], I. K. Lakomiec[81a], N. Lalloue[56], J. E. Lambert[125], S. Lammers[63], W. Lampl[6], C. Lampoudis[159], E. Lançon[27], U. Landgraf[50], M. P. J. Landon[90], V. S. Lang[50], J. C. Lange[51], R. J. Langenberg[100], A. J. Lankford[167], F. Lanni[27], K. Lantzsch[22], A. Lanza[68a], A. Lapertosa[53a,53b], J. F. Laporte[141], T. Lari[66a], F. Lasagni Manghi[21b], M. Lassnig[34], V. Latonova[137], T. S. Lau[60a], A. Laudrain[97], A. Laurier[32], M. Lavorgna[67a,67b], S. D. Lawlor[91], M. Lazzaroni[66a,66b], B. Le[98], B. Leban[89], A. Lebedev[76], M. LeBlanc[34], T. LeCompte[5], F. Ledroit-Guillon[56], A. C. A. Lee[92], C. A. Lee[27], G. R. Lee[15], L. Lee[57], S. C. Lee[155], S. Lee[76], L. L. Leeuw[31c], B. Lefebvre[164a], H. P. Lefebvre[91], M. Lefebvre[172], C. Leggett[16], K. Lehmann[149], N. Lehmann[18], G. Lehmann Miotto[34], W. A. Leight[44], A. Leisos[159,w], M. A. L. Leite[78c], C. E. Leitgeb[44], R. Leitner[139], K. J. C. Leney[40], T. Lenz[22], S. Leone[69a], C. Leonidopoulos[48], A. Leopold[132], C. Leroy[107], R. Les[104], C. G. Lester[30], M. Levchenko[134], J. Levêque[4], D. Levin[103], L. J. Levinson[176], D. J. Lewis[19], B. Li[13b], B. Li[58b], C. Li[58a], C-Q. Li[58c,58d], H. Li[58a], H. Li[58b], J. Li[58c], K. Li[145], L. Li[58c], M. Li[13a,13d], Q. Y. Li[58a], S. Li[58c,58d,c], X. Li[44], Y. Li[44], Z. Li[58b], Z. Li[131], Z. Li[101], Z. Li[88], Z. Liang[13a], M. Liberatore[44], B. Liberti[71a], K. Lie[60c], K. Lin[104], R. A. Linck[63], R. E. Lindley[6], J. H. Lindon[2], A. Linss[44], A. L. Lionti[52], E. Lipeles[133], A. Lipniacka[15], T. M. Liss[169,aj], A. Lister[171], J. D. Little[7], B. Liu[13a], B. X. Liu[149], J. B. Liu[58a], J. K. K. Liu[35], K. Liu[58c,58d], M. Liu[58a], M. Y. Liu[58a], P. Liu[13a], X. Liu[58a], Y. Liu[44], Y. Liu[13c,13d], Y. L. Liu[103], Y. W. Liu[58a], M. Livan[68a,68b], A. Lleres[56], J. Llorente Merino[149], S. L. Lloyd[90], E. M. Lobodzinska[44], P. Loch[6], S. Loffredo[71a,71b], T. Lohse[17], K. Lohwasser[146], M. Lokajicek[137], J. D. Long[169], R. E. Long[87], I. Longarini[70a,70b], L. Longo[34], R. Longo[169], I. Lopez Paz[12], A. Lopez Solis[44], J. Lorenz[111], N. Lorenzo Martinez[4], A. M. Lory[111], A. Lösle[50], X. Lou[43a,43b], X. Lou[13a], A. Lounis[62], J. Love[5], P. A. Love[87], J. J. Lozano Bahilo[170], G. Lu[13a], M. Lu[58a], S. Lu[133], Y. J. Lu[61], H. J. Lubatti[145], C. Luci[70a,70b], F. L. Lucio Alves[13c], A. Lucotte[56], F. Luehring[63], I. Luise[152], L. Luminari[70a], B. Lund-Jensen[151], N. A. Luongo[128], M. S. Lutz[158], D. Lynn[27], H. Lyons[88], R. Lysak[137], E. Lytken[94], F. Lyu[13a], V. Lyubushkin[77], T. Lyubushkina[77], H. Ma[27], L. L. Ma[58b], Y. Ma[92], D. M. Mac Donell[172], G. Maccarrone[49], C. M. Macdonald[146], J. C. MacDonald[146], R. Madar[36], W. F. Mader[46], M. Madugoda Ralalage Don[126], N. Madysa[46], J. Maeda[80], T. Maeno[27], M. Maerker[46], V. Magerl[50], J. Magro[64a,64c], D. J. Mahon[37], C. Maidantchik[78b], A. Maio[136a,136b,136d], K. Maj[81a], O. Majersky[26a], S. Majewski[128], N. Makovec[62], B. Malaescu[132], Pa. Malecki[82], V. P. Maleev[134], F. Malek[56], D. Malito[39a,39b], U. Mallik[75], C. Malone[30], S. Maltezos[9], S. Malyukov[77], J. Mamuzic[170], G. Mancini[49], J. P. Mandalia[90], I. Mandić[89], L. Manhaes de Andrade Filho[78a], I. M. Maniatis[159], M. Manisha[141], J. Manjarres Ramos[46], K. H. Mankinen[94], A. Mann[111], A. Manousos[74], B. Mansoulie[141], I. Manthos[159], S. Manzoni[116], A. Marantis[159,w], L. Marchese[131], G. Marchiori[132], M. Marcisovsky[137], L. Marcoccia[71a,71b], C. Marcon[94], M. Marjanovic[125], Z. Marshall[16], S. Marti-Garcia[170], T. A. Martin[174], V. J. Martin[48], B. Martin dit Latour[15], L. Martinelli[70a,70b], M. Martinez[12,x], P. Martinez Agullo[170], V. I. Martinez Outschoorn[100], S. Martin-Haugh[140], V. S. Martoiu[25b], A. C. Martyniuk[92], A. Marzin[34], S. R. Maschek[112], L. Masetti[97], T. Mashimo[160], R. Mashinistov[108], J. Masik[98], A. L. Maslennikov[118a,118b], L. Massa[21b], P. Massarotti[67a,67b], P. Mastrandrea[69a,69b], A. Mastroberardino[39a,39b], T. Masubuchi[160], D. Matakias[27], T. Mathisen[168], A. Matic[111], N. Matsuzawa[160], J. Maurer[25b], B. Maček[89], D. A. Maximov[118a,118b], R. Mazini[155], I. Maznas[159], S. M. Mazza[142], C. Mc Ginn[27], J. P. Mc Gowan[101], S. P. Mc Kee[103], T. G. McCarthy[112], W. P. McCormack[16], E. F. McDonald[102], A. E. McDougall[116], J. A. Mcfayden[153], G. Mchedlidze[156b], M. A. McKay[40], K. D. McLean[172], S. J. McMahon[140], P. C. McNamara[102], R. A. McPherson[172,aa], J. E. Mdhluli[31f], Z. A. Meadows[100], S. Meehan[34], T. Megy[36], S. Mehlhase[111], A. Mehta[88], B. Meirose[41], D. Melini[157], B. R. Mellado Garcia[31f], F. Meloni[44], A. Melzer[22], E. D. Mendes Gouveia[136a], A. M. Mendes Jacques Da Costa[19], H. Y. Meng[163], L. Meng[34], S. Menke[112], M. Mentink[34], E. Meoni[39a,39b], S. A. M. Merkt[135], C. Merlassino[131], P. Mermod[52,*], L. Merola[67a,67b], C. Meroni[66a], G. Merz[103], O. Meshkov[108,110], J. K. R. Meshreki[148], J. Metcalfe[5], A. S. Mete[5], C. Meyer[63], J-P. Meyer[141], M. Michetti[17], R. P. Middleton[140], L. Mijović[48], G. Mikenberg[176], M. Mikestikova[137],

M. Mikuž[89], H. Mildner[146], A. Milic[163], C. D. Milke[40], D. W. Miller[35], L. S. Miller[32], A. Milov[176], D. A. Milstead[43a,43b], A. A. Minaenko[119], I. A. Minashvili[156b], L. Mince[55], A. I. Mincer[122], B. Mindur[81a], M. Mineev[77], Y. Minegishi[160], Y. Mino[83], L. M. Mir[12], M. Miralles Lopez[170], M. Mironova[131], T. Mitani[175], V. A. Mitsou[170], M. Mittal[58c], O. Miu[163], P. S. Miyagawa[90], Y. Miyazaki[85], A. Mizukami[79], J. U. Mjörnmark[94], T. Mkrtchyan[59a], M. Mlynarikova[117], T. Moa[43a,43b], S. Mobius[51], K. Mochizuki[107], P. Moder[44], P. Mogg[111], A. F. Mohammed[13a], S. Mohapatra[37], G. Mokgatitswane[31f], B. Mondal[148], S. Mondal[138], K. Mönig[44], E. Monnier[99], A. Montalbano[149], J. Montejo Berlingen[34], M. Montella[124], F. Monticelli[86], N. Morange[62], A. L. Moreira De Carvalho[136a], M. Moreno Llácer[170], C. Moreno Martinez[12], P. Morettini[53b], M. Morgenstern[157], S. Morgenstern[174], D. Mori[149], M. Morii[57], M. Morinaga[160], V. Morisbak[130], A. K. Morley[34], A. P. Morris[92], L. Morvaj[34], P. Moschovakos[34], B. Moser[116], M. Mosidze[156b], T. Moskalets[50], P. Moskvitina[115], J. Moss[29,o], E. J. W. Moyse[100], S. Muanza[99], J. Mueller[135], D. Muenstermann[87], G. A. Mullier[94], J. J. Mullin[133], D. P. Mungo[66a,66b], J. L. Munoz Martinez[12], F. J. Munoz Sanchez[98], M. Murin[98], P. Murin[26b], W. J. Murray[140,174], A. Murrone[66a,66b], J. M. Muse[125], M. Muškinja[16], C. Mwewa[27], A. G. Myagkov[119,ag], A. A. Myers[135], G. Myers[63], M. Myska[138], B. P. Nachman[16], O. Nackenhorst[45], A.Nag Nag[46], K. Nagai[131], K. Nagano[79], J. L. Nagle[27], E. Nagy[99], A. M. Nairz[34], Y. Nakahama[113], K. Nakamura[79], H. Nanjo[129], F. Napolitano[59a], R. Narayan[40], I. Naryshkin[134], M. Naseri[32], C. Nass[22], T. Naumann[44], G. Navarro[20a], J. Navarro-Gonzalez[170], P. Y. Nechaeva[108], F. Nechansky[44], T. J. Neep[19], A. Negri[68a,68b], M. Negrini[21b], C. Nellist[115], C. Nelson[101], K. Nelson[103], M. E. Nelson[43a,43b], S. Nemecek[137], M. Nessi[34,g], M. S. Neubauer[169], F. Neuhaus[97], J. Neundorf[44], R. Newhouse[171], P. R. Newman[19], C. W. Ng[135], Y. S. Ng[17], Y. W. Y. Ng[167], B. Ngair[33e], H. D. N. Nguyen[99], T. Nguyen Manh[107], R. B. Nickerson[131], R. Nicolaidou[141], D. S. Nielsen[38], J. Nielsen[142], M. Niemeyer[51], N. Nikiforou[10], V. Nikolaenko[119,ag], I. Nikolic-Audit[132], K. Nikolopoulos[19], P. Nilsson[27], H. R. Nindhito[52], A. Nisati[70a], N. Nishu[2], R. Nisius[112], T. Nitta[175], T. Nobe[160], D. L. Noel[30], Y. Noguchi[83], I. Nomidis[132], M. A. Nomura[27], M. B. Norfolk[146], R. R. B. Norisam[92], J. Novak[89], T. Novak[44], O. Novgorodova[46], L. Novotny[138], R. Novotny[114], L. Nozka[127], K. Ntekas[167], E. Nurse[92], F. G. Oakham[32,ak], J. Ocariz[132], A. Ochi[80], I. Ochoa[136a], J. P. Ochoa-Ricoux[143a], K. O'Connor[24], S. Oda[85], S. Odaka[79], S. Oerdek[168], A. Ogrodnik[81a], A. Oh[98], C. C. Ohm[151], H. Oide[161], R. Oishi[160], M. L. Ojeda[163], Y. Okazaki[83], M. W. O'Keefe[88], Y. Okumura[160], A. Olariu[25b], L. F. Oleiro Seabra[136a], S. A. Olivares Pino[143d], D. Oliveira Damazio[27], D. Oliveira Goncalves[78a], J. L. Oliver[1], M. J. R. Olsson[167], A. Olszewski[82], J. Olszowska[82], Ö. O. Öncel[22], D. C. O'Neil[149], A. P. O'neill[131], A. Onofre[136a,136e], P. U. E. Onyisi[10], H. Oppen[130], R. G. Oreamuno Madriz[117], M. J. Oreglia[35], G. E. Orellana[86], D. Orestano[72a,72b], N. Orlando[12], R. S. Orr[163], V. O'Shea[55], R. Ospanov[58a], G. Otero y Garzon[28], H. Otono[85], P. S. Ott[59a], G. J. Ottino[16], M. Ouchrif[33d], J. Ouellette[27], F. Ould-Saada[130], A. Ouraou[141,*], Q. Ouyang[13a], M. Owen[55], R. E. Owen[140], V. E. Ozcan[11c], N. Ozturk[7], S. Ozturk[11c], J. Pacalt[127], H. A. Pacey[30], K. Pachal[47], A. Pacheco Pages[12], C. Padilla Aranda[12], S. Pagan Griso[16], G. Palacino[63], S. Palazzo[48], S. Palestini[34], M. Palka[81b], P. Palni[81a], D. K. Panchal[10], C. E. Pandini[52], J. G. Panduro Vazquez[91], P. Pani[44], G. Panizzo[64a,64c], L. Paolozzi[52], C. Papadatos[107], S. Parajuli[40], A. Paramonov[5], C. Paraskevopoulos[9], D. Paredes Hernandez[60b], S. R. Paredes Saenz[131], B. Parida[176], T. H. Park[163], A. J. Parker[29], M. A. Parker[30], F. Parodi[53a,53b], E. W. Parrish[117], J. A. Parsons[37], U. Parzefall[50], L. Pascual Dominguez[158], V. R. Pascuzzi[16], F. Pasquali[116], E. Pasqualucci[70a], S. Passaggio[53b], F. Pastore[91], P. Pasuwan[43a,43b], J. R. Pater[98], A. Pathak[177], J. Patton[88], T. Pauly[34], J. Pearkes[150], M. Pedersen[130], L. Pedraza Diaz[115], R. Pedro[136a], T. Peiffer[51], S. V. Peleganchuk[118a,118b], O. Penc[137], C. Peng[60b], H. Peng[58a], M. Penzin[162], B. S. Peralva[78a], M. M. Perego[62], A. P. Pereira Peixoto[136a], L. Pereira Sanchez[43a,43b], D. V. Perepelitsa[27], E. Perez Codina[164a], M. Perganti[9], L. Perini[66a,66b], H. Pernegger[34], S. Perrella[34], A. Perrevoort[116], K. Peters[44], R. F. Y. Peters[98], B. A. Petersen[34], T. C. Petersen[38], E. Petit[99], V. Petousis[138], C. Petridou[159], P. Petroff[62], F. Petrucci[72a,72b], M. Pettee[179], N. E. Pettersson[34], K. Petukhova[139], A. Peyaud[141], R. Pezoa[143e], L. Pezzotti[68a,68b], G. Pezzullo[179], T. Pham[102], P. W. Phillips[140], M. W. Phipps[169], G. Piacquadio[152], E. Pianori[16], F. Piazza[66a,66b], A. Picazio[100], R. Piegaia[28], D. Pietreanu[25b], J. E. Pilcher[35], A. D. Pilkington[98], M. Pinamonti[64a,64c], J. L. Pinfold[2], C. Pitman Donaldson[92], D. A. Pizzi[32], L. Pizzimento[71a,71b], A. Pizzini[116], M.-A. Pleier[27], V. Plesanovs[50], V. Pleskot[139], E. Plotnikova[77], P. Podberezko[118a,118b], R. Poettgen[94], R. Poggi[52], L. Poggioli[132], I. Pogrebnyak[104], D. Pohl[22], I. Pokharel[51], G. Polesello[68a], A. Poley[149,164a], A. Policicchio[70a,70b], R. Polifka[139], A. Polini[21b], C. S. Pollard[44], Z. B. Pollock[124], V. Polychronakos[27], D. Ponomarenko[109], L. Pontecorvo[34], S. Popa[25a], G. A. Popeneciu[25d], L. Portales[4], D. M. Portillo Quintero[56],

S. Pospisil[138], P. Postolache[25c], K. Potamianos[131], I. N. Potrap[77], C. J. Potter[30], H. Potti[1], T. Poulsen[44], J. Poveda[170], T. D. Powell[146], G. Pownall[44], M. E. Pozo Astigarraga[34], A. Prades Ibanez[170], P. Pralavorio[99], M. M. Prapa[42], S. Prell[76], D. Price[98], M. Primavera[65a], M. A. Principe Martin[96], M. L. Proffitt[145], N. Proklova[109], K. Prokofiev[60c], F. Prokoshin[77], S. Protopopescu[27], J. Proudfoot[5], M. Przybycien[81a], D. Pudzha[134], P. Puzo[62], D. Pyatiizbyantseva[109], J. Qian[103], Y. Qin[98], A. Quadt[51], M. Queitsch-Maitland[34], G. Rabanal Bolanos[57], F. Ragusa[66a,66b], G. Rahal[95], J. A. Raine[52], S. Rajagopalan[27], K. Ran[13a,13d], D. F. Rassloff[59a], D. M. Rauch[44], S. Rave[97], B. Ravina[55], I. Ravinovich[176], M. Raymond[34], A. L. Read[130], N. P. Readioff[146], D. M. Rebuzzi[68a,68b], G. Redlinger[27], K. Reeves[41], D. Reikher[158], A. Reiss[97], A. Rej[148], C. Rembser[34], A. Renardi[44], M. Renda[25b], M. B. Rendel[112], A. G. Rennie[55], S. Resconi[66a], E. D. Resseguie[16], S. Rettie[92], B. Reynolds[124], E. Reynolds[19], M. Rezaei Estabragh[178], O. L. Rezanova[118a,118b], P. Reznicek[139], E. Ricci[73a,73b], R. Richter[112], S. Richter[44], E. Richter-Was[81b], M. Ridel[132], P. Rieck[112], P. Riedler[34], O. Rifki[44], M. Rijssenbeek[152], A. Rimoldi[68a,68b], M. Rimoldi[44], L. Rinaldi[21a,21b], T. T. Rinn[169], M. P. Rinnagel[111], G. Ripellino[151], I. Riu[12], P. Rivadeneira[44], J. C. Rivera Vergara[172], F. Rizatdinova[126], E. Rizvi[90], C. Rizzi[52], B. A. Roberts[174], S. H. Robertson[101,aa], M. Robin[44], D. Robinson[30], C. M. Robles Gajardo[143e], M. Robles Manzano[97], A. Robson[55], A. Rocchi[71a,71b], C. Roda[69a,69b], S. Rodriguez Bosca[59a], A. Rodriguez Rodriguez[50], A. M. Rodríguez Vera[164b], S. Roe[34], J. Roggel[178], O. Røhne[130], R. A. Rojas[143e], B. Roland[50], C. P. A. Roland[63], J. Roloff[27], A. Romaniouk[109], M. Romano[21b], N. Rompotis[88], M. Ronzani[122], L. Roos[132], S. Rosati[70a], G. Rosin[100], B. J. Rosser[133], E. Rossi[163], E. Rossi[4], E. Rossi[67a,67b], L. P. Rossi[53b], L. Rossini[44], R. Rosten[124], M. Rotaru[25b], B. Rottler[50], D. Rousseau[62], D. Rousso[30], G. Rovelli[68a,68b], A. Roy[10], A. Rozanov[99], Y. Rozen[157], X. Ruan[31f], A. J. Ruby[88], T. A. Ruggeri[1], F. Rühr[50], A. Ruiz-Martinez[170], A. Rummler[34], Z. Rurikova[50], N. A. Rusakovich[77], H. L. Russell[34], L. Rustige[36], J. P. Rutherfoord[6], E. M. Rüttinger[146], M. Rybar[139], E. B. Rye[130], A. Ryzhov[119], J. A. Sabater Iglesias[44], P. Sabatini[170], L. Sabetta[70a,70b], H.F-W. Sadrozinski[142], R. Sadykov[77], F. Safai Tehrani[70a], B. Safarzadeh Samani[153], M. Safdari[150], P. Saha[117], S. Saha[101], M. Sahinsoy[112], A. Sahu[178], M. Saimpert[141], M. Saito[160], T. Saito[160], D. Salamani[52], G. Salamanna[72a,72b], A. Salnikov[150], J. Salt[170], A. Salvador Salas[12], D. Salvatore[39a,39b], F. Salvatore[153], A. Salzburger[34], D. Sammel[50], D. Sampsonidis[159], D. Sampsonidou[58c,58d], J. Sánchez[170], A. Sanchez Pineda[4], V. Sanchez Sebastian[170], H. Sandaker[130], C. O. Sander[44], I. G. Sanderswood[87], J. A. Sandesara[100], M. Sandhoff[178], C. Sandoval[20b], D. P. C. Sankey[140], M. Sannino[53a,53b], Y. Sano[113], A. Sansoni[49], C. Santoni[36], H. Santos[136a,136b], S. N. Santpur[16], A. Santra[176], K. A. Saoucha[146], A. Sapronov[77], J. G. Saraiva[136a,136d], J. Sardain[99], O. Sasaki[79], K. Sato[165], C. Sauer[59b], F. Sauerburger[50], E. Sauvan[4], P. Savard[163,ak], R. Sawada[160], C. Sawyer[140], L. Sawyer[93], I. Sayago Galvan[170], C. Sbarra[21b], A. Sbrizzi[64a,64c], T. Scanlon[92], J. Schaarschmidt[145], P. Schacht[112], D. Schaefer[35], L. Schaefer[133], U. Schäfer[97], A. C. Schaffer[62], D. Schaile[111], R. D. Schamberger[152], E. Schanet[111], C. Scharf[17], N. Scharmberg[98], V. A. Schegelsky[134], D. Scheirich[139], F. Schenck[17], M. Schernau[167], C. Schiavi[53a,53b], L. K. Schildgen[22], Z. M. Schillaci[24], E. J. Schioppa[65a,65b], M. Schioppa[39a,39b], B. Schlag[97], K. E. Schleicher[50], S. Schlenker[34], K. Schmieden[97], C. Schmitt[97], S. Schmitt[44], L. Schoeffel[141], A. Schoening[59b], P. G. Scholer[50], E. Schopf[131], M. Schott[97], J. Schovancova[34], S. Schramm[52], F. Schroeder[178], H-C. Schultz-Coulon[59a], M. Schumacher[50], B. A. Schumm[142], Ph. Schune[141], A. Schwartzman[150], T. A. Schwarz[103], Ph. Schwemling[141], R. Schwienhorst[104], A. Sciandra[142], G. Sciolla[24], F. Scuri[69a], F. Scutti[102], C. D. Sebastiani[88], K. Sedlaczek[45], P. Seema[17], S. C. Seidel[114], A. Seiden[142], B. D. Seidlitz[27], T. Seiss[35], C. Seitz[44], J. M. Seixas[78b], G. Sekhniaidze[67a], S. J. Sekula[40], L. P. Selem[4], N. Semprini-Cesari[21a,21b], S. Sen[47], C. Serfon[27], L. Serin[62], L. Serkin[64a,64b], M. Sessa[58a], H. Severini[125], S. Sevova[150], F. Sforza[53a,53b], A. Sfyrla[52], E. Shabalina[51], R. Shaheen[151], J. D. Shahinian[133], N. W. Shaikh[43a,43b], D. Shaked Renous[176], L. Y. Shan[13a], M. Shapiro[16], A. Sharma[34], A. S. Sharma[1], S. Sharma[44], P. B. Shatalov[120], K. Shaw[153], S. M. Shaw[98], P. Sherwood[92], L. Shi[92], C. O. Shimmin[179], Y. Shimogama[175], J. D. Shinner[91], I. P. J. Shipsey[131], S. Shirabe[52], M. Shiyakova[77], J. Shlomi[176], M. J. Shochet[35], J. Shojaii[102], D. R. Shope[151], S. Shrestha[124], E. M. Shrif[31f], M. J. Shroff[172], E. Shulga[176], P. Sicho[137], A. M. Sickles[169], E. Sideras Haddad[31f], O. Sidiropoulou[34], A. Sidoti[21b], F. Siegert[46], Dj. Sijacki[14], M. V. Silva Oliveira[34], S. B. Silverstein[43a], S. Simion[62], R. Simoniello[34], S. Simsek[11b], P. Sinervo[163], V. Sinetckii[110], S. Singh[149], S. Sinha[44], S. Sinha[31f], M. Sioli[21a,21b], I. Siral[128], S.Yu. Sivoklokov[110], J. Sjölin[43a,43b], A. Skaf[51], E. Skorda[94], P. Skubic[125], M. Slawinska[82], K. Sliwa[166], V. Smakhtin[176], B. H. Smart[140], J. Smiesko[139], S.Yu. Smirnov[109], Y. Smirnov[109], L. N. Smirnova[110,s], O. Smirnova[94], E. A. Smith[35], H. A. Smith[131], M. Smizanska[87],

K. Smolek[138], A. Smykiewicz[82], A. A. Snesarev[108], H. L. Snoek[116], S. Snyder[27], R. Sobie[172,aa], A. Soffer[158], F. Sohns[51], C. A. Solans Sanchez[34], E.Yu. Soldatov[109], U. Soldevila[170], A. A. Solodkov[119], S. Solomon[50], A. Soloshenko[77], O. V. Solovyanov[119], V. Solovyev[134], P. Sommer[146], H. Son[166], A. Sonay[12], W. Y. Song[164b], A. Sopczak[138], A. L. Sopio[92], F. Sopkova[26b], S. Sottocornola[68a,68b], R. Soualah[64a,64c], A. M. Soukharev[118a,118b], Z. Soumaimi[33e], D. South[44], S. Spagnolo[65a,65b], M. Spalla[112], M. Spangenberg[174], F. Spanò[91], D. Sperlich[50], T. M. Spieker[59a], G. Spigo[34], M. Spina[153], D. P. Spiteri[55], M. Spousta[139], A. Stabile[66a,66b], B. L. Stamas[117], R. Stamen[59a], M. Stamenkovic[116], A. Stampekis[19], M. Standke[22], E. Stanecka[82], B. Stanislaus[34], M. M. Stanitzki[44], M. Stankaityte[131], B. Stapf[44], E. A. Starchenko[119], G. H. Stark[142], J. Stark[99], D. M. Starko[164b], P. Staroba[137], P. Starovoitov[59a], S. Stärz[101], R. Staszewski[82], G. Stavropoulos[42], P. Steinberg[27], A. L. Steinhebel[128], B. Stelzer[149,164a], H. J. Stelzer[135], O. Stelzer-Chilton[164a], H. Stenzel[54], T. J. Stevenson[153], G. A. Stewart[34], M. C. Stockton[34], G. Stoicea[25b], M. Stolarski[136a], S. Stonjek[112], A. Straessner[46], J. Strandberg[151], S. Strandberg[43a,43b], M. Strauss[125], T. Strebler[99], P. Strizenec[26b], R. Ströhmer[173], D. M. Strom[128], L. R. Strom[44], R. Stroynowski[40], A. Strubig[43a,43b], S. A. Stucci[27], B. Stugu[15], J. Stupak[125], N. A. Styles[44], D. Su[150], S. Su[58a], W. Su[58c,58d,145], X. Su[58a], N. B. Suarez[135], K. Sugizaki[160], V. V. Sulin[108], M. J. Sullivan[88], D. M. S. Sultan[52], S. Sultansoy[3c], T. Sumida[83], S. Sun[103], S. Sun[177], X. Sun[98], O. Sunneborn Gudnadottir[168], C. J. E. Suster[154], M. R. Sutton[153], M. Svatos[137], M. Swiatlowski[164a], T. Swirski[173], I. Sykora[26a], M. Sykora[139], T. Sykora[139], D. Ta[97], K. Tackmann[44,y], A. Taffard[167], R. Tafirout[164a], E. Tagiev[119], R. H. M. Taibah[132], R. Takashima[84], K. Takeda[80], T. Takeshita[147], E. P. Takeva[48], Y. Takubo[79], M. Talby[99], A. A. Talyshev[118a,118b], K. C. Tam[60b], N. M. Tamir[158], A. Tanaka[160], J. Tanaka[160], R. Tanaka[62], Z. Tao[171], S. Tapia Araya[76], S. Tapprogge[97], A. Tarek Abouelfadl Mohamed[104], S. Tarem[157], K. Tariq[58b], G. Tarna[25b,f], G. F. Tartarelli[66a], P. Tas[139], M. Tasevsky[137], E. Tassi[39a,39b], G. Tateno[160], Y. Tayalati[33e], G. N. Taylor[102], W. Taylor[164b], H. Teagle[88], A. S. Tee[177], R. Teixeira De Lima[150], P. Teixeira-Dias[91], H. Ten Kate[34], J. J. Teoh[116], K. Terashi[160], J. Terron[96], S. Terzo[12], M. Testa[49], R. J. Teuscher[163,aa], N. Themistokleous[48], T. Theveneaux-Pelzer[17], D. W. Thomas[91], J. P. Thomas[19], E. A. Thompson[44], P. D. Thompson[19], E. Thomson[133], E. J. Thorpe[90], Y. Tian[51], V. O. Tikhomirov[108,ah], Yu.A. Tikhonov[118a,118b], S. Timoshenko[109], P. Tipton[179], S. Tisserant[99], S. H. Tlou[31f], A. Tnourji[36], K. Todome[21a,21b], S. Todorova-Nova[139], S. Todt[46], M. Togawa[79], J. Tojo[85], S. Tokár[26a], K. Tokushuku[79], E. Tolley[124], R. Tombs[30], M. Tomoto[79,113], L. Tompkins[150], P. Tornambe[100], E. Torrence[128], H. Torres[46], E. Torró Pastor[170], M. Toscani[28], C. Tosciri[35], J. Toth[99,z], D. R. Tovey[146], A. Traeet[15], C. J. Treado[122], T. Trefzger[173], A. Tricoli[27], I. M. Trigger[164a], S. Trincaz-Duvoid[132], D. A. Trischuk[171], W. Trischuk[163], B. Trocmé[56], A. Trofymov[62], C. Troncon[66a], F. Trovato[153], L. Truong[31c], M. Trzebinski[82], A. Trzupek[82], F. Tsai[152], A. Tsiamis[159], P. V. Tsiareshka[105,af], A. Tsirigotis[159,w], V. Tsiskaridze[152], E. G. Tskhadadze[156a], M. Tsopoulou[159], I. I. Tsukerman[120], V. Tsulaia[16], S. Tsuno[79], O. Tsur[157], D. Tsybychev[152], Y. Tu[60b], A. Tudorache[25b], V. Tudorache[25b], A. N. Tuna[34], S. Turchikhin[77], D. Turgeman[176], I. Turk Cakir[3b,u], R. J. Turner[19], R. Turra[66a], P. M. Tuts[37], S. Tzamarias[159], P. Tzanis[9], E. Tzovara[97], K. Uchida[160], F. Ukegawa[165], G. Unal[34], M. Unal[10], A. Undrus[27], G. Unel[167], F. C. Ungaro[102], K. Uno[160], J. Urban[26b], P. Urquijo[102], G. Usai[7], R. Ushioda[161], M. Usman[107], Z. Uysal[11d], V. Vacek[138], B. Vachon[101], K. O. H. Vadla[130], T. Vafeiadis[34], C. Valderanis[111], E. Valdes Santurio[43a,43b], M. Valente[164a], S. Valentinetti[21a,21b], A. Valero[170], L. Valéry[44], R. A. Vallance[19], A. Vallier[99], J. A. Valls Ferrer[170], T. R. Van Daalen[12], P. Van Gemmeren[5], S. Van Stroud[92], I. Van Vulpen[116], M. Vanadia[71a,71b], W. Vandelli[34], M. Vandenbroucke[141], E. R. Vandewall[126], D. Vannicola[70a,70b], L. Vannoli[53a,53b], R. Vari[70a], E. W. Varnes[6], C. Varni[53a,53b], T. Varol[155], D. Varouchas[62], K. E. Varvell[154], M. E. Vasile[25b], L. Vaslin[36], G. A. Vasquez[172], F. Vazeille[36], D. Vazquez Furelos[12], T. Vazquez Schroeder[34], J. Veatch[51], V. Vecchio[98], M. J. Veen[116], I. Veliscek[131], L. M. Veloce[163], F. Veloso[136a,136c], S. Veneziano[70a], A. Ventura[65a,65b], A. Verbytskyi[112], M. Verducci[69a,69b], C. Vergis[22], M. Verissimo De Araujo[78b], W. Verkerke[116], A. T. Vermeulen[116], J. C. Vermeulen[116], C. Vernieri[150], P. J. Verschuuren[91], M. L. Vesterbacka[122], M. C. Vetterli[149,ak], N. Viaux Maira[143e], T. Vickey[146], O. E. Vickey Boeriu[146], G. H. A. Viehhauser[131], L. Vigani[59b], M. Villa[21a,21b], M. Villaplana Perez[170], E. M. Villhauer[48], E. Vilucchi[49], M. G. Vincter[32], G. S. Virdee[19], A. Vishwakarma[48], C. Vittori[21a,21b], I. Vivarelli[153], V. Vladimirov[174], E. Voevodina[112], M. Vogel[178], P. Vokac[138], J. Von Ahnen[44], S. E. von Buddenbrock[31f], E. Von Toerne[22], V. Vorobel[139], K. Vorobev[109], M. Vos[170], J. H. Vossebeld[88], M. Vozak[98], N. Vranjes[14], M. Vranjes Milosavljevic[14], V. Vrba[138,*], M. Vreeswijk[116], N. K. Vu[99], R. Vuillermet[34], I. Vukotic[35], S. Wada[165], C. Wagner[100], P. Wagner[22],

W. Wagner[178], S. Wahdan[178], H. Wahlberg[86], R. Wakasa[165], M. Wakida[113], V. M. Walbrecht[112], J. Walder[140], R. Walker[111], S. D. Walker[91], W. Walkowiak[148], A. M. Wang[57], A. Z. Wang[177], C. Wang[58a], C. Wang[58c], H. Wang[16], J. Wang[60a], P. Wang[40], R.-J. Wang[97], R. Wang[57], R. Wang[117], S. M. Wang[155], S. Wang[58b], T. Wang[58a], W. T. Wang[58a], W. X. Wang[58a], X. Wang[169], Y. Wang[58a], Z. Wang[103], C. Wanotayaroj[34], A. Warburton[101], C. P. Ward[30], R. J. Ward[19], N. Warrack[55], A. T. Watson[19], M. F. Watson[19], G. Watts[145], B. M. Waugh[92], A. F. Webb[10], C. Weber[27], M. S. Weber[18], S. A. Weber[32], S. M. Weber[59a], C. Wei[58a], Y. Wei[131], A. R. Weidberg[131], J. Weingarten[45], M. Weirich[97], C. Weiser[50], T. Wenaus[27], B. Wendland[45], T. Wengler[34], S. Wenig[34], N. Wermes[22], M. Wessels[59a], K. Whalen[128], A. M. Wharton[87], A. S. White[57], A. White[7], M. J. White[1], D. Whiteson[167], W. Wiedenmann[177], C. Wiel[46], M. Wielers[140], N. Wieseotte[97], C. Wiglesworth[38], L. A. M. Wiik-Fuchs[50], D. J. Wilbern[125], H. G. Wilkens[34], L. J. Wilkins[91], D. M. Williams[37], H. H. Williams[133], S. Williams[30], S. Willocq[100], P. J. Windischhofer[131], I. Wingerter-Seez[4], F. Winklmeier[128], B. T. Winter[50], M. Wittgen[150], M. Wobisch[93], A. Wolf[97], R. Wölker[131], J. Wollrath[167], M. W. Wolter[82], H. Wolters[136a,136c], V. W. S. Wong[171], A. F. Wongel[44], S. D. Worm[44], B. K. Wosiek[82], K. W. Woźniak[82], K. Wraight[55], J. Wu[13a,13d], S. L. Wu[177], X. Wu[52], Y. Wu[58a], Z. Wu[58a,141], J. Wuerzinger[131], T. R. Wyatt[98], B. M. Wynne[48], S. Xella[38], J. Xiang[60c], X. Xiao[103], X. Xie[58a], I. Xiotidis[153], D. Xu[13a], H. Xu[58a], H. Xu[58a], L. Xu[58a], R. Xu[133], W. Xu[103], Y. Xu[13b], Z. Xu[58b], Z. Xu[150], B. Yabsley[154], S. Yacoob[31a], N. Yamaguchi[85], Y. Yamaguchi[161], M. Yamatani[160], H. Yamauchi[165], T. Yamazaki[16], Y. Yamazaki[80], J. Yan[58c], Z. Yan[23], H. J. Yang[58c,58d], H. T. Yang[16], S. Yang[58a], T. Yang[60c], X. Yang[58a], X. Yang[13a], Y. Yang[160], Z. Yang[58a,103], W-M. Yao[16], Y. C. Yap[44], H. Ye[13c], J. Ye[40], S. Ye[27], I. Yeletskikh[77], M. R. Yexley[87], P. Yin[37], K. Yorita[175], K. Yoshihara[76], C. J. S. Young[34], C. Young[150], R. Yuan[58b,j], X. Yue[59a], M. Zaazoua[33e], B. Zabinski[82], G. Zacharis[9], E. Zaffaroni[52], A. M. Zaitsev[119,ag], T. Zakareishvili[156b], N. Zakharchuk[32], S. Zambito[34], D. Zanzi[50], S. V. Zeißner[45], C. Zeitnitz[178], G. Zemaityte[131], J. C. Zeng[169], O. Zenin[119], T. Ženiš[26a], S. Zenz[90], S. Zerradi[33a], D. Zerwas[62], M. Zgubič[131], B. Zhang[13c], D. F. Zhang[13b], G. Zhang[13b], J. Zhang[5], K. Zhang[13a], L. Zhang[13c], M. Zhang[169], R. Zhang[177], S. Zhang[103], X. Zhang[58c], X. Zhang[58b], Z. Zhang[62], P. Zhao[47], Y. Zhao[142], Z. Zhao[58a], A. Zhemchugov[77], Z. Zheng[103], D. Zhong[169], B. Zhou[103], C. Zhou[177], H. Zhou[6], N. Zhou[58c], Y. Zhou[6], C. G. Zhu[58b], C. Zhu[13a,13d], H. L. Zhu[58a], H. Zhu[13a], J. Zhu[103], Y. Zhu[58a], X. Zhuang[13a], K. Zhukov[108], V. Zhulanov[118a,118b], D. Zieminska[63], N. I. Zimine[77], S. Zimmermann[50,*], M. Ziolkowski[148], L. Živković[14], A. Zoccoli[21a,21b], K. Zoch[52], T. G. Zorbas[146], O. Zormpa[42], W. Zou[37], L. Zwalinski[34]

[1] Department of Physics, University of Adelaide, Adelaide, Australia
[2] Department of Physics, University of Alberta, Edmonton, AB, Canada
[3] [(a)]Department of Physics, Ankara University, Ankara, Turkey; [(b)]Istanbul Aydin University, Application and Research Center for Advanced Studies, Istanbul, Turkey; [(c)]Division of Physics, TOBB University of Economics and Technology, Ankara, Turkey
[4] LAPP, Univ. Savoie Mont Blanc, CNRS/IN2P3, Annecy, France
[5] High Energy Physics Division, Argonne National Laboratory, Argonne, IL, USA
[6] Department of Physics, University of Arizona, Tucson, AZ, USA
[7] Department of Physics, University of Texas at Arlington, Arlington, TX, USA
[8] Physics Department, National and Kapodistrian University of Athens, Athens, Greece
[9] Physics Department, National Technical University of Athens, Zografou, Greece
[10] Department of Physics, University of Texas at Austin, Austin, TX, USA
[11] [(a)]Faculty of Engineering and Natural Sciences, Bahcesehir University, Istanbul, Turkey; [(b)]Istanbul Bilgi University, Faculty of Engineering and Natural Sciences, Istanbul, Turkey; [(c)]Department of Physics, Bogazici University, Istanbul, Turkey; [(d)]Department of Physics Engineering, Gaziantep University, Gaziantep, Turkey
[12] Institut de Física d'Altes Energies (IFAE), Barcelona Institute of Science and Technology, Barcelona, Spain
[13] [(a)]Institute of High Energy Physics, Chinese Academy of Sciences, Beijing, China; [(b)]Physics Department, Tsinghua University, Beijing, China; [(c)]Department of Physics, Nanjing University, Nanjing, China; [(d)]University of Chinese Academy of Science (UCAS), Beijing, China
[14] Institute of Physics, University of Belgrade, Belgrade, Serbia
[15] Department for Physics and Technology, University of Bergen, Bergen, Norway
[16] Physics Division, Lawrence Berkeley National Laboratory and University of California, Berkeley, CA, USA

[17] Institut für Physik, Humboldt Universität zu Berlin, Berlin, Germany
[18] Albert Einstein Center for Fundamental Physics and Laboratory for High Energy Physics, University of Bern, Bern, Switzerland
[19] School of Physics and Astronomy, University of Birmingham, Birmingham, UK
[20] [(a)]Facultad de Ciencias y Centro de Investigaciónes, Universidad Antonio Nariño, Bogotá, Colombia; [(b)]Departamento de Física, Universidad Nacional de Colombia, Bogotá, Colombia
[21] [(a)]Dipartimento di Fisica e Astronomia A. Righi, Università di Bologna, Bologna, Italy; [(b)]INFN Sezione di Bologna, Bologna, Italy
[22] Physikalisches Institut, Universität Bonn, Bonn, Germany
[23] Department of Physics, Boston University, Boston, MA, USA
[24] Department of Physics, Brandeis University, Waltham, MA, USA
[25] [(a)]Transilvania University of Brasov, Brasov, Romania; [(b)]Horia Hulubei National Institute of Physics and Nuclear Engineering, Bucharest, Romania; [(c)]Department of Physics, Alexandru Ioan Cuza University of Iasi, Iasi, Romania; [(d)]National Institute for Research and Development of Isotopic and Molecular Technologies, Physics Department, Cluj-Napoca, Romania; [(e)]University Politehnica Bucharest, Bucharest, Romania; [(f)]West University in Timisoara, Timisoara, Romania
[26] [(a)]Faculty of Mathematics, Physics and Informatics, Comenius University, Bratislava, Slovakia; [(b)]Department of Subnuclear Physics, Institute of Experimental Physics of the Slovak Academy of Sciences, Kosice, Slovak Republic
[27] Physics Department, Brookhaven National Laboratory, Upton, NY, USA
[28] Departamento de Física (FCEN) and IFIBA, Universidad de Buenos Aires and CONICET, Buenos Aires, Argentina
[29] California State University, Long Beach, CA, USA
[30] Cavendish Laboratory, University of Cambridge, Cambridge, UK
[31] [(a)]Department of Physics, University of Cape Town, Cape Town, South Africa; [(b)]iThemba Labs, Western Cape, South Africa; [(c)]Department of Mechanical Engineering Science, University of Johannesburg, Johannesburg, South Africa; [(d)]National Institute of Physics, University of the Philippines Diliman (Philippines), Quezon, Philippines; [(e)]Department of Physics, University of South Africa, Pretoria, South Africa; [(f)]School of Physics, University of the Witwatersrand, Johannesburg, South Africa
[32] Department of Physics, Carleton University, Ottawa, ON, Canada
[33] [(a)]Faculté des Sciences Ain Chock, Réseau Universitaire de Physique des Hautes Energies - Université Hassan II, Casablanca, Morocco; [(b)]Faculté des Sciences, Université Ibn-Tofail, Kénitra, Morocco; [(c)]Faculté des Sciences Semlalia, Université Cadi Ayyad, LPHEA-Marrakech, Marrakech, Morocco; [(d)]LPMR, Faculté des Sciences, Université Mohamed Premier, Oujda, Morocco; [(e)]Faculté des sciences, Université Mohammed V, Rabat, Morocco; [(f)]Mohammed VI Polytechnic University, Ben Guerir, Morocco
[34] CERN, Geneva, Switzerland
[35] Enrico Fermi Institute, University of Chicago, Chicago, IL, USA
[36] LPC, Université Clermont Auvergne, CNRS/IN2P3, Clermont-Ferrand, France
[37] Nevis Laboratory, Columbia University, Irvington, NY, USA
[38] Niels Bohr Institute, University of Copenhagen, Copenhagen, Denmark
[39] [(a)]Dipartimento di Fisica, Università della Calabria, Rende, Italy; [(b)]INFN Gruppo Collegato di Cosenza, Laboratori Nazionali di Frascati, Frascati, Italy
[40] Physics Department, Southern Methodist University, Dallas, TX, USA
[41] Physics Department, University of Texas at Dallas, Richardson, TX, USA
[42] National Centre for Scientific Research "Demokritos", Agia Paraskevi, Greece
[43] [(a)]Department of Physics, Stockholm University, Stockholm, Sweden; [(b)]Oskar Klein Centre, Stockholm, Sweden
[44] Deutsches Elektronen-Synchrotron DESY, Hamburg and Zeuthen, Germany
[45] Lehrstuhl für Experimentelle Physik IV, Technische Universität Dortmund, Dortmund, Germany
[46] Institut für Kern- und Teilchenphysik, Technische Universität Dresden, Dresden, Germany
[47] Department of Physics, Duke University, Durham, NC, USA
[48] SUPA-School of Physics and Astronomy, University of Edinburgh, Edinburgh, UK
[49] INFN e Laboratori Nazionali di Frascati, Frascati, Italy
[50] Physikalisches Institut, Albert-Ludwigs-Universität Freiburg, Freiburg, Germany
[51] II. Physikalisches Institut, Georg-August-Universität Göttingen, Göttingen, Germany
[52] Département de Physique Nucléaire et Corpusculaire, Université de Genève, Geneva, Switzerland

[53] [(a)]Dipartimento di Fisica, Università di Genova, Genoa, Italy; [(b)]INFN Sezione di Genova, Genoa, Italy
[54] II. Physikalisches Institut, Justus-Liebig-Universität Giessen, Giessen, Germany
[55] SUPA-School of Physics and Astronomy, University of Glasgow, Glasgow, UK
[56] LPSC, Université Grenoble Alpes, CNRS/IN2P3, Grenoble INP, Grenoble, France
[57] Laboratory for Particle Physics and Cosmology, Harvard University, Cambridge, MA, USA
[58] [(a)]Department of Modern Physics and State Key Laboratory of Particle Detection and Electronics, University of Science and Technology of China, Hefei, China; [(b)]Institute of Frontier and Interdisciplinary Science and Key Laboratory of Particle Physics and Particle Irradiation (MOE), Shandong University, Qingdao, China; [(c)]School of Physics and Astronomy, Shanghai Jiao Tong University, Key Laboratory for Particle Astrophysics and Cosmology (MOE), SKLPPC, Shanghai, China; [(d)]Tsung-Dao Lee Institute, Shanghai, China
[59] [(a)]Kirchhoff-Institut für Physik, Ruprecht-Karls-Universität Heidelberg, Heidelberg, Germany; [(b)]Physikalisches Institut, Ruprecht-Karls-Universität Heidelberg, Heidelberg, Germany
[60] [(a)]Department of Physics, Chinese University of Hong Kong , Shatin, N.T., Hong Kong; [(b)]Department of Physics, University of Hong Kong, Lung Fu Shan, Hong Kong; [(c)]Department of Physics and Institute for Advanced Study, Hong Kong University of Science and Technology, Clear Water Bay, Kowloon, Hong Kong, China
[61] Department of Physics, National Tsing Hua University, Hsinchu, Taiwan
[62] IJCLab, Université Paris-Saclay, CNRS/IN2P3, 91405 Orsay, France
[63] Department of Physics, Indiana University, Bloomington, IN, USA
[64] [(a)]INFN Gruppo Collegato di Udine, Sezione di Trieste, Udine, Italy; [(b)]ICTP, Trieste, Italy; [(c)]Dipartimento Politecnico di Ingegneria e Architettura, Università di Udine, Udine, Italy
[65] [(a)]INFN Sezione di Lecce, Lecce, Italy; [(b)]Dipartimento di Matematica e Fisica, Università del Salento, Lecce, Italy
[66] [(a)]INFN Sezione di Milano, Milan, Italy; [(b)]Dipartimento di Fisica, Università di Milano, Milan, Italy
[67] [(a)]INFN Sezione di Napoli, Naples, Italy; [(b)]Dipartimento di Fisica, Università di Napoli, Naples, Italy
[68] [(a)]INFN Sezione di Pavia, Pavia, Italy; [(b)]Dipartimento di Fisica, Università di Pavia, Pavia, Italy
[69] [(a)]INFN Sezione di Pisa, Pisa, Italy; [(b)]Dipartimento di Fisica E. Fermi, Università di Pisa, Pisa, Italy
[70] [(a)]INFN Sezione di Roma, Rome, Italy; [(b)]Dipartimento di Fisica, Sapienza Università di Roma, Rome, Italy
[71] [(a)]INFN Sezione di Roma Tor Vergata, Rome, Italy; [(b)]Dipartimento di Fisica, Università di Roma Tor Vergata, Rome, Italy
[72] [(a)]INFN Sezione di Roma Tre, Rome, Italy; [(b)]Dipartimento di Matematica e Fisica, Università Roma Tre, Rome, Italy
[73] [(a)]INFN-TIFPA, Povo, Italy; [(b)]Università degli Studi di Trento, Trento, Italy
[74] Institut für Astro- und Teilchenphysik, Leopold-Franzens-Universität, Innsbruck, Austria
[75] University of Iowa, Iowa City, IA, USA
[76] Department of Physics and Astronomy, Iowa State University, Ames, IA, USA
[77] Joint Institute for Nuclear Research, Dubna, Russia
[78] [(a)]Departamento de Engenharia Elétrica, Universidade Federal de Juiz de Fora (UFJF), Juiz de Fora, Brazil ; [(b)]Universidade Federal do Rio de Janeiro COPPE/EE/IF, Rio de Janeiro, Brazil; [(c)]Instituto de Física, Universidade de São Paulo, São Paulo, Brazil
[79] KEK, High Energy Accelerator Research Organization, Tsukuba, Japan
[80] Graduate School of Science, Kobe University, Kobe, Japan
[81] [(a)]Faculty of Physics and Applied Computer Science, AGH University of Science and Technology, Krakow, Poland; [(b)]Marian Smoluchowski Institute of Physics, Jagiellonian University, Krakow, Poland
[82] Institute of Nuclear Physics Polish Academy of Sciences, Krakow, Poland
[83] Faculty of Science, Kyoto University, Kyoto, Japan
[84] Kyoto University of Education, Kyoto, Japan
[85] Research Center for Advanced Particle Physics and Department of Physics, Kyushu University, Fukuoka , Japan
[86] Instituto de Física La Plata, Universidad Nacional de La Plata and CONICET, La Plata, Argentina
[87] Physics Department, Lancaster University, Lancaster, UK
[88] Oliver Lodge Laboratory, University of Liverpool, Liverpool, UK
[89] Department of Experimental Particle Physics, Jožef Stefan Institute and Department of Physics, University of Ljubljana, Ljubljana, Slovenia
[90] School of Physics and Astronomy, Queen Mary University of London, London, UK
[91] Department of Physics, Royal Holloway University of London, Egham, UK
[92] Department of Physics and Astronomy, University College London, London, UK

[93] Louisiana Tech University, Ruston, LA, USA
[94] Fysiska institutionen, Lunds universitet, Lund, Sweden
[95] Centre de Calcul de l'Institut National de Physique Nucléaire et de Physique des Particules (IN2P3), Villeurbanne, France
[96] Departamento de Física Teorica C-15 and CIAFF, Universidad Autónoma de Madrid, Madrid, Spain
[97] Institut für Physik, Universität Mainz, Mainz, Germany
[98] School of Physics and Astronomy, University of Manchester, Manchester, UK
[99] CPPM, Aix-Marseille Université, CNRS/IN2P3, Marseille, France
[100] Department of Physics, University of Massachusetts, Amherst, MA, USA
[101] Department of Physics, McGill University, Montreal, QC, Canada
[102] School of Physics, University of Melbourne, Melbourne, VIC, Australia
[103] Department of Physics, University of Michigan, Ann Arbor, MI, USA
[104] Department of Physics and Astronomy, Michigan State University, East Lansing, MI, USA
[105] B.I. Stepanov Institute of Physics, National Academy of Sciences of Belarus, Minsk, Belarus
[106] Research Institute for Nuclear Problems of Byelorussian State University, Minsk, Belarus
[107] Group of Particle Physics, University of Montreal, Montreal, QC, Canada
[108] P.N. Lebedev Physical Institute of the Russian Academy of Sciences, Moscow, Russia
[109] National Research Nuclear University MEPhI, Moscow, Russia
[110] D.V. Skobeltsyn Institute of Nuclear Physics, M.V. Lomonosov Moscow State University, Moscow, Russia
[111] Fakultät für Physik, Ludwig-Maximilians-Universität München, München, Germany
[112] Max-Planck-Institut für Physik (Werner-Heisenberg-Institut), München, Germany
[113] Graduate School of Science and Kobayashi-Maskawa Institute, Nagoya University, Nagoya, Japan
[114] Department of Physics and Astronomy, University of New Mexico, Albuquerque, NM, USA
[115] Institute for Mathematics, Astrophysics and Particle Physics, Radboud University/Nikhef, Nijmegen, The Netherlands
[116] Nikhef National Institute for Subatomic Physics and University of Amsterdam, Amsterdam, The Netherlands
[117] Department of Physics, Northern Illinois University, DeKalb, IL, USA
[118] [(a)]Budker Institute of Nuclear Physics and NSU, SB RAS, Novosibirsk, Russia; [(b)]Novosibirsk State University Novosibirsk, Novosibirsk, Russia
[119] Institute for High Energy Physics of the National Research Centre Kurchatov Institute, Protvino, Russia
[120] Institute for Theoretical and Experimental Physics named by A.I. Alikhanov of National Research Centre "Kurchatov Institute", Moscow, Russia
[121] [(a)]New York University Abu Dhabi, Abu Dhabi, United Arab Emirates; [(b)]United Arab Emirates University, Al Ain, United Arab Emirates; [(c)]University of Sharjah, Sharjah, United Arab Emirates
[122] Department of Physics, New York University, New York, NY, USA
[123] Ochanomizu University, Otsuka, Bunkyo-ku, Tokyo, Japan
[124] Ohio State University, Columbus, OH, USA
[125] Homer L. Dodge Department of Physics and Astronomy, University of Oklahoma, Norman, OK, USA
[126] Department of Physics, Oklahoma State University, Stillwater, OK, USA
[127] Palacký University, Joint Laboratory of Optics, Olomouc, Czech Republic
[128] Institute for Fundamental Science, University of Oregon, Eugene, OR, USA
[129] Graduate School of Science, Osaka University, Osaka, Japan
[130] Department of Physics, University of Oslo, Oslo, Norway
[131] Department of Physics, Oxford University, Oxford, UK
[132] LPNHE, Sorbonne Université, Université de Paris, CNRS/IN2P3, Paris, France
[133] Department of Physics, University of Pennsylvania, Philadelphia, PA, USA
[134] Konstantinov Nuclear Physics Institute of National Research Centre "Kurchatov Institute", PNPI, St. Petersburg, Russia
[135] Department of Physics and Astronomy, University of Pittsburgh, Pittsburgh, PA, USA

[136] [(a)]Laboratório de Instrumentação e Física Experimental de Partículas-LIP, Lisbon, Portugal; [(b)]Departamento de Física, Faculdade de Ciências, Universidade de Lisboa, Lisbon, Portugal; [(c)]Departamento de Física, Universidade de Coimbra, Coimbra, Portugal; [(d)]Centro de Física Nuclear da Universidade de Lisboa, Lisbon, Portugal; [(e)]Departamento de Física, Universidade do Minho, Braga, Portugal; [(f)]Departamento de Física Teórica y del Cosmos, Universidad de Granada, Granada, Spain; [(g)]Dep Física and CEFITEC of Faculdade de Ciências e Tecnologia, Universidade Nova de Lisboa, Caparica, Portugal; [(h)]Instituto Superior Técnico, Universidade de Lisboa, Lisbon, Portugal
[137] Institute of Physics of the Czech Academy of Sciences, Prague, Czech Republic
[138] Czech Technical University in Prague, Prague, Czech Republic
[139] Charles University, Faculty of Mathematics and Physics, Prague, Czech Republic
[140] Particle Physics Department, Rutherford Appleton Laboratory, Didcot, UK
[141] IRFU, CEA, Université Paris-Saclay, Gif-sur-Yvette, France
[142] Santa Cruz Institute for Particle Physics, University of California Santa Cruz, Santa Cruz, CA, USA
[143] [(a)]Departamento de Física, Pontificia Universidad Católica de Chile, Santiago, Chile; [(b)]Universidad de la Serena, La Serena, Chile; [(c)]Department of Physics, Universidad Andres Bello, Santiago, Chile; [(d)]Instituto de Alta Investigación, Universidad de Tarapacá, Arica, Chile; [(e)]Departamento de Física, Universidad Técnica Federico Santa María, Valparaíso, Chile
[144] Universidade Federal de São João del Rei (UFSJ), São João del Rei, Brazil
[145] Department of Physics, University of Washington, Seattle, WA, USA
[146] Department of Physics and Astronomy, University of Sheffield, Sheffield, UK
[147] Department of Physics, Shinshu University, Nagano, Japan
[148] Department Physik, Universität Siegen, Siegen, Germany
[149] Department of Physics, Simon Fraser University, Burnaby, BC, Canada
[150] SLAC National Accelerator Laboratory, Stanford, CA, USA
[151] Department of Physics, Royal Institute of Technology, Stockholm, Sweden
[152] Departments of Physics and Astronomy, Stony Brook University, Stony Brook, NY, USA
[153] Department of Physics and Astronomy, University of Sussex, Brighton, UK
[154] School of Physics, University of Sydney, Sydney, Australia
[155] Institute of Physics, Academia Sinica, Taipei, Taiwan
[156] [(a)]E. Andronikashvili Institute of Physics, Iv. Javakhishvili Tbilisi State University, Tbilisi, Georgia; [(b)]High Energy Physics Institute, Tbilisi State University, Tbilisi, Georgia
[157] Department of Physics, Technion, Israel Institute of Technology, Haifa, Israel
[158] Raymond and Beverly Sackler School of Physics and Astronomy, Tel Aviv University, Tel Aviv, Israel
[159] Department of Physics, Aristotle University of Thessaloniki, Thessaloniki, Greece
[160] International Center for Elementary Particle Physics and Department of Physics, University of Tokyo, Tokyo, Japan
[161] Department of Physics, Tokyo Institute of Technology, Tokyo, Japan
[162] Tomsk State University, Tomsk, Russia
[163] Department of Physics, University of Toronto, Toronto, ON, Canada
[164] [(a)]TRIUMF, Vancouver, BC, Canada; [(b)]Department of Physics and Astronomy, York University, Toronto, ON, Canada
[165] Division of Physics and Tomonaga Center for the History of the Universe, Faculty of Pure and Applied Sciences, University of Tsukuba, Tsukuba, Japan
[166] Department of Physics and Astronomy, Tufts University, Medford, MA, USA
[167] Department of Physics and Astronomy, University of California Irvine, Irvine, CA, USA
[168] Department of Physics and Astronomy, University of Uppsala, Uppsala, Sweden
[169] Department of Physics, University of Illinois, Urbana, IL, USA
[170] Instituto de Física Corpuscular (IFIC), Centro Mixto Universidad de Valencia-CSIC, Valencia, Spain
[171] Department of Physics, University of British Columbia, Vancouver, BC, Canada
[172] Department of Physics and Astronomy, University of Victoria, Victoria, BC, Canada
[173] Fakultät für Physik und Astronomie, Julius-Maximilians-Universität Würzburg, Würzburg, Germany
[174] Department of Physics, University of Warwick, Coventry, UK
[175] Waseda University, Tokyo, Japan
[176] Department of Particle Physics and Astrophysics, Weizmann Institute of Science, Rehovot, Israel
[177] Department of Physics, University of Wisconsin, Madison, WI, USA

[178] Fakultät für Mathematik und Naturwissenschaften, Fachgruppe Physik, Bergische Universität Wuppertal, Wuppertal, Germany
[179] Department of Physics, Yale University, New Haven, CT, USA

[a] Also at Borough of Manhattan Community College, City University of New York, New York, NY, USA
[b] Also at Bruno Kessler Foundation, Trento, Italy
[c] Also at Center for High Energy Physics, Peking University, China
[d] Also at Centro Studi e Ricerche Enrico Fermi, Rome, Italy
[e] Also at CERN, Geneva, Switzerland
[f] Also at CPPM, Aix-Marseille Université, CNRS/IN2P3, Marseille, France
[g] Also at Département de Physique Nucléaire et Corpusculaire, Université de Genève, Geneva, Switzerland
[h] Also at Departament de Fisica de la Universitat Autonoma de Barcelona, Barcelona, Spain
[i] Also at Department of Financial and Management Engineering, University of the Aegean, Chios, Greece
[j] Also at Department of Physics and Astronomy, Michigan State University, East Lansing, MI, USA
[k] Also at Department of Physics and Astronomy, University of Louisville, Louisville, KY, USA
[l] Also at Department of Physics, Ben Gurion University of the Negev, Beer Sheva, Israel
[m] Also at Department of Physics, California State University, East Bay, USA
[n] Also at Department of Physics, California State University, Fresno, USA
[o] Also at Department of Physics, California State University, Sacramento, USA
[p] Also at Department of Physics, King's College London, London, UK
[q] Also at Department of Physics, St. Petersburg State Polytechnical University, St. Petersburg, Russia
[r] Also at Department of Physics, University of Fribourg, Fribourg, Switzerland
[s] Also at Faculty of Physics, M.V. Lomonosov Moscow State University, Moscow, Russia
[t] Also at Faculty of Physics, Sofia University, 'St. Kliment Ohridski', Sofia, Bulgaria
[u] Also at Giresun University, Faculty of Engineering, Giresun, Turkey
[v] Also at Graduate School of Science, Osaka University, Osaka, Japan
[w] Also at Hellenic Open University, Patras, Greece
[x] Also at Institucio Catalana de Recerca i Estudis Avancats, ICREA, Barcelona, Spain
[y] Also at Institut für Experimentalphysik, Universität Hamburg, Hamburg, Germany
[z] Also at Institute for Particle and Nuclear Physics, Wigner Research Centre for Physics, Budapest, Hungary
[aa] Also at Institute of Particle Physics (IPP), Victoria, Canada
[ab] Also at Institute of Physics, Azerbaijan Academy of Sciences, Baku, Azerbaijan
[ac] Also at Institute of Theoretical Physics, Ilia State University, Tbilisi, Georgia
[ad] Also at Instituto de Fisica Teorica, IFT-UAM/CSIC, Madrid, Spain
[ae] Also at Department of Physics, Istanbul University, Istanbul, Turkey
[af] Also at Joint Institute for Nuclear Research, Dubna, Russia
[ag] Also at Moscow Institute of Physics and Technology State University, Dolgoprudny, Russia
[ah] Also at National Research Nuclear University MEPhI, Moscow, Russia
[ai] Also at Physikalisches Institut, Albert-Ludwigs-Universität Freiburg, Freiburg, Germany
[aj] Also at The City College of New York, New York, NY, USA
[ak] Also at TRIUMF, Vancouver, BC, Canada
[al] Also at Universita di Napoli Parthenope, Naples, Italy
[am] Also at University of Chinese Academy of Sciences (UCAS), Beijing, China
[an] Also at Physics Department, Yeditepe University, Istanbul, Turkey
*Deceased